
# Study of sinter reactions when fine iron ore is replaced with coarse ore, using an infrared furnace and sinter pot tests

by

**MUTOMBO NYEMBWE**

Supervisor: Prof. AM Garbers - Craig

A dissertation submitted in partial fulfilment of the
requirements for the degree of

**Master of Science**

Department of Materials Science and Metallurgical Engineering, Faculty of Engineering, Built Environment and Information Technology, University of Pretoria, Pretoria.

November 2011

## Acknowledgements

I would like to thank God for being with me every step of my life.

I express sincere gratitude to Prof. AM Garbers - Craig for his continuous guidance and supervision throughout the course of this dissertation.

Thanks to Prof de Villiers for his pertinent comments and suggestions.

Anglo American Kumba Iron Ore (Value-in-Use group) is greatly acknowledged for providing different raw materials and technical support.

To all my family, thank you for your support.

## Abstract

The effect of replacing fine ore by coarse ore on sintering reactions was investigated using an infrared furnace on laboratory scale and sinter pots on pilot plant scale. Five sinter mixes were prepared by changing the percentage coarse ore from 0% to 100% in 25% increments.

Coarse ore fraction, sintering temperature, holding time and oxygen partial pressure were selected as sintering parameters, and two-level factorial design was used for identification of parameters that significantly influence the formation of sinter phases. Experimental results showed that the coarse ore fraction has a higher effect on the sintering process compared to those of other parameters. The experiment design also enabled to set these parameters to their optimum values.

The porosity of compacted pellets was measured using a helium pycnometer. The replacement of fine ore by coarse ore resulted in a decrease in porosity (increase in packing density) of compacted pellets. The particles are closer to each other in pellets consisting of more coarse particles than fine particles.

Laboratory experiments were performed at 1300℃ in air, using a high heating rate (15℃/s). The holding time was set to 2.5 minutes. X-ray diffraction (XRD), reflected light microscopy (RLM), scanning electron microscopy (SEM) and energy dispersive spectrometry (EDS) were used to characterize sintering reactions and sinter phases.

XRD analysis revealed that sintered pellets consisted of hematite, SFCA, SFCA-I and calcium silicate. The proportions of SFCA slightly increased when the fraction of coarse ore varied from 0% to 25%, but decreased with a further increase in percentage coarse ore. At 25% coarse ore fraction, the porosity of the compacted pellets decreased, resulting in an increase in packing density and sintering rate. More hematite reacted, resulting in the formation of high amounts of SFCA. Above 25% coarse ore fraction, the amount of hematite increased, and the concentrations of columnar SFCA decreased despite a further decrease in porosity. This was attributed to the decrease in reaction surface area for coarse ore, and the short reaction time,

which limited the extent of reaction of the coarse particles. The variation of SFCA-I and calcium silicate was not significant under laboratory conditions.

Reflected light microscopy and SEM analysis easily identified two major sinter phases: hematite and SFCA. A clear distinction between the different types of SFCA could not be made using EDS analysis.

Sinter pot tests were carried out in order to examine the effect of coarse ore fraction on physical and metallurgical properties of sinters. The tumbler and reduction disintegration indexes increased with increasing coarse ore fraction in the sinter bed. This was presumably due to the increase in amounts of hematite and decrease in surface area for reaction. Consequently, the reducibility of sinter decreased as the percentage coarse ore increased.

This study has concluded that the presence of 25% coarse ore in the sinter mix led to enhance sintering reactions. The amounts of SFCA increased, and sinter quality was improved.

It is recommended that in future work, sintering reactions should further be investigated by also measuring the permeability of the sinter bed and the reaction surface area of solid particles.

**Keywords**: Coarse ore, sintering reactions, XRD analysis, SFCA, sinter quality

# Table of contents

## List of abbreviations

| | |
|---|---|
| $C_2F$ | : $2CaO.Fe_2O_3$ |
| $C_2S$ | : $2CaO.SiO_2$ |
| $C_3S_2$ | : $3CaO.2SiO_2$ |
| $C_4S_3$ | : $4CaO.3SiO_2$ |
| CA | : $CaO.Al_2O_3$ |
| $CA_2$ | : $CaO.2Al_2O_3$ |
| $CA_6$ | : $CaO.6Al_2O_3$ |
| CF | : $CaO.Fe_2O_3$ |
| $CF_2$ | : $CaO.2Fe_2O_3$ |
| $CF_3$ | : $CaO.3Fe_2O_3$ |
| CS | : $CaO.SiO_2$ |
| EDS | : Energy dispersive spectrometry |
| Hem or H | : Hematite |
| ISO | : International Standards Organisation |
| M or Mt | : Magnetite |
| SEM | : Scanning electron microscopy |
| SFC | : Silico-ferrite of calcium |
| SFCA | : Silico-ferrite of calcium and aluminium |
| SFCA-I | : Acicular SFCA |
| Thaba | : Thabazimbi |
| XRD | : X-ray diffraction |
| XRF | : X-ray fluorescence |

# I Introduction

The production of most pig iron in the world is based on the use of iron ore sinter which consists of various mineral phases produced by sintering iron ores with fluxes and coke breeze. During the sintering process, the chemical reactions are taking place at high temperature and iron ores and fluxes are combined together and form a sinter cake composed of iron ore, silico-ferrites of calcium and aluminium (SFCA), dicalcium silicate and a glassy phase. Sintering reactions also regulate the volume fraction of each mineral which may affect sinter quality and hence, the performance of the blast furnace [1,2].

In principle, the sintering reactions involve reactions of fine ores with fluxes resulting in the formation of a melting phase which is used during solid-liquid reactions for the assimilation of coarse ore. The melt that forms during sintering acts as the bonding phase. As SFCA is considered the most important component of the bonding phase due to its abundance in iron ore sinter and its significant influence on sinter quality, sintering reactions have specifically been studied with regard to the control of the concentration and microstructure of the SFCA phase that forms during the sintering process [3,4].

The volume of the melting phase plays a significant role during sintering. Excessive melting will result in a homogeneous glassy structure, which has a low reducibility, whereas a very low concentration of melting will cause insufficient sinter strength, resulting in a high amount of return fines [5,6].

The effect of changing ore particle size during the sintering process was also examined by Debrincat *et al.* [6]. They found that the assimilation ability of fine ores was greater than that of coarse particles. The reaction surface area for fine particles is high resulting in high reaction rates. However, the formation of higher concentrations of melt might lead to the increase in the viscosity of the melt, resulting in a decrease in the melt fluidity. The inclusion of coarse particles into the sinter mix can therefore be necessary to improve the permeability of the sinter bed, which is

associated with an increase in large-scale movements between the melt and solid particles.

Kamijo *et al.*[7] also studied the sinterability of the sinter bed in which large particles were incorporated. They found that the use of larger ore particles resulted in improved permeability of the sinter bed as well as the sintering reactions during the process. When large particles were placed in the bed, low-density areas were formed around the particles. Due to the increase in permeability of the sinter bed, the gas flow rate as well as the flame front speed was higher around the large particles than with fine particles. The melt reaction and the assimilation might therefore occur quickly around the large particles due to the high fluidity of the melt.

Studies by German [8] and Rahaman [9] examined the effect of particle size distribution on the packing density of compacted pellets, which influences sintering rates. The results reported that the packing density of mixtures consisting of fine particles can be improved by replacing some of them by coarse particles. During compaction, the solid particles can move closer together, resulting in a high number of contacts between particles and a high packing density (low porosity). German [8] and Rahaman [9] also reported that the replacement of fine particles by large particles leads to an increase in the packing density up to a maximum, after which it decreases for higher fractions of coarse particles. The maximum packing density occurs at the point where all the voids between the coarse particles are filled by small particles. The presence of coarse particles can therefore produce compacted powders with a higher packing density (lower porosity), resulting in an increase in sintering rates.

## II Aim of project

Sinter quality is dependent on the formation of the bonding phase which, in turn depends on the sintering ability of iron ores. On the other hand, the reactivity of iron ore is considerably influenced by their grain size which determines the reaction surface area and packing density (porosity) of the sinter mix. The particle size of iron ores is therefore important to control sintering reactions during the sintering process.

The objective of this study was to examine sintering reactions on a small scale when fine iron ore is replaced with coarse ore using an infrared heating furnace. An emphasis was placed on sintering temperature, holding time and sintering atmosphere to determine their combined influence on phase formation during sintering. The coarse ore/fine iron ore ratio at which the sinters have optimum physical and metallurgical properties was then examined on a pilot plant scale.

# III Literature review

## III.1 Sintering process description

Iron ore sintering is a generic term that is used to describe the process whereby a green mix of iron ore fines, fluxes, fuel and plant fines (e.g. mill scale, blast-furnace dust and returned sinter fines) are converted into a particular form of agglomerate. The sinter product produced should be able to withstand the operating pressures and temperatures inside the blast furnace [10-14].

Prior to the sintering process, the granulation of the ore mixture is commonly performed in a rotary drum for several minutes with the addition of 6-8% water. Fine particles (< 0.250 mm) adhere onto the surface of large particles (> 0.750 mm) and then form granules called quasi-particles or pseudo-particles. Intermediate particles (0.250 - 0.750 mm) are difficult to granulate and do not have a well-defined role [10]. In practice, the amount of intermediate particles needs to be minimized because of their detrimental influence on granulation and adverse effect on permeability of the sinter bed [9-12]. An increase in water content of the sinter mix can lead the intermediate particles to act as adhering fines, which poorly adhere onto the coarse particles, and can detach during the drying stage. The intermediate particles can also act as nuclei and form quasi-particles with small size compared to those formed with coarser nuclei. This can sensibly reduce the permeability of the sinter bed as well as the productivity of the sintering process [10].

After granulation, the raw mix is fed onto the sintering machine as shown in Figure 1. The top of the sinter bed is heated by a gas burner and ignited for a short time. During the sintering process, the flame front descends down the sinter bed under the application of suction until the entire mass of the material has been converted into a porous but physically strong block. Subsequently, the sinter is cooled by the cold air supplied by the suction fan. The sinter formed is finally crushed and screened to a pre-determined maximum particle size. The fraction of undersized sinter is recycled to the sintering machine [12].

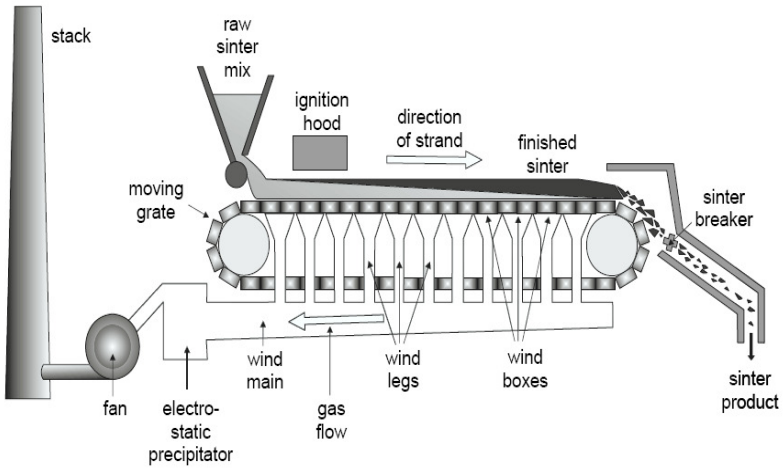


**Figure 1.** Typical sintering machine [12]

Studies by Yang *et al.* [13,14] reported that the combustion of coke generates a high temperature zone (combustion zone) which moves downwards through the sinter bed. Fine particles react faster, and form the primary melt which partially dissolves coarse ore particles. A sinter bed cross section of an interrupted sintering process is shown in Figure 2. Progress of the coke combustion determines the temperature profile and the formation of different zones in the bed. As the combustion zone moves down, the solidification of melting phase occurs by air suction, resulting in the formation of the sintered zone. The zone below the combustion zone is composed of the raw mix (un-reacted material) and can be split into two regions. The region immediately below the combustion zone corresponds to the dehydration of the raw mix by the hot gas from the combustion zone, while the zone below this region is the cold part of the sinter bed where the steam is condensed.

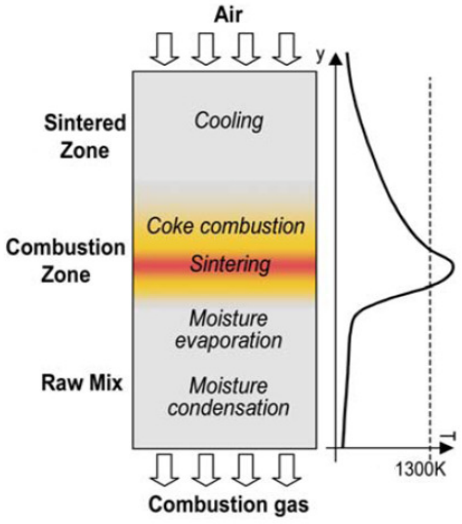


**Figure 2.** Schematic representation of a sinter bed cross section [13]

## III.2 Characterization of iron ore sinters

Iron ore sinters are considered as multi-phase materials, with a heterogeneous microstructure. Usually, the main mineral phases are: hematite, magnetite, SFCA and silicates. The mineralogical distribution of different phases determines the microstructure of the sinter which imparts the quality of the sinter such as mechanical strength and behaviour during reduction stages [1-4,15-19].

### III.2.1 Phases and microstructures of sinter

The microstructure of the sinter has been examined by considering the chemical composition, the mineralogy, the morphology and the spatial arrangement of the various mineral phases formed during sintering [15-18]. Studies by Scarlett *et al.*[18] reported that the sinter structure is composed of the following phases: iron oxides (~ 40 -70 vol%), ferrites (mostly SFCA, a silicoferrite of calcium and aluminium (~20 - 50 vol%)), glassy phases (up to ~10 vol%) and dicalcium silicates (up to ~10 vol%). Some phases such as sulphides (FeS), pyroxenes ($(Mg,Fe)SiO_3$), quartz and lime can be present but in very small proportion. Renard Chaigneau [16] also stated that the sinter product can be defined as an aggregate of the bonding phases, the relict solid particles and the pores.

#### III.2.1.1 Bonding phases

During the sintering process, the formation of the melt occurs in the flame front where the temperature is above 1100 °C [15,16,19]. Thereafter, the melt solidifies to become the bonding phases which make up the majority of other phases within a sinter. The bonding phase is generally composed of the SFCA phase in association with iron oxides and silicates. SFCA is considered to be the most important bonding phase because of its great influence on the properties of sinter [3,4,15,16,19].

### III.2.1.1.1 Silicoferrite of Calcium and Aluminium

The major bonding phase produced in iron ore sinter has been identified as a solid solution of $CaO.2Fe_2O_3$ with small amounts of dissolved $Al_2O_3$ and $SiO_2$. This phase has also been considered as a complex quaternary phase, known as SFCA (silico-ferrite of calcium and aluminium) [15-24]. The SFCA phases form a series of solid solutions which can also contain $Fe^{2+}$ and $Mg^{2+}$ [20,21].

Considered as the major bonding phase in iron ore sintering, SFCA has been extensively studied on account of its important role in producing sinter with high mechanical strength, high reducibility and low reduction disintegration [2-4,15-21].

Mumme *et al*. [20] and Mumme [21] examined the synthetic SFCA made from a mixture of analytical reagents of $Fe_2O_3$, $SiO_2$, $Al_2O_3$ and $CaCO_3$. The analysis of the SFCA crystal revealed the coexistence of homologue structures that can be represented by the following formula: $M_{14+6n}O_{20+8n}$ with n = 0, 1 and M=Al, Ca, Fe and Si. Two different structures of SFCA were identified, SFCA ($M_{14}O_{20}$) and SFCA-I ($M_{20}O_{28}$). The same authors also suggested a third homologue structure corresponding to SFCA-II ($M_{34}O_{48}$), in which the unit cell volume is nearly the sum of the cell volumes of SFCA and SFCA-I [20,21].

Further investigations by Mumme [21] reported the existence of another homologue structure ($M_{25}O_{36}$). The analysis of SFCA revealed XRD patterns that are similar to that of $Ca_5Si_2(Fe,Al)_{18}O_{36}$. This structure was then predicted to be the possible next member of the series, corresponding to n =2. As the structure of SFCA covered a large series of chemical compositions, studies by Hancart *et al*.[22] also proposed that the complex ferrites might be represented with the general formula $xFe_2O_3$ -$ySiO_2$ -$zAl_2O_3$ -5CaO where x + y + z = 12.

Studies by Scarlett *et al*. [18] examined the microstructure of SFCA phases on the basis of their chemical composition and morphology. The results also showed the coexistence of two main types of SFCA phases as shown in Figure 3. SFCA-I is characterized by a high amount of Fe and low Si content. Its morphology is platy and may be acicular or needle-like in a cross section. However, the morphology of SFCA

is columnar, blocky or lath shaped, contains less Fe and is more stable at high temperature (>1300°C). A third type of structure was also observed which has a dendritic morphology. This structure is very fine and forms SFCA-II.

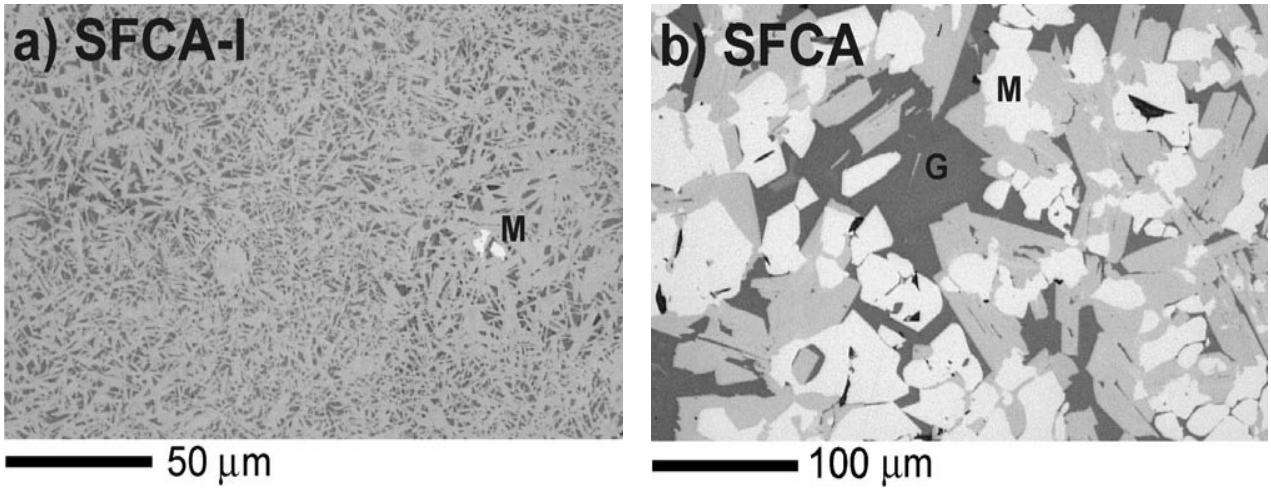


**Figure 3.** (*a*) and (*b*) Optical photomicrographs showing typical SFCA-I and SFCA textures in iron ore sinter. In both images, the bright phase is magnetite (M), SFCA-I and SFCA are light gray phases whilst the dark phase is glass (G) [18]

Dawson *et al.*[23] also examined the crystal size and the formation of SFCA. They found that the SFCA-II phase is the first to form during the sintering process, and its crystal size is smaller than 4 microns. When the temperature increases from 1200°C to 1300°C, the crystal grows and forms the SFCA-I phase with a size up to 10 microns. At 1300°C, acicular SFCA melts and precipitates as columnar SFCA characterized by a large crystal size (>10 µm).

Pownceby and Clout [24] used phase diagrams to locate the mineral compositions of SFCA phases as shown in Figure 4. The starting compositions were designed in order to lie within a plane that connects the end members $CF_3$ ($CaO{\cdot}3Fe_2O_3$), $CA_3$ ($CaO{\cdot}3Al_2O_3$), and $C_4S_3$ ($4CaO{\cdot}3SiO_2$) or within the $Fe_2O_3$ - $Al_2O_3$ - CaO plane. The shaded area in Figure 4a, represents most SFCA compositions encountered in industrial sintering [24]. Pownceby and Clout [24] reported that SFCA forms a series of solid solutions, SFCA, SFCA-I, and SFCA-II (Figure 4b).

In practice, different forms of SFCA can coexist and their relative proportions are dependent on the sintering conditions (for instance, oxygen potential) and physical properties (particle size, porosity) and chemical composition of the raw materials.

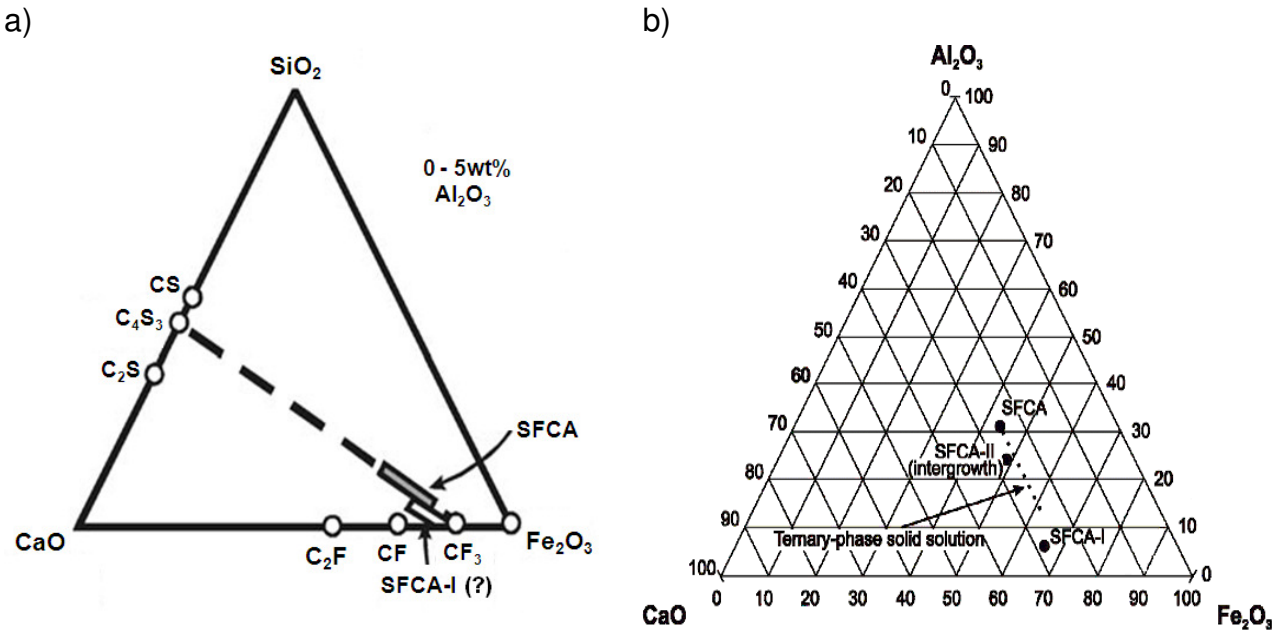


**Figure 4.** Schematic diagrams showing (*a*) the compositional relationship between SFCA and SFCA-I within the $Fe_2O_3$-$Al_2O_3$-CaO-$SiO_2$ pseudo quaternary system and (*b*) the compositional relationship between SFCA, SFCA-I and SFCA-II [24]

### III.2.1.1.2 Iron oxides

The second group of major constituents in the bonding phases are composed of iron oxides which precipitate from the melt [16]. Hematite is referred to as secondary hematite characterized by a polygonal skeletal structure, as opposed to the relict hematite which is the principal iron ore. Skeletal hematite is often polycrystalline with a granular structure and internal pores. Tertiary hematite is identified as oxidized magnetite. Secondary magnetite may form by the reduction of hematite under low oxygen partial pressure. The presence of $Mg^{2+}$ in the melt can lead to the formation of magnesio-spinels [16].

### III.2.1.1.3 Silicates

The silicate phases include the slag phase and calcium silicate. The slag phase can be formed by partial melting of fluxes, which is favoured by low basicity and higher sintering temperatures (>1300℃) [16]. The slag phase can precipitate from a silicate melt with higher viscosity and be present as extremely small capillary fillings between the other micro-constituents [16].

The most common crystalline silicate in fluxed sinters is larnite (β-$2CaO.SiO_2$) in which a substantial amount of calcium may be substituted by $Fe^{2+}$. Silicates can contain up to 40% of iron oxide and other impurities such as aluminium, magnesium, phosphorous and different alkalis [15,16]. The silicate crystals can also be favourable sites for crystallization of SFCA [15,16].

### III.2.1.2 Relict particles

Relict particles refer to principal ore which has been partially reacted or rearranged during the sintering process [15,16,]. Most of the relict particles are coarse ore (nuclei), but sometimes un-reacted fluxes such as lime are also present. Generally the large particles of iron ores react with the surrounding melt, but this assimilation reaction is not complete. One fraction of relict particles may maintain regular external forms of the original crystals, while other fractions may present subhedral and anhedral edges as consequences of recrystallization, sintering of pores, dehydration and oxidation [15,16]. Compared to the original ore, these changes can improve sinter quality such as reducibility [15,16].

The volume of the relict iron ores is strongly dependent on the size of the ore particles and the sintering conditions. During the sintering process fine particles react faster, resulting in complete reaction, while sintering reactions of coarse particles are slow and result in a high level of relict particles [3,4].

### III.2.1.3 Pores

The structure of sinter may also be considered to contain two constituents, mineral phases and pores. The presence of pores plays an important role in controlling the sinter quality such as the reducibility and the strength of sinter [25,26]. During the reduction of sinters, the pores provide the diffusion path for the reactant gases, resulting in an increase in surface area for the reaction to take place. Without pores, reaction can only occur through the exterior surface thereby leaving the core of the sinter unreacted and resulting in a low reduction rate [25,26].

### III.2.2 Quality of sinter

Sinters are not only characterised by their microstructures but also by their physical and metallurgical properties that are determined by standard methods (ISO) [27,28,29]. Generally, the quality of a sinter is defined by assessing the reducibility index, reduction disintegration index and cold strength index.

It has been established that the quality of sinter is dependent on the mineral phases formed during the sintering process. SFCA is reported to be the main bonding phase which strongly influences sinter quality. The presence of cracks and pores also influence the properties of sinter [16,25].

Cores *et al.* [30] studied the influence of different compositions of iron ore mixtures on the sinter quality. They found that the cold strength and the reducibility of the sinter are strongly dependent on the presence of calcium ferrites in the microstructure of the sinter. Cores *et al.* [30] also reported that the optimum structure for high sinter quality is formed with a hematite nucleus surrounded by SFCA-I. This can be attributed to the porous structure of acicular SFCA (SFCA-I) which can hinder the propagation of cracks and provide a large surface contact during reduction reactions [16,25,30].

#### III.2.2.1 Sinter strength

The cold strength is considered to be the prime factor in assessing overall sinter quality, and is measured by the Tumble Index (TI) and the Abrasion Index (AI) [16,25]. According to the ISO 3271 test [27], the cold strength of the sinter is determined by tumbling a portion of 15 kg into a circular drum for 200 revolutions at a speed of 25 rpm, followed by sieving to 6.30 mm. The percentage of +6.30 mm fraction is reported as the tumble index, while the abrasion index is expressed as the -0.5 mm fraction after the tumble test.

The tumble index (TI) as well as the abrasion index (AI) can be calculated as follows:

$$TI = [m_1/m_0]*100$$

$$AI = [\{m_0-(m_2+m_1)\}/m_0]*100$$

where

- $m_0$ = mass of the test portion before tumbling, in grams.
- $m_1$ = mass of the oversize fraction retained on the 6.30 mm sieve, in grams.
- $m_2$ = mass of -6.3 +0.5 mm fraction of the tumbled test portion, in grams.

Sinter should have sufficient strength to withstand, without significant breakage, the normal handling which occurs during transportation between the sinter plant and the blast furnace [16,25]. A good sinter is assumed to have a tumble index more than 70% and an abrasion index less than 5% [16,25].

It has been reported that the sinter strength is highly dependent on the ability of the individual phases of the sinter to resist cracking and crack propagation [16,31,32]. Although, the primary hematite has a higher fracture toughness than the secondary hematite, magnetite and SFCA, SFCA-I with a porous microstructure can prevent the propagation of cracks and therefore prevent further breakdown of sinter [16,31,32].

A study on the effects of mineral composition and microstructure on crack resistance of sintered ore reported that acicular SFCA is the major component that influences the resistance to crack propagation [32]. Cracks can be initiated in columnar SFCA, magnetite and silicate when the load is 245 mN, while crack initiation was not observed in acicular SFCA until the load was increased to 490 mN [32]. Zi-wei *et al.*[32] also stated that crack initiation in fine acicular SFCA started appearing when the load reached 1960 mN [32].

### III.2.2.2 Reducibility index

The reducibility index (RI) evaluates the reduction behaviour of various iron ore burden materials in the middle zone of the blast furnace. The test is done according to the ISO 4695 procedure where a test portion of -12.5 +10mm is reduced isothermally at 950℃ with a gas mixture of 40% CO and 60% $N_2$. The test portion is weighed at specified time intervals. The percentage loss of oxygen per minute therefore represents the value of the reducibility index [28]. For blast furnace users, the reducibility index above 1%/min is acceptable.

The reducibility of sinter is largely governed by the porosity and mineral composition of sinter cake [33]. Further studies on the effect of pores on sinter quality reported that the sinter reducibility is strongly influenced by the morphology of the SFCA. The porous structure of acicular SFCA provides a large reaction area available for solid-gas contact. The reducibility of the sinter will consequently be improved, compared to that of columnar SFCA [31,32,33].

High reducibility has also been attributed to a sinter with high concentrations of granular and relict hematite, and low magnetite content [36].

Hida *et al.* [37] reported that the reducibility of a sinter is directly related to the internal pore volume and the surface area of the ore. Dense ore and coarse particles will definitely affect the reducibility of the final sinter. The solid-gas reaction is limited to the exterior surface of dense particles, resulting in a lower degree of reducibility compared to porous ores where the reduction reaction is extended into the pores [37].

### III.2.2.3 Reduction disintegration Index

The reduction disintegration index (RDI) is defined as a quantitative measure of the disintegration or breakdown of the sinter during reduction in the upper part of the blast furnace. The primary cause of high disintegration of sinter is due to the crystalline transformation from hexagonal hematite to cubic magnetite accompanied by volume expansion and lattice distortion [16,31,38]. The volumetric change can generate stresses and cracks within the mineral phase, resulting in a disintegration of the sinter [16,31,38]. Husslage *et al.* [31] and Ghost *et al.* [38] also reported that a porous structure can absorb stresses and prevent the cracks from propagating.

Husslage *et al.* [31] also stated that the skeletal rhombohedral hematite is the major cause for high disintegration values. The presence of columnar SFCA, glassy silicate phase and coarse secondary hematite can also increase the disintegration of sinter [31]. The addition of MgO can also lead to the formation of magnesio-ferrite and decreases the hematite content, resulting in a decrease in the disintegration of the sinter material [31].

According to the ISO 4696-1 test, the reduction disintegration index is determined by performing a static reduction of a test portion of -12.5 +10mm at 500℃ in an atmosphere consisting of 20%$CO_2$, 20%CO, 2%$H_2$ and 58%$N_2$. After one hour of reduction, the test portion is cooled to a temperature below 100℃, and tumbled by using a small tumbler drum for 300 revolutions in total, followed by screening with test sieves of 6.30 mm, 3.15 mm and 500 µm [29].

The reduction disintegration index is expressed as percentage masses of material greater than 6.30 mm, less than 3.15 mm and less than 500 µm, and can be calculated from the following equations:

$$RDI_{+6.3} = [m_1/m_0]*100$$

$$RDI_{-3.15} = [\{m_0-(m_2+m_1)\}/m_0]*100$$

$$RDI_{-0.5} = [\{m_0-(m_3+m_2+m_1)\}/m_0]*100$$

where

- $m_0$ = mass of the test portion after reduction and before tumbling, in grams.
- $m_1$ = mass of the oversize fraction retained on the 6.30 mm sieve, in grams.
- $m_2$ = mass of the oversize fraction retained on the 3.15 mm sieve, in grams.
- $m_3$ = mass of the oversize fraction retained on the 500 µm sieve, in grams.

Acceptable levels in industry require that the fractions of +6.30 mm, -3.15 mm and -0.5 mm should respectively be above 70%, below 30% and less than 5%.

## III.3.Sintering reactions

### III.3.1 Introduction

During the sintering process, several chemical reactions between iron ores and fluxes are taking place at a specific maximum temperature, resulting in conversion of loose materials into a solid mass. These reactions are defined as sintering reactions

and involve the formation of the melting phase followed by the assimilation of large particles into the melt [39,40,41].

Studies by Malysheva and Mansurova [39] investigated the sequence of formation of phases during iron ore sintering. They found that the sintering reactions occurred in the flame front and consisted of reactions between a fraction of iron ore and the principal flux. This led to the formation of a liquid phase which formed the bonding phase. Malysheva and Mansurova [39] also found that the sintering reactions start within the layer of adhering fines where fine reactive ores and fluxes are in intimate contact. Solid - solid reactions are therefore the first reactions to occur, generating the primary melt. However, large particles are almost inactive during this first stage due to their large reaction area.

The sintering reactions were also studied by Loo *et al.* [40]. Their results showed that sintering reactions consist of melt formation and assimilation reactions (Figure 5). A relevant starting point was a pseudo-particle consisting of a large core particle (nucleus) and a coating layer of adhering fines and fluxes. Figure 5a represents the basic structure of pseudo-particles formed during the granulation. Loo *et al.* [40] reported that sintering reactions begin within the layer of adhering fines, where fine materials are in intimate contact. With the increase in temperature (at about 1100°C), calcium ferrites are the first product to form by solid-solid reactions between hematite and lime. At approximately 1200°C, calcium ferrites decompose and form the initial liquid melt, which can dissolve silica and alumina. This stage of the sintering process is schematically represented in Figure 5b. As the sintering process progresses, the liquid melt starts reacting with the nucleus particles, resulting in a dissolution of the nucleus particle and formation of more melt (Figure 5c). The assimilation reaction depends on the properties of both the initial melt and nucleus particle. The more reactive the melt, the greater its ability to dissolve the solid nucleus. Similarly, the greater the reactivity of the solid nucleus, the more the amount that will be assimilated [40].

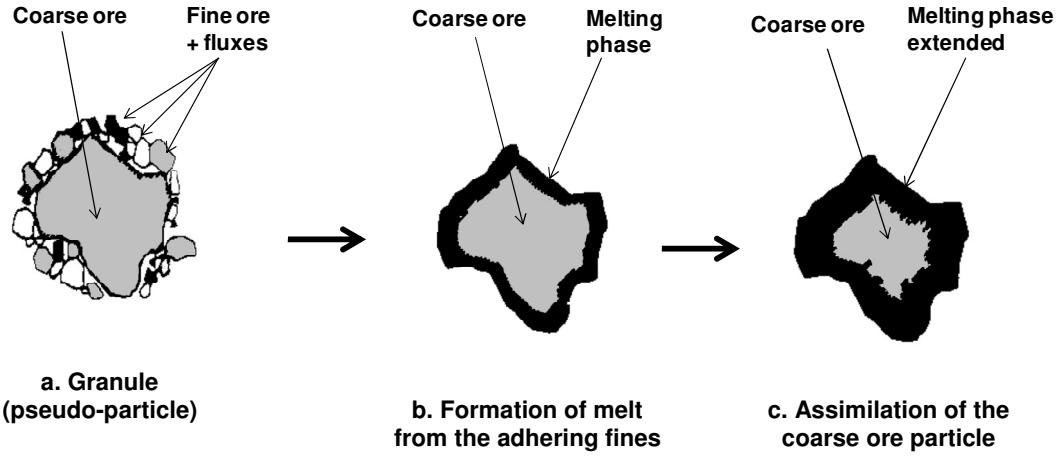


**Figure 5.** Schematic representation of the sintering of a pseudo-particle [40]

Chakraborti *et al.* [41] examined the effect of sintering temperature on textural microstructures of the sinter product. Their results showed that the change of sintering temperatures lead to the formation of two types of microstructures, homogeneous and heterogeneous. At low temperatures (< 1220℃), the assimilation is expected to be low and the sinter contains a significant amount of relict ore resulting in a heterogeneous texture. Sinters formed at high temperatures (above 1300℃) are characterised by a more homogeneous structure due to the high degree of superheat and melt mobility. The reaction rates are high, resulting in a low amount of relict particles. A schematic representation of these routes of formation is given in Figure 6.

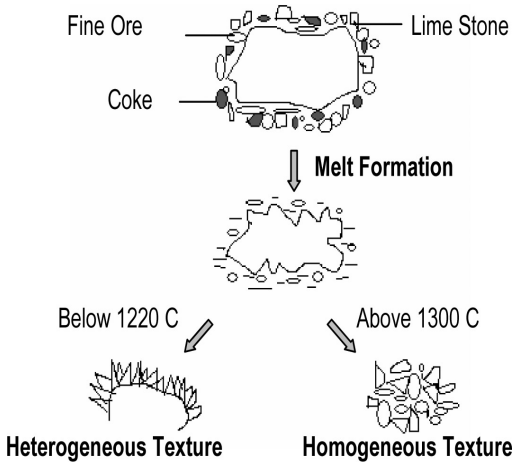


**Figure 6.** Formation of heterogeneous and homogeneous texture [41]

### III.3.2 Basic mechanisms of sintering reactions

Most experimental and theoretical studies related to the production of iron ore sinter stated that the sintering process is a thermal operation involving melting and assimilation reactions [2,16,39-43]. The initial melt is generated from adhering fines during heating via reaction between iron ores and fluxes. Thereafter, nucleus particles are partially assimilated or dissolved into the primary melt to form more melt. Before complete melting is achieved, the sintering temperature drops due to the short residence time at the maximum temperature and then the melt solidifies and mineral phases precipitate, resulting in the formation of the bonding phases.

#### III.3.2.1 Melt formation

The first stage of a two step sintering process is the formation of the melt which involves the reaction between fine iron ore particles and fluxes. In iron ore sintering, the main starting materials are lime, silica and iron ores. This system can be compared to the crystallization of ferrite and silicate phases within the ternary phase diagram of CaO-$SiO_2$-FeOx (x=1 or 1.5) [16]. The following phase diagrams were selected to understand the formation of the melt during sintering:

##### III.3.2.1.1 The binary CaO – $Fe_2O_3$ system

During the sintering process, the basic reaction is reported to be the solid-solid interaction between lime and hematite [16,24,42,43]. Study on sintering reactions reported that the reaction of hematite and lime started taking place at low temperatures (< 800℃) and produced dicalcium ferrites ($C_2F$). Increasing the temperature up to 1000℃, dicalcium ferrite reacted with hematite and formed monocalcium ferrite (CF). At a temperature of 1205℃, the liquid phase started forming [16,24,40-43]. This temperature corresponds to the eutectic transformation of dicalcium ferrite and monocalcium ferrite into melt, as shown in Figure 7 [16,24,42,43].

Further investigation examined the solid state interactions in the CaO-$Fe_2O_3$ system (Figure 7), using X-ray diffraction at 900℃-1200℃ and for a duration of 360 min [43]. The conditions of complete interaction between lime and hematite were assumed to

be achieved [43]. The results showed that a mixture of both $CaFe_2O_4$ and $Ca_2Fe_2O_5$ in different concentrations was formed.

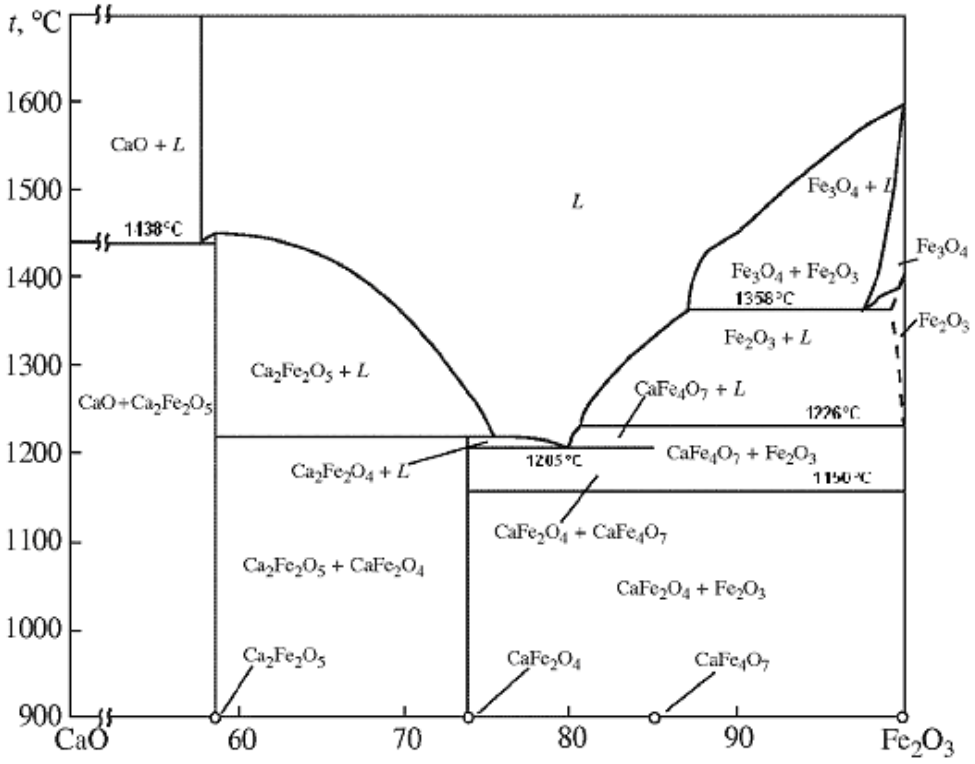


**Figure 7.** Binary phase diagram $CaO\text{-}Fe_2O_3$ in air [16,42,43]

### III.3.2.1.2 The CaO - $SiO_2$ - $Fe_2O_3$ system

Studies conducted by Levin *et al.* [44] examined the effect that silica has on the ternary system $CaO\text{-}SiO_2\text{-}Fe_2O_3$. The results showed that the presence of silica can modify the chemical compositions as well as the properties of the melt. In Figure 8, two regions α and β with a melting point below 1300 °C represent the compositions of the melt that formed during the sintering process. The melt of composition β can form more calcium ferrites from the reaction between CaO and a high amount of iron ores ($Fe_2O_3$). This reaction is known to be faster than the reaction of lime (CaO) with silica ($SiO_2$) or alumina ($Al_2O_3$) at low temperatures. Further investigations also revealed that the diffusion of $Ca^{2+}$ is faster than that of $Si^{4+}$ in the calcium ferrites at low temperatures (~900 °C) [16,44]. During the sintering process, the sinter mix is constituted in such a way as to promote the reaction between CaO and $Fe_2O_3$, which

is more likely to occur at low temperatures, and may form more calcium ferrite as bonding phase [16,44].

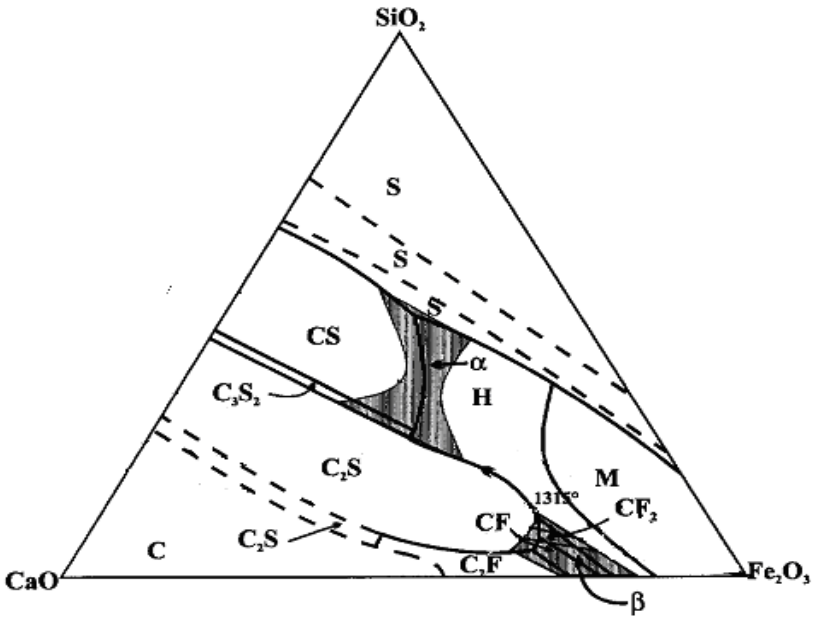


**Figure 8.** Ternary phase diagram CaO-$SiO_2$-$Fe_2O_3$ in air, with melt regions α and β below 1300 C, based on %wt [44]

Levin *et al.* [44] stated that the melt with composition α may form when more silica is added to the sinter mix, which basically consists of $Fe_2O_3$ and CaO. The reaction between hematite and quartz is very limited, and the rate of formation of calcium silicates is relatively slow. The development of such a melt is therefore less probable at low temperatures and can only be observed in the vicinity of quartz grains [16,44].

### III.3.2.1.3 The CaO-$Fe_2O_3$-$SiO_2$-$Al_2O_3$ system

The forth component, alumina ($Al_2O_3$), is very important in the stabilization and formation of SFCA [16,45]. The effect of alumina can be explained from Figures 9a and 9b. The region β is extended by the formation of a new domain γ, which contains the τ field (Figure 9a) [16,45,46,]. It can also be seen that the solid solution phase $C(A,F)_3$ can crystallize out of the τ field (Figure 9b). Its composition may vary along the hatched line [16,46,]. Lister and Glasser [46] reported that the entire primary phase field of $C(A,F)_3$ may have an incongruent melting point in air and is stable only in contact with liquid phases containing some $SiO_2$.

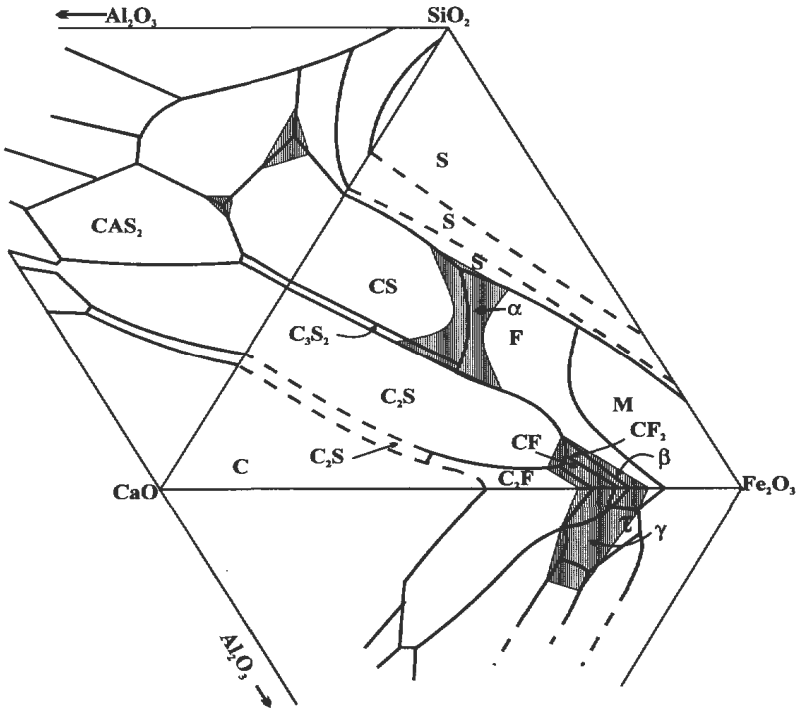


**Figure 9a.** The combination of three ternary phase diagrams with the melt regions below 1300 ℃ (indicated in gray) [16]

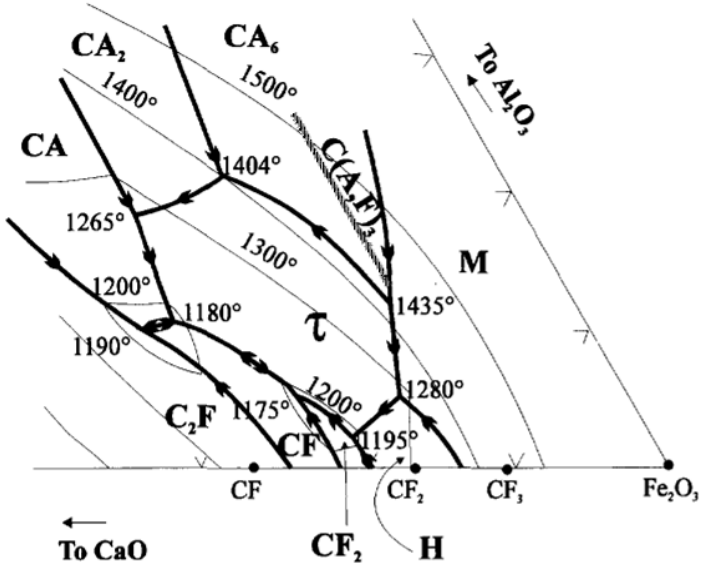


**Figure 9b.** Ternary phase diagram of $CaO$-$Al_2O_3$-$Fe_2O_3$ in air [46]

### III.3.2.1.4. The $CaO$-$Fe_2O_3$-$SiO_2$-$FeO$ system

In industrial sintering, the presence of $Fe^{2+}$ is inevitable in small amounts as magnetite also forms. Due to the presence of $Fe^{2+}$, the melt regions α and β are combined into one and extended to melt region δ, as shown in Figure 10. The formation of calcium ferrites is therefore hindered to the detriment of the formation of

calcium silicates as bonding phases, and the final product can be composed of calcium silicates and iron oxides [16,47]. Magnetite can be the major iron oxide in the sinter material if reducing conditions are maintained during cooling [16,47].

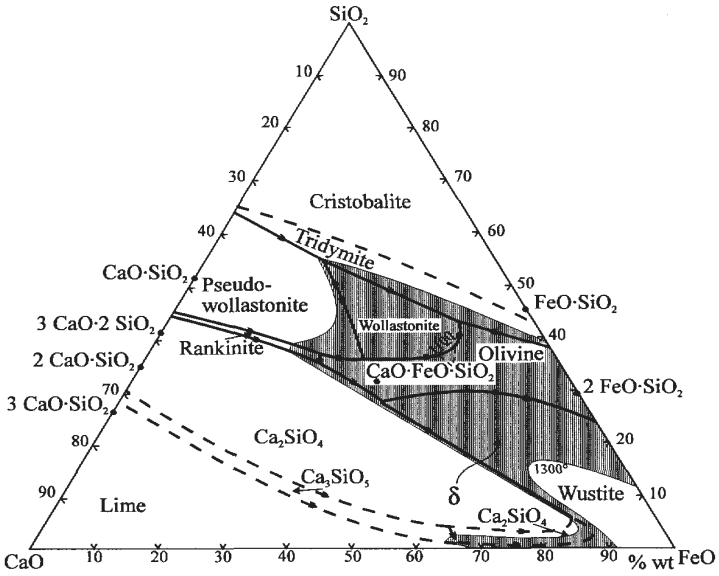


**Figure 10.** Phase diagram CaO - FeO - $SiO_2$ at $pO_2 = 10^{-2}$ atm with melt region δ below 1300 °C [47]

### III.3.2.2 Assimilation of coarse particles

The assimilation of coarse particles is defined as the second step during sintering reactions, and involves reactions between the primary melt phase and coarse particles [40,48]. For particles with high porosity, the primary melt readily penetrates into the ores through open pores, resulting in a high assimilation rate, while the assimilation behaviour of dense coarse ore is reported to be low due to low penetration of melt into the ore [25,26,40,48].

Loo and Matthews [48] determined the parameters that generally control the assimilation reaction during the sintering process. They stated that the assimilation of large particles into the primary melt can be compared to the usual dissolution of a solid by a liquid. A conceptual model was therefore used to describe the assimilation of solid particles into a liquid phase. The breaking down of the solid lattice structure by the dissolution reaction followed by the diffusion of the species to and away from the interface as the material is transferred into the bulk of the melt, is schematically shown in Figure 11.

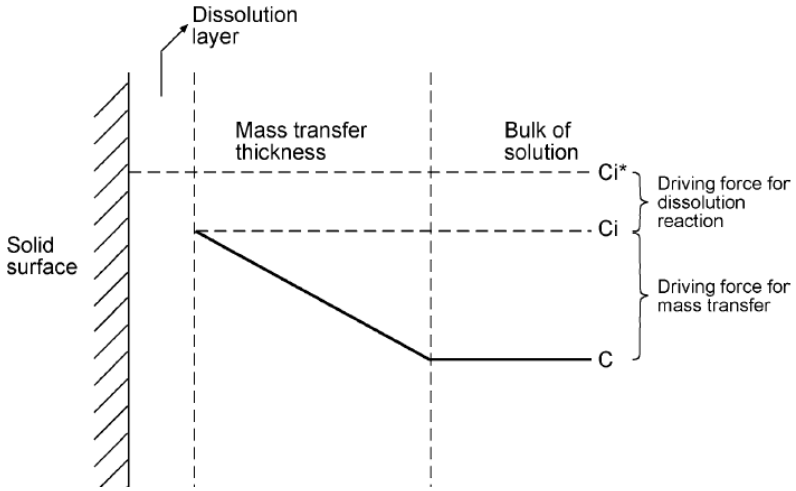


**$C_i$*; Saturation concentration of solid at the temperature of the solid surface**

**$C_i$ : Concentration of solid at mass transfer thickness/dissolution layer interface**

**C : Concentration of solid in bulk solution**

**Figure 11.** Conceptual model for dissolution of solid particles [48]

The rate at which the solid particle is transferred into the liquid phase can be described as a function of a driving force (concentration difference) and a surface area. According to Perry's chemical reaction considerations [49], the rate of the dissolution of the solid particle into the melt can be expressed by the following equation:

$$\frac{dm}{dt} = K \cdot A_r \cdot \Delta c^n$$

Where:

- ***m*** represents the mass of solid assimilated,
- ***t*** is reaction time,
- ***K*** is proportionality constant,
- $A_r$ is the area normal to the direction of mass transfer,
- $\Delta c$ is the concentration driving force or concentration difference,
- ***n*** is a constant.

The nature and value of constant, K, are dependent on the mechanisms that control the dissolution of solid particles [40,48]. If mass transfer is the rate-determining step, K is the mass-transfer coefficient, and the temperature will affect the viscosity of the liquid phase and diffusion rates. If the process is controlled by the dissolution

reaction, the value K is the reaction rate constant, and depends on the temperature according to the Arrhenius equation [40,48].

The constant n is also dependent on the type of mechanisms that control the assimilation process. If mass transfer is important, the value of n is 1, while n is greater than 1 if the dissolution reaction is the rate-determining step [40,48].

Studies conducted by Loo and Matthews [48], reported that the assimilation rate is rapidly increased when nuclear particles are very porous, because of their high reaction surface area. The adhering fines can be embedding in the crevices of the rough surface of the ore where the melt can react quickly with the nuclear particles [48]. However the assimilation of dense nuclear ore particles is low because it is only dependent on their outside surface [48]. Figure 12 illustrates the variation of the amount of relict fraction in final sinter with the ratio of adhering fines to coarse particles for two hematite ores with different porosities (ore 2 is more porous than ore 1). The amount of relict ore decreased with an increase in the ratio of adhering fines to coarse ore. For a high fine/coarse ore ratio, the volume of melt increased, resulting in an increase in the ability of the melt to react with more coarse ore. This implies that the volume of dissolved particles (concentration difference) will increase and the percentage of relict particles will be reduced. Loo and Matthews [48] also stated that the increase in the concentration of fine fraction corresponds to the increase in the area normal to the direction of mass transfer ($A_r$) if insufficient melt is formed to cover the surface of the solid particles [48]. From Figure 12, it can be seen that the fraction of relict particles in the sinter material is lower when particles are porous than when particles are dense, for the same ratio of adhering fines to coarse particles. Hematite ore with a high porosity is therefore more reactive due to the likely penetration of melt through the pores.

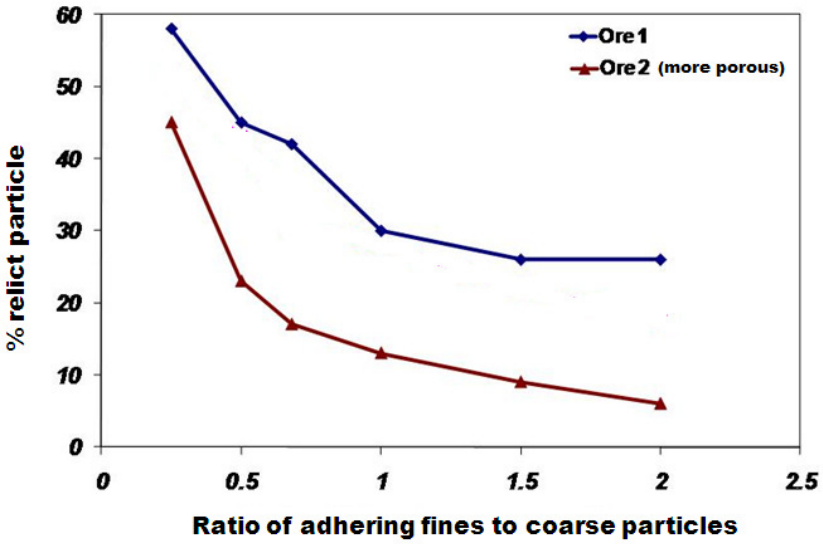


**Figure 12.** Variation of amount of relict ore vs fine: coarse particle ratio [48]

Loo and Matthews [48] investigated the effect of sintering temperature on the assimilation reaction. The same two hematite ores were sintered under similar conditions. The results showed that the fraction of relict ore in all sinters decreased when the maximum temperature changed from 1250℃ to 1350℃. This means that the assimilation for each ore increased with increasing temperature, as shown in Figure 13. Loo and Matthews [48] also reported that the variation of the sintering temperature can alter the degree of superheat which in turn, may affect the variation of the viscosity and the fluidity of the melt.

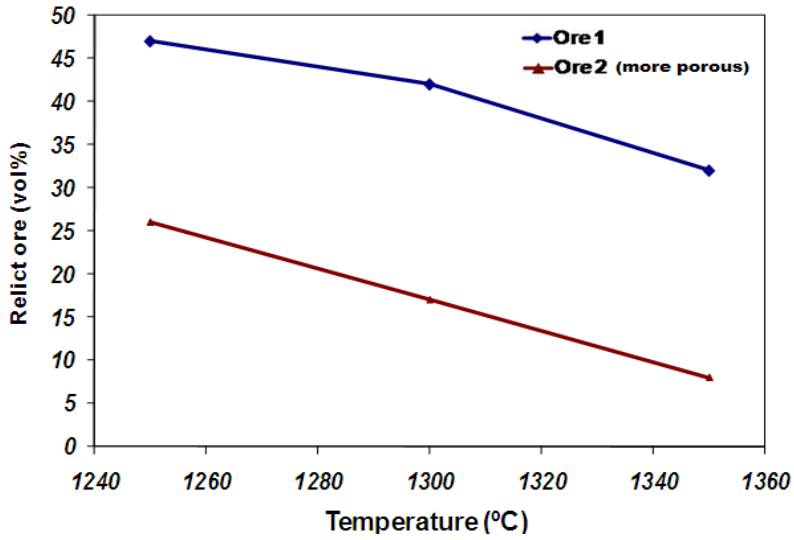


**Figure 13.** Variation of relict ore percent vs sintering temperature [48]

### III.3.3 Reaction sequences during iron ore sintering

During the sintering process, reactions of iron ores and fluxes convert the loose raw materials into a porous but physically strong sinter cake. The starting raw materials consist of the fine ores (generally the - 1mm fraction), lime and coke breeze, and are heated to temperatures of around 1220 ℃ to 1300 ℃**.** The formed sinter is then composed of iron oxides, SFCA and silicate phases.

Most studies reported that the reactions that are taking place during iron ore sintering can occur simultaneously or in successive steps, and mainly consist of solid-solid and liquid-solid reactions [2,24,50,51].

Studies conducted by Pownceby *et al.* [24] described the sequences of sintering reactions using in-situ X-ray diffraction. The starting mixture was composed of analytical reagents of hematite, calcite, gibbsite and quartz. They observed that the dicalcium ferrite ($C_2F$) was the first product formed at low temperatures (~750 ℃ to 780℃). With an increase in sintering temperature, the dicalcium ferrites started to react with hematite and formed the calcium ferrite (CF). At ~ 1050℃, quartz started reacting and formed SFCA-I and SFCA. From 1220 ℃ to 1240 ℃, SFCA-I broke down, and formed SFCA.

In-situ X-ray diffraction was also used by Scarlett *et al.*[2] in order to examine different sintering reactions that are taking place during the sintering process. This technique enables the identification of microstructural changes in real time compared to “ex-situ or post-mortem” techniques. Experimental sintering was conducted at low temperatures (22 ℃ to 1260 ℃), using a mixture of calcite ($CaCO_3$), hematite ($Fe_2O_3$), quartz ($SiO_2$) and gibbsite ($Al(OH)_3$). The heating rate was lower than in the industrial sintering process in order to ensure accuracy in the identification of phase changes and the quantification of phases. The variation of the amount of different phases with sintering temperature is given in Figure 14.

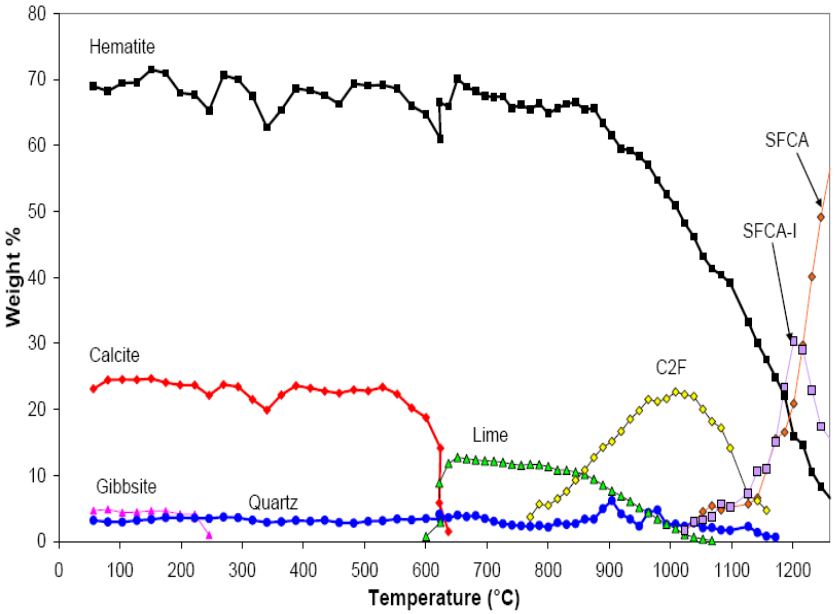


**Figure 14.** Quantitative phase analysis of iron ore sinter phases using in-situ XRD [2]

Based on the results described in Figure 14, the reaction sequences involved in the formation of SFCA phases can be summarized as follows [2,52]:

- From ~ 200 ℃, Gibbsite starts to decompose.
  $Al(OH)_2 = Al_2O_3(amorphous) + 3H_2O$
- From ~ 550 ℃, Calcite decomposes into lime and carbon dioxide.
  $CaCO_3 = CaO + CO_2$
- From ~ 750 ℃, hematite starts to react with CaO forming dicalcium ferrite ($C_2F$)
  $Fe_2O_3 + 2\ CaO = 2CaO.Fe_2O_3$
- From ~ 950 ℃, more hematite react with CaO forming calcium ferrite (CF)
  $Fe_2O_3 + CaO. = CaO.Fe_2O_3$
- Above ~ 1050 ℃, the two main types of SFCA start to form simultaneously.
  $CaO.Fe_2O_3 + Fe_2O_3 + CaO + Al_2O_3 + SiO_2 = SFCA + SFCA\text{-}I$
- From ~ 1200 ℃, SFCA-I is consumed and SFCA is produced.
  $SFCA\text{-}I + Fe_2O_3 + CaO + Al_2O_3 + SiO_2 = SFCA$

The heat/quench techniques [50] have been used to investigate the reactions involved during the formation of SFCA. A mixture of $Fe_2O_3$, CaO, $SiO_2$ and $Al_2O_3$ was prepared and heated between 900℃ and 1400℃ in air and quenched rapidly. The experimental results showed that reactions occur in the solid-state up to 1200℃.

Calcium ferrites formed between 900℃ and 1000℃. At temperatures lower than 1150℃, $SiO_2$ started to react with CaO but this reaction is very slow. At temperatures up to 1200℃, calcium ferrites melt and reacted with quartz to form SFCA-I. A further increase in temperature allows more quartz and alumina to dissolve into the melt resulting in the formation of columnar SFCA.

Similar observations were reported by the studies conducted by Hida *et al.* [51]. A scanning electron microscope was used to analyze the microstructural changes that occur into a sample composed of iron ore particles and CaO powder when heated at 300℃/min and under a stream of oxygen at a constant rate of 10 ml/min. The results showed that hematite and lime react at low temperatures (<1200℃) via solid reactions forming calcium ferrites ($C_2F$ and CF). Above 1200℃, the calcium ferrites melt and start to cover the ore particle surface. The assimilation reaction between hematite and the melt quickly forms the acicular SFCA-I. At high temperatures, more silica and alumina are assimilated into the melt and the columnar SFCA forms.

### III.3.4 Parameters controlling sintering reactions

Sintering reactions are identified as a combination of the formation of the primary melt within the adhering fines and the assimilation of nuclear particles. Generally, these two reactions produce SFCA and are taking place in a complex system composed of $Fe_2O_3$, CaO, $SiO_2$ and $Al_2O_3$. Thermodynamic and kinetics studies also showed that sintering reactions are dependent on parameters such as the time-temperature profile in the sinter bed, sintering atmosphere, particle size distribution and chemical composition of the raw materials [40,48]. The variation of each parameter may bring dramatic change in the mineralogical composition of sinters and may have a negative impact on their mechanical and physical properties [40,48].

#### III.3.4.1 Particle size of iron ores

The formation of sinter phases depends on the grain size distribution, which determines the permeability of the sinter bed and the packing density of the compacted powders. Particle size distribution has therefore been considered as a key parameter in agglomeration (iron ores) and the industry of ceramics.

Most studies on the packing of solid particles in the sintering process showed that the incorporation of coarse particles increases either the permeability of the sinter bed or the packing density of compacted powders [39,40,48,53-56].

### III.3.4.1.1 Particle density of a powder mixture

German [7] as well as Cumberland and Crawford [53] extensively studied the effect of particle size distribution on the packing density. Prior to sintering, a mixture of loose particles needs to be shaped. The compaction process involves particle arrangement, deformation and possibly fractures, and can produce a pellet with specific packing density [54]. High compaction pressure can move the particles closer together, resulting in a high number of contacts between particles, and high packing density and a high sintering rate can be achieved. Compacted powders (granules) can have high sintering rates and produce higher sintered densities than those obtained from loose powders [7]. The maximum packing density occurs at the point where small particles fill all the voids between the coarse particles [7].

Rahaman [8] also examined the variation of packing density of bimodal mixtures of spheres. He reported that the packing density of an arrangement of large spheres can be increased by filling the interstitial holes with small spheres. Similarly, the density of an aggregate of fine spheres can be increased by replacing some of them by large spheres. Rahaman [8] reported that the packing density for the two types of particle packing is dependent on the ratio of the sphere diameters and the fraction of the large or small spheres in the mixture [8]. Maximum packing densities for mixtures of large spheres with different fine spheres are shown in Figure 15. It can be seen that the replacement of fine particles by large particles leads to an increase in the packing density up to a maximum, after which it decreases for higher fractions of coarse particles. It can also be seen that the packing density is decreased with a decrease in the size ratio of large particles to fine particles (Figure 15). A mixture of coarse particles (3.15mm) and very fine particles (0.191mm) was the lowest ratio (0.191mm/3.15mm) of fine to coarse particles that was examined and had the highest packing density (~80%).

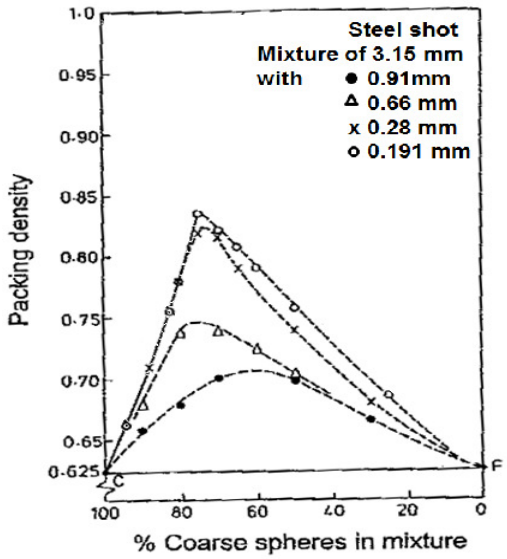


**Figure 15.** Binary packing of spheres showing the packing density as a function of the composition of the mixture and ratio of large sphere diameter to small sphere diameter [8]

Rui-Ping Zou *et al.* [54] studied the packing density of binary mixtures of spheres with the addition of water. The presence of water generates liquid bridges between particles, resulting in formation of agglomerates. Two types of agglomerates can be identified: agglomerates formed by only fine particles and those that are formed by both fine and coarse particles. Their results indicated that there is a similarity between dry and wet packing. Furthermore, the packing density decreases with the increase in moisture content, for binary mixtures of spheres (Figure 16).

For complex structures of agglomerates, Rui-Ping Zou et al. [54] stated that the formation of agglomerates requires more fundamental studies to quantify the effects of porosity, particle size ratio and moisture on particle packing.

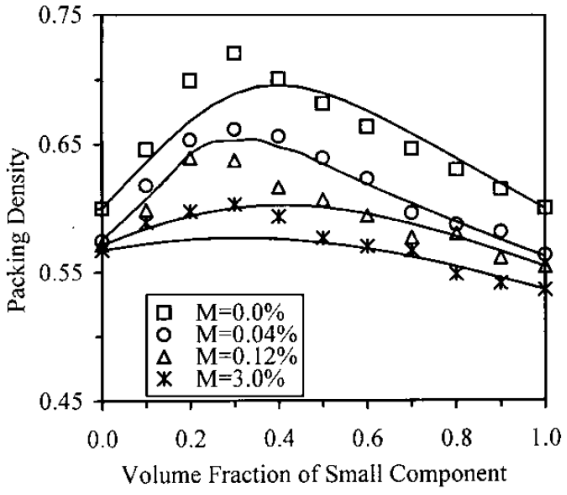


**Figure 16.** Packing of binary mixtures of spheres with moisture content (M) [54] (ratio of fine particle diameter to coarse particle diameter: 1mm/4mm)

### III.3.4.1.2 Permeability of the sinter bed

The particle size distribution of iron ores is a determining parameter that controls the size of granules or pseudo-particles, which determines the permeability of the sinter bed as well as the sinter productivity. Increasing the permeability of the sinter bed can improve the airflow rate and the flame front speed through the sinter bed, resulting in an increase in sintering rate and sinter productivity [6,7,36].

Debricant *et al.*[6] studied the effect of coarse particles on permeability of the sinter bed and fluidity of the melt. A sinter bed consisting of only fine particles has a low permeability, and the high volume of melt during sintering cannot easily flow through the sinter bed. This can retard the progress of the sintering process, resulting in a low productivity of the sinter pot. Debricant *et al.*[6] also reported that the presence of coarse ore leads to an improvement in the permeability of the sinter bed, which results in an increase in the large-scale movements between the melt and solid particles.

Studies by Kamijo *et al.*[7] examined the impact that the incorporation of dense coarse particles has on the permeability of the sinter bed. Their results showed that the presence of coarse particles improves the permeability of the sinter bed and forms low-density areas around the particles. The gas flow rate and the flame front speed therefore increase compared to other parts of the sinter bed, resulting in high sintering rates around the coarse particles.

Umadevi *et al.* [36] also studied the effect of iron ore mean particle size on the permeability of the sinter bed, which in turn, influences sinter microstructure and productivity. They stated that larger particles favour diffusion bonding, and smaller particles favour slag bonding in the sintering process. A high fraction of small particles forms excessive amounts of melt, resulting in a deterioration of the sinter quality, while the sinter from large amounts of coarse particles consists of more relict particles, and results in a decrease in the sinter strength. Umadevi *et al.* [36] found that the increase in iron ore mean particle size increased the sinter productivity. Sinters made with coarser and finer iron ore mean particles consisted of higher concentrations of relict hematite and lower concentrations of magnetite compared to

the sinters prepared from intermediate mean particle size. This is presumably due to respectively an increase and decrease in the sinter permeability (speed of flame front) with coarser and finer iron ore mean particle size.

### III.3.4.3 Holding time

The holding time also plays an important role in the formation of SFCA during the sintering process. A study by Loo and Matthews [48] examined the influence of holding time on the ore assimilation ability. Sintering tests were carried out using the standard adhering fines and two types of iron ores (ore 1 and ore 2) as nuclear particles. The maximum temperature was kept constant at 1300℃ while the time was varied between 2 min, 5 min and 10 min. The results showed that more iron ore was dissolved into the melt with an increase in holding time for all sinters (Figure 17). The fraction of relict iron ore subsequently decreased. It can also be seen that the assimilation of ore 2 (with high porosity) is high from 2min to 5min, and does not change with a further increase in holding time. The saturation concentration of the melt is quickly attained due to their high reactivity. The melt can therefore dissolve only small concentrations of solid particles [48].

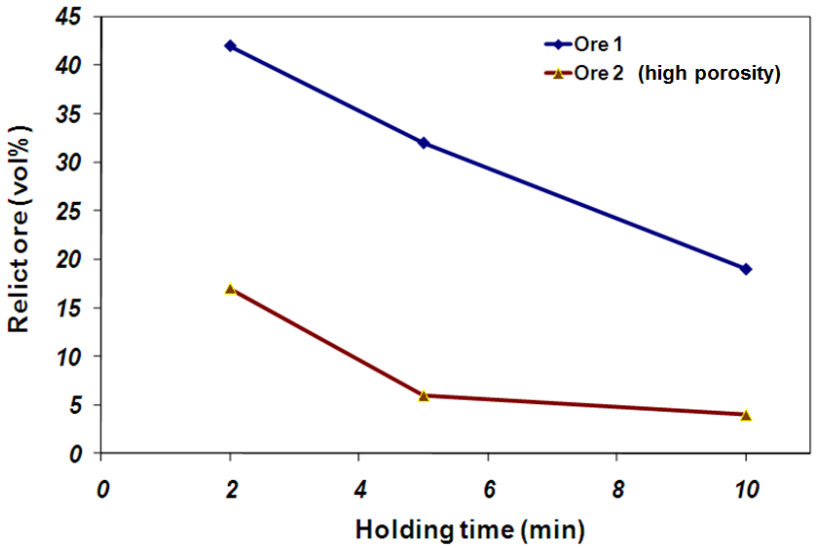


**Figure 17.** Variation of relict ore content vs holding time [48]

Scarlett *et al.* [18] studied the effect of holding time on the stability of phases formed during the sintering process. Starting materials consisting of 82.36% $Fe_2O_3$, 14.08% CaO and 3.56% $SiO_2$ were used in order to produce SFCA phases, and the variation of sinter phases was obtained using an in-situ powder XRD system. Each sinter mix was sedimented directly onto the Pt strip heater and heated under partial vacuum at a rate of 10℃/min to 600℃. The heating rate was then decreased to 5℃/min. The maximum temperature was increased up to 1215℃, and the sinter was held at this maximum temperature for 40 min to examine the variation of sinter phase fraction with holding time. The sinter produced at 1215℃ consisted of approximately 12% SFCA, 28% SFCA-I and 28% hematite (Figure 18). An increase in the residence time led to a decrease in abundance of SFCA-I and hematite contents, and an increase in the concentrations in SFCA. After the total decomposition of SFCA-I, the variation of SFCA continued as a function of time. The final product consisted of a higher amount of SFCA (~ 30 wt%) than that which had formed at 0 min holding time.

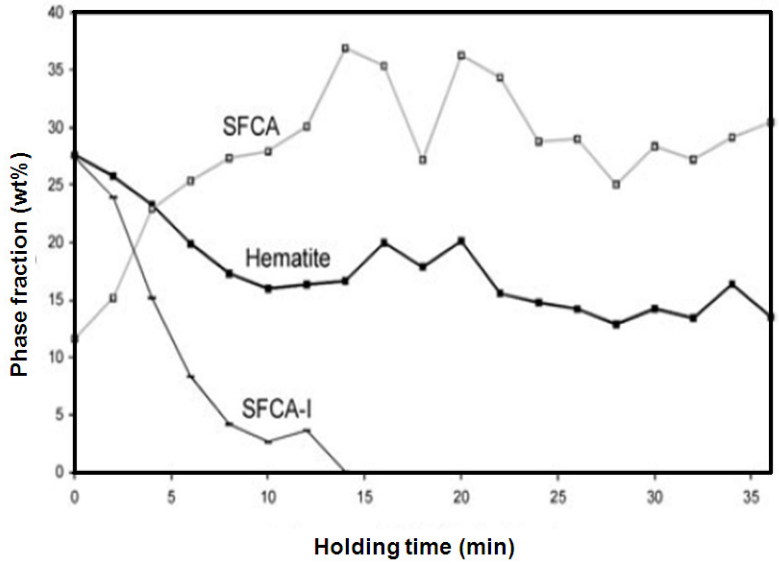


**Figure 18.** Variation of hematite, SFCA and SFCA-I vs holding time [18]

### III.3.4.4 Chemical composition of iron ore

The behaviour of sinter mixtures during the sintering process depends on their chemical compositions. Several studies have been conducted in order to investigate the effect of the chemical compositions of the sinter mix on melt formation and the assimilation reactions. Small changes in chemical composition of iron ores may induce significant modifications in phase formation during sintering [40,48].

Studies relating to melt formation found that melt formation is the first stage of sintering reactions and depends on the chemical composition of the iron ores [40,48]. It has also been established that hematite ores are more reactive than magnetite, and more readily participate in sintering reactions to form SFCA. Magnetite cannot form SFCA. For this reason, magnetite must be oxidized into hematite before sintering, resulting in a partial transformation of the $Fe_3O_4$-CaO-$SiO_2$-$Al_2O_3$ system into the $Fe_2O_3$-CaO-$SiO_2$-$Al_2O_3$ system [55,56].

It has been established that the percentage of iron in the ore may influence the microstructure of the SFCA that forms during the sintering process [24]. Low iron grade ores (< 62 % Fe) preferentially form SFCA as the bonding phase while medium grade ores (62-65% Fe) form a mixture of SFCA and SFCA-I. High grade iron ores of 65-68% Fe largely produce SFCA-I.

Loo and Matthews [48], found that the variation of the chemical compositions of iron ores showed noticeable effects on the assimilation of large ore particles (ore 1 and ore 2 where ore 2 is more porous) into the melt. Three types of adhering fines were considered: the first one was referred to as standard adhering fines, the second had a low $Fe_2O_3$ content and the third a high $Fe_2O_3$ content, compared to the standard adhering fines. The basicity was kept at 2. The results reported that the degree of assimilation of investigated hematite ores (low relict hematite) is more significant for adhering fines with low hematite than with high hematite content. This was attributed to the degree of saturation of the melt which is dependent on the amount of dissolved hematite. Loo and Matthews [48] also reported that an increase in solid particles in the melt results in an increase in the viscosity of the melt. The fluidity of the melt is therefore reduced, resulting in a decrease in the assimilation rate. It can also be seen that the fraction of relict ore in the final product increases with the increase in concentration of $Fe_2O_3$ content in the adhering fines (Figure 19).

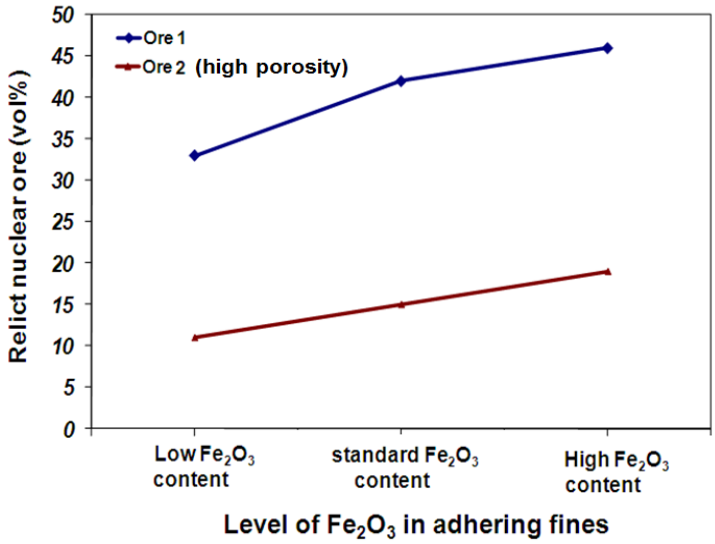


**Figure 19.** Variation of relict ore content vs $Fe_2O_3$ content in adhering fines [48]

### III.3.4.5 Sintering atmosphere

The atmosphere around the sample is another parameter that influences the sintering process. In practice, the sinter mix is heated in a reducing atmosphere and then cooled under an oxidizing atmosphere. Studies by Hsieh and Whiteman [57] examined phase formation during the sintering process under different oxygen partial pressures. The results showed that acicular calcium ferrites can form easily at low temperature (<1180℃) even under reducing conditions. At high temperatures (>1300℃), acicular SFCA can start to transform into magnetite and silicate melt. If reducing conditions are maintained on cooling, magnetite and calcium silicates can be the major constituents of the final sinter. During cooling, magnetite can react with the silicate melt under oxidizing conditions and form SFCA.

The effect of oxygen partial pressure on phase formation was also investigated using the equilibrium phase relations in the Fe-rich portion of the system $Fe_2O_3$-CaO-$SiO_2$ (FCS) at 1240℃-1300℃ [24,58,59]. The experimental tests were performed in air and at low oxygen partial pressure ($pO_2$ of $5x10^{-3}$ atm). The $Fe_2O_3$-CaO-$SiO_2$ pseudo-ternary systems at $pO_2$ of $5x10^{-3}$ atm and in air at temperatures of 1240℃ and 1255℃ are shown in Figure 20. It can be seen that the liquid phase field segregates in two melt regions for an oxygen partial pressure of 0.21 atm (Figures 20a and 20b). The $L_\alpha$ liquid phase field is associated with high $Fe_2O_3$ hematite contents and a

basicity of 2, and can preferentially lead to predominant crystallization of calcium ferrites during cooling. The second melt field has a high $SiO_2$ content and low basicity (B<1.8), and will precipitate calcium silicates and hematite on cooling.

At low oxygen partial pressure of $5x10^{-3}$ atm (Figures 20c and 20d), the two melt regions expand and form one liquid phase field. The phase fields of magnetite + liquid and calcium silicates + liquid are enlarged over a larger region compared to the phase field consisting of calcium ferrites with a liquid [58]. It is clear that the reducing conditions (low oxygen partial pressure) are not favourable for the crystallization of calcium ferrites as a bonding phase in low Al-sinter.

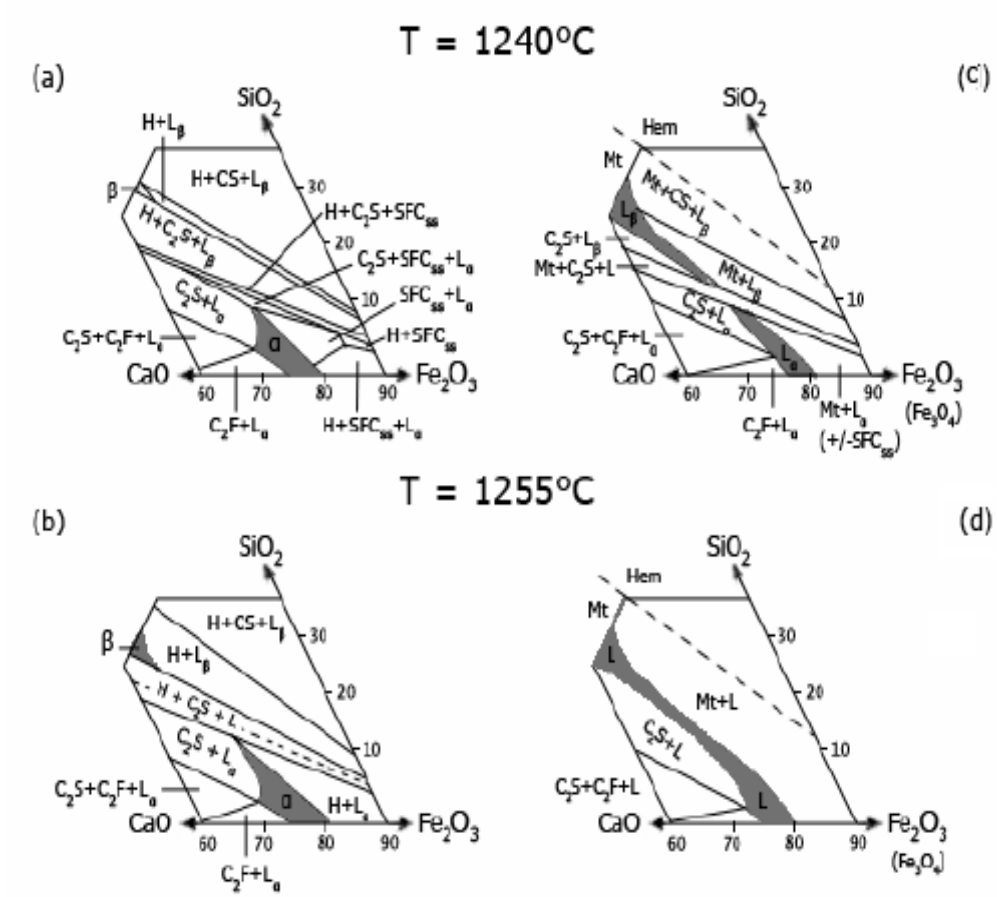


**Figure 20.** Summary of phase relations determined for the $Fe_2O_3$-CaO-$SiO_2$ ternary system at 1240°C-1255°C. (Figure 20(a-b) from experiments conducted in air, while Figure 20(c-d) from experiments conducted at $pO_2$ of $5x10^{-3}$ atm) [58]

## III.4 Conclusion

During sintering, the replacement of fine iron ore by coarse ore may affect reactions that take place between iron ores and fluxes. Sintering reactions occur in the combustion zone, and include the formation of melt followed by the assimilation of coarse ore into the melting phase, and the crystallization of sinter phases (hematite, magnetite, SFCA, calcium silicates and glassy phase) from the melt during cooling. Studies on compacted pellets and sinter pot samples reported that the formation of sinter phases and the variation in sinter mineralogy mainly depend on parameters such as particle size and chemical composition of the raw materials, maximum temperature, holding time, oxygen partial pressure, heating rate, basicity and cooling rate.
In this study, the relationship between the coarse ore/fine iron ore ratio, the variation in mineralogy of the sinter and the sinter quality were examined.

Studies of sintering reactions reported that melt formation and assimilation of the iron are strongly dependent on reaction surface area. Fine ores provide large reaction areas and react faster to form more melt. Coarse ores remain inactive during the early stage of sintering, due to their low reaction area. Furthermore, the assimilation reaction is limited only to the out layer of coarse ore if it is dense. The final sinter will consist of high relict ore fractions. For porous coarse particles, the melt easily penetrates into pores, and the assimilation ability is high due to the large intra-particle reaction area, whereby the concentration of relict ore will decrease.

Further investigations into sintering reactions reported that the assimilation ability of coarse ore depends on the sintering temperature, holding time and properties of the melt. Experimental results showed that the assimilation reaction is controlled by the transport of species from the solid-liquid interface to the bulk of the liquid. The increase in sintering temperature and time improves the ability of the melt to dissolve more coarse particles, except when the melt is saturated with the solid particles. During sintering, small nuclear particles react faster and can form a melt with high viscosity, resulting in a reduction of the large-scale movements of melt. However, the presence of large particles with low assimilation rate allows the melt to remain fairly mobile, and can improve the large-scale movements of the melt and solid particles.

The properties of melts that form in the flame front during sintering were also reported to be determinant of the sinter bonding phases. In the $CaO$-$SiO_2$-$Fe_2O_3$ pseudo-ternary system, the variation of basicity of the melt generates two liquid phase fields. A melt of low basicity is associated with the melt region where the crystallization of calcium silicates is more probable. At high viscosity, the melt composition falls into the second melt region where calcium ferrites are likely to be formed as bonding phase. Studies on melt formation demonstrated that more SFCA forms during sintering at low temperatures (1220 ℃ -1300℃) and in the basicity range 1.8 - 2.0.

As the sintering reactions take place under both reducing and oxidizing conditions, studies confirmed the strong effect of changing oxygen partial pressure on sintering reactions and crystallization sequences during sintering. If the $CaO$-$SiO_2$-$Fe_2O_3$ pseudo-ternary system is considered, sintering atmospheres and the basicity determine the bonding phases which form during crystallization. In air, the liquid phase field is composed of two regions with different basicities. The region with high basicity leads to crystallization of calcium ferrites as the bonding phase. In the second region (of low basicity), calcium silicates will form as bonding phase.
At low oxygen partial pressure, the two melt regions combine into one large melt region, resulting in an enlargement of the phase fields of (magnetite + liquid) and (calcium silicates + liquid). The phase field of (calcium ferrites + liquid) significantly shrinks. A reduction of oxygen partial pressure will therefore allow calcium silicates to crystallize during cooling.

The effect of particle size on assimilation ability was investigated using a pot grate test. The results showed that the presence of large ore particles in the sinter mix increases the permeability of the sinter bed and forms low density areas around the large particles. This leads to an increase in the gas flow rate and the flame front speed around the particles, which in turn, improves the melting and assimilation reaction rates and sinter quality. For porous and fine particles, sintering reactions are fast in the early stages of the process. More melt is quickly formed allowing the viscosity of the melt to increase. This has an adverse effect on the sintering process as the large scale movements of the melt and solid particles are reduced.

Sinter quality is strongly affected by the variation in sinter mineralogy. A high reducibility of the sinter is attributed to easy access of gas to the sinter material, provided by porous phases such as acicular SFCA and granular hematite. Magnetite decreases the reducibility of the sinter.

The disintegration of sinter is influenced by volume expansion and lattice distortion that occur during phase transformation of hematite into magnetite at low temperature. This volume change can generate stresses and cracks within the mineral phase, leading to the disintegration of the sinter material. A porous microstructure consisting of acicular SFCA and relict hematite can absorb the propagation of these cracks and minimize their effects. The presence of columnar SFCA, silicate phase and coarse secondary hematite and magnetite cause the breakage of the sinter in the upper zone of the blast furnace.

The cold strength is also dependent on the ability of sinter phases to resist the formation and propagation of cracks. The cold strength of sinter is also improved by primary hematite and porous SFCA.

# IV. Experimental procedure

## IV.1 Materials

The starting materials used in this study were supplied by Value-In-Use, Anglo-American KUMBA IRON ORE, Pretoria West. The raw materials were selected on the basis of the study conducted by Elie Lwamba [60]: He reported that sinter mixtures with good permeability can be produced by mixing 50 mass% of Thabazimbi fine iron ore and 50 mass% of Sishen fine iron ore, together with sized coke and limestone. All experiments were therefore conducted using sinter mixtures consisting of the same proportions of both types of iron ores. The addition of limestone was necessary to adjust the basicity ($CaO/SiO_2$) of the sinter mix up to 2.

### IV.1.1 Particle size and chemical compositions of raw materials

The two iron ores and limestone were milled and screened to obtain particles with a broad particle size distribution. Very fine iron ore particles ranged between 0 - 125 microns, fine iron ore 0.125 - 250 microns, and coarse particles of 0.710 - 1.00 mm were used to simulate nucleus particles. The particle size distribution and the chemical compositions of the raw materials are given in Table 1.

**Table 1** Particle size and chemical compositions of raw materials

| Raw materials | Particle size (mm) | Chemical composition (mass %) | | | | | |
|---|---|---|---|---|---|---|---|
| | | T Fe | $SiO_2$ | $Al_2O_3$ | $Fe_2O_3$ | CaO | LOI |
| Thabazimbi ore | 0 - 0.125 | 61.06 | 5.19 | 2.32 | 87.23 | 0.34 | 1.97 |
| | 0.125 - 0.250 | 62.59 | 4.85 | 2.32 | 89.41 | 0.49 | 1.70 |
| Sishen ore | 0 - 0.125 | 63.18 | 4.06 | 3.20 | 90.26 | 0.37 | 0.45 |
| | 0.125 - 0.250 | 63.18 | 4.04 | 1.84 | 90.26 | 0.53 | 0.55 |
| | 0.710 - 1.000 | 65.55 | 2.19 | 1.55 | 93.65 | 0.28 | 0.51 |
| Limestone | 0 - 0.250 | 0.87 | 1.26 | 0.31 | 1.24 | 52.69 | 42.44 |

T Fe : Total iron
LOI : Loss on ignition

The chemical compositions show that Thabazimbi ore has a higher loss of mass during ignition (LOI) than Sishen ore (Table 1). This implies that more pores can be created by evaporation of gas from the solid particles, resulting in an increase in the reaction area. Sishen ore contains more $Fe_2O_3$ and less $SiO_2$ compared to similar fractions of Thabazimbi ore.

### IV.1.2. Sample preparation

Different fractions of iron ores (Sishen and Thabazimbi) and limestone were mixed together, and used to produce cylindrical pellets with a diameter of 6.5mm. A small amount of water was used as binder. Each sinter mix weighed about 1.00 gram, and was pressed into a pellet using a steel mould and a laboratory hydraulic press at room temperature. A low pressure of 5MPa was applied for 2 minutes, and was kept low in order to minimize the fracture of nuclear particles.

Five sinter mixtures (Mix 1, Mix 2, Mix 3. Mix 4 and Mix 5) with specific ratios of coarse ore to fine iron ore were used, and are given in Table 2. The basicities of the sinter mixtures were adjusted by addition of limestone, and were all kept constant at 2.

**Table 2** Sinter mixtures that were used

| | **Mass %** | | | | |
|---|---|---|---|---|---|
| | **Mix 1** | **Mix 2** | **Mix 3** | **Mix 4** | **Mix 5** |
| **Thabazimbi fines** | 42.5 | 32.5 | 22.1 | 11.3 | 0 |
| **Sishen fines** | 42.5 | 32.5 | 22.1 | 11.3 | 0 |
| **Sishen Coarse** | 0 | 22.0 | 44.2 | 68.0 | 92.3 |
| **Limestone** | 15.0 | 13.0 | 11.6 | 9.5 | 7.7 |
| **%Coarse/%Fine** | 0 /100 | 25 /75 | 50 /50 | 75/25 | 100/0 |

The chemical compositions of the five sinter mixtures are given in Table 3. Mix 1 was composed of only fine ore particles, and has the lowest mass percent of $Fe_2O_3$ (76.08%), while the total replacement of fine iron ore by coarse ore is associated with

sinter mix 5, which has with the highest hematite content (86.53%). It can also be seen that silica, alumina and calcium oxide content is decreased with an increase in the coarse ore fraction of the sinter mix.

**Table 3** Chemical compositions of the sinter mixtures

| | Mass % | | | | | |
|---|---|---|---|---|---|---|
| | **Fe** | **$SiO_2$** | **$Al_2O_3$** | **$Fe_2O_3$** | **CaO** | **LOI** |
| **Mix 1** | 53.26 | 4.04 | 2.10 | 76.08 | 8.27 | 7.36 |
| **Mix 2** | 55.16 | 3.59 | 1.95 | 78.80 | 7.19 | 6.39 |
| **Mix 3** | 56.70 | 3.12 | 1.79 | 81.00 | 6.43 | 5.67 |
| **Mix 4** | 58.79 | 2.64 | 1.63 | 83.98 | 5.29 | 4.65 |
| **Mix 5** | 60.57 | 2.12 | 1.46 | 86.53 | 4.31 | 3.74 |

## IV.2. Experimental equipment

The sintering process can be simulated on a small scale by using an infrared furnace (IR-furnace). In this study, the infrared heating Model E4-10 ChamberIR was used, which consists of four elliptical aluminium reflectors and four infrared lamps. Each lamp consists of a quartz glass tube with tungsten filament sealed in it, which provides a radiant energy which is reflected on the internal elliptical surface of the furnace and focused on a centred zone as shown in Figure 21 [61]. By absorbing the reflected rays, the sample which is located in this zone is heated. The Model ChamberIR can provide a clean and efficient heat source, which does not contact the product being heated [61]. The infrared furnace can heat up to 10 times faster than competitive convection systems. The infrared lamps can reach 90% of full operating temperature within 3 seconds after a cold start, and the radiant energy can dissipate to ten percent within five seconds after power switch-off [61]. There is no time wasted on start-ups, or waiting for the furnace to cool down [61]. This feature can offer a rapid heating rate up to 20℃/s [40,48].

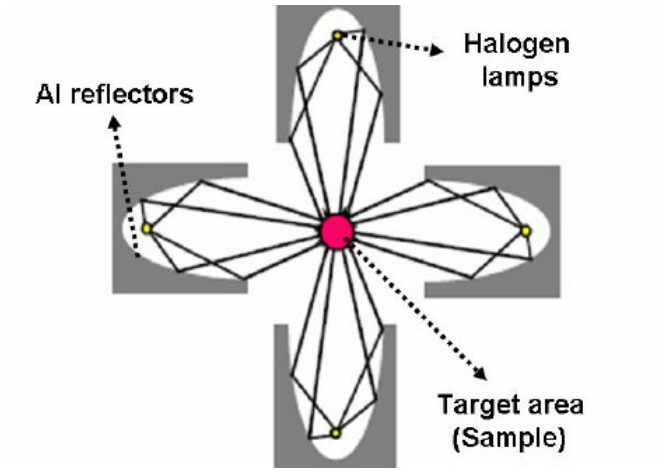


**Figure 21.** Radial heating configuration in Infrared furnace [61]

A schematic layout of the infrared furnace with quartz reaction tube is given in Figure 22. A pellet was set on a perforated quartz plate and positioned at the centre of the infrared furnace through the reaction tube. The heat treatment was similar to the temperature profile used in industrial sintering. The specimen was heated from room temperature up to 500˚C at 2℃/s and held at this temperature for 1min in order to minimize the thermal gradient during the process. Then the temperature was increased at 15℃/s to the desired maximum temperature. After holding at this temperature for a given time, the pellet was cooled to 350℃ at 2℃/s. The temperature of the furnace was controlled using a Pt-Pt10%Rh thermocouple with an exposed junction in intimate contact with the surface of the sample.
The temperature profile of the sample was recorded as shown in Figure 23.

A gas mixture composed of air and argon was blown through the quartz reaction tube in order to regulate the oxygen partial pressure during the sintering process. The atmosphere of the furnace could therefore be controlled at a specific oxygen partial pressure throughout the experimental sintering process.

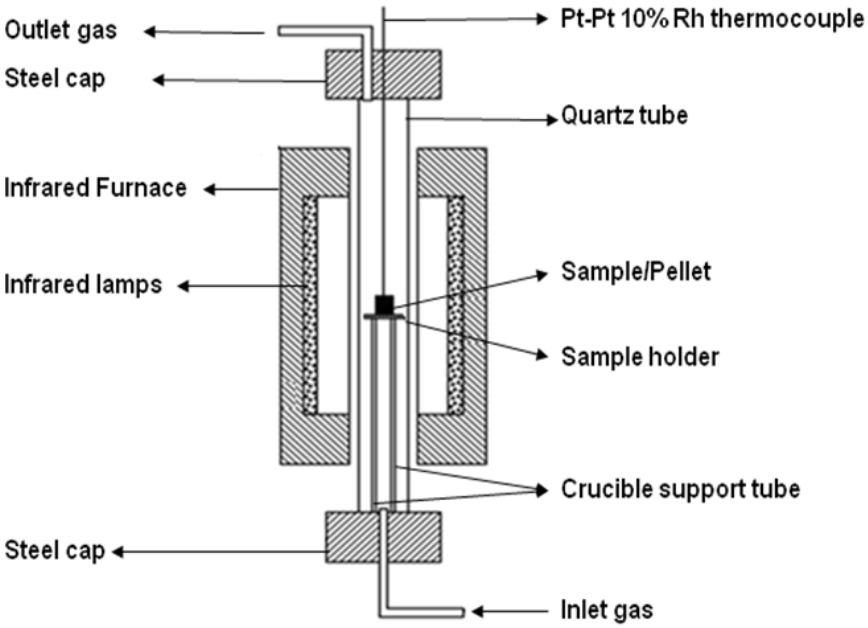


**Figure 22.** Schematic diagram of the experimental setup

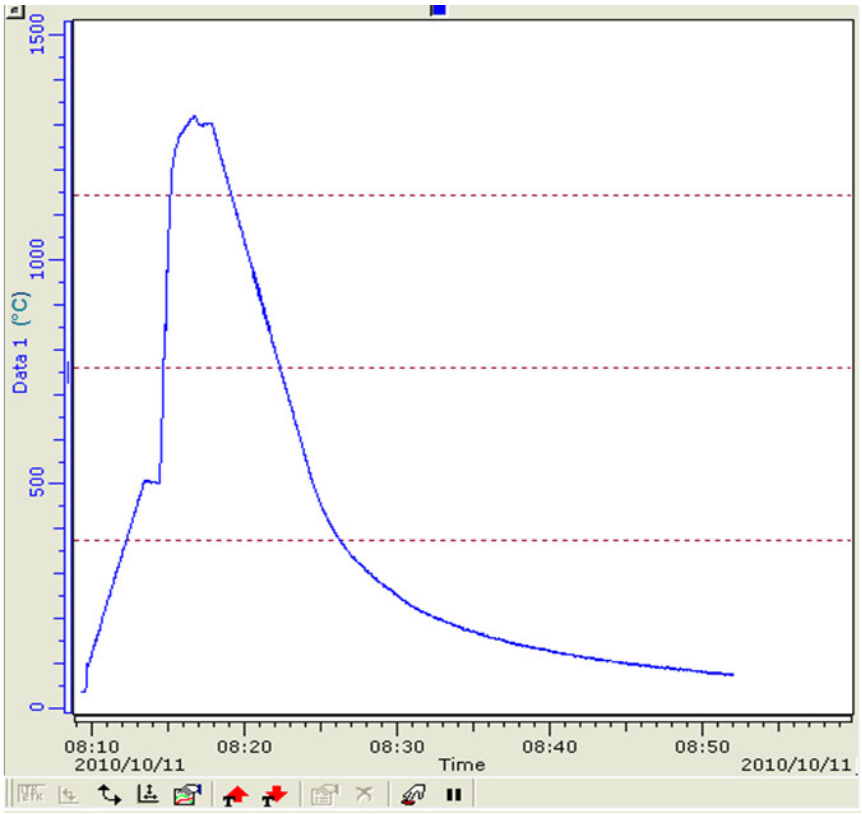


**Figure 23**. Typical time-temperature profile of a pellet

## IV.3. Analysis techniques

### IV.3.1 X-ray diffraction

X-ray diffraction analysis (XRD) is a technique which is generally used for analysis of sinter phases. This technique typically provides qualitative and quantitative analyses of crystalline phase from characteristic diffraction patterns. XRD experiments are typically performed on powders milled as fine as possible (< 75 µm) in order to get a random crystallographic orientation. Afterwards, a thin layer of the sample powder is mounted onto the sample holder, which is placed in the center of the diffractometer. The specimen is irradiated with a monochromatic beam of X-rays, and the scattered portion of the beam is recorded by a detector [62,63].

A typical diffractometer with the X-ray source, specimen and detector is schematically represented in Figure 24.

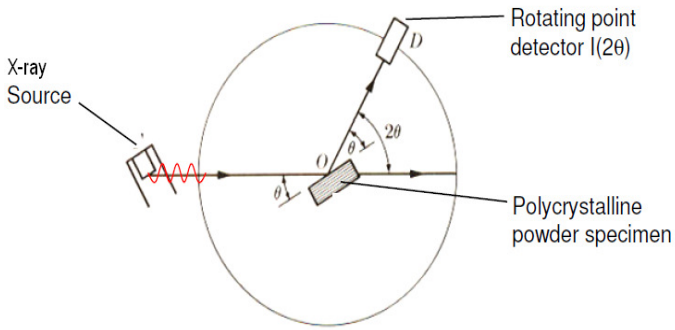


**Figure 24.** Schematic diagram of a typical diffractometer [62]

The X-ray diffraction analysis is based on Bragg's law, which is mathematically expressed as follows [62,63]:

$$2d \sin\theta = n\lambda$$

Where n is an integer, λ is the wavelength of the X-ray source, d is the spacing between the planes in the atomic lattice and θ is the angle between the X-ray source and the crystalline planes (Figure 25).

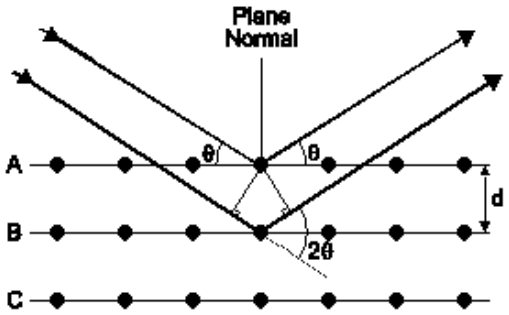


**Figure 25**. Diffraction of a monochromatic x-ray beam by a single crystal [64]

In this investigation, the Rietveld method was used to quantify the crystalline phases. It is based on comparing the experimental diffraction pattern with one calculated from known crystal structure data, and can provide a very reproducible and reliable quantification of the major phases formed during the sintering process [62].

### IV.3.2 Optical microscopy

The iron ore sinters have a microstructure characterized by a heterogeneous arrangement of different phases. Optical microscopy is typically applied to characterize iron ore sinter because it is capable of distinguishing the sinter phases based on their difference in reflectivity. This technique can provide fundamental information such as morphology, porosity and mineralogy of mineral phases.

The sinter specimen is mounted in epoxy resin and polished. After polishing, the specimen is analyzed by visual examination using a reflected light microscope. The images or micrographs that are observed can be captured at different magnifications if the microscope is equipped with a digital camera.

### IV.3.3 Scanning electron microscopy

The Scanning Electron Microscope (SEM) is a microscope that uses a beam of high-energy electrons rather than light to form an image. The electron-sample interactions generate a variety of signals that can reveal information about the sample such as morphology, chemical composition and crystalline structure [64].

Different types of signals result from interaction between the beam of electrons and the surface of the specimen, and include secondary electrons (SE), back scattered electrons (BSE) and characteristic X-rays. The analysis of a sample surface can therefore produce micrographs with high resolution (details about 1 to 5 nm in size can be revealed) [64].

In this study, scanning electron microscopy was also used for examination of morphological changes in the sintered pellets at high magnification, and determination of typical bonding phases that formed during the sintering process. Energy dispersive x-ray spectrometry (EDS) analysis was used to determine the chemical compositions of the different phases present in the sinter samples. The chemical analyses could therefore be used to determine the different types of SFCA phases by comparing these compositions to those reported in the literature.

### IV.4. Experiment design

The design of experiments (DOE) or experiment design (ED) is an efficient strategy for planning experiments so that the data obtained can produce valid and objective conclusions. This experimental method is a useful tool in identification of the important factors and their levels for a specific process [65]. The experiment design also enables the user to estimate how changes in input factors affect the response of a specific process in today's engineering world. Furthermore the use of experiment design presents an advantage to obtain necessary information about a new product or process development using a limited number of experimental tests [65].

According to the objective of this study, the experimental design was used to find out the most influential variables between fraction of coarse particles, sintering temperature, holding time and oxygen partial pressure on the formation of sinter phases during laboratory experiments. The screening design was selected for identification of the key variables or factors that have a significant effect on phase formation.

### IV.4.1. Identification of parameters

A broad number of parameters influence the production of sinter cake and particularly the formation of sinter phases. In this study, emphasis was on measuring the effects of the fraction of coarse ore, sintering temperature, oxygen partial pressure, and residence time on the formation of sinter phases.
The basicity, heating rate and cooling rate were all kept constant throughout the sintering tests.

### IV.4.2. Identification of levels of each parameter

Two-level designs are the most popular experiment designs used by engineers because they are simple, economical and the associated statistical analyses are simple. A 2-level full factorial design was used in this study to measure the effects of four investigated parameters on the formation of sinter phases [65].

The values of each factorial level were identified on the basis of previous experiments, whereby high and low levels of each factor were determined. It was found that measurable amounts of both types of SFCA form in the temperature range between 1200℃-1300℃. Hida [51] reported that solid-solid reactions occur quickly between hematite and lime at low temperatures (750℃-1100℃), and form calcium ferrites ($C_2F$ and CF). Above 1200℃, SFCA-I start to form while SFCA will considerably form only at temperatures around 1300℃. An increase in sintering temperature above 1300℃ can result in the decomposition of SFCA into calcium silicates and iron oxides. Scarlett *et al.* [18] as well as Loo and Matthews [48] found that SFCA start to form at low temperatures (~ 1050℃-1100℃) when the heating rate is low (~10℃/min). At high heating rate, a significant overstepping of the equilibrium SFCA formation temperature is noticed before a measurable amount of SFCA is formed.
The holding time is another important parameter that deserves to be investigated. At maximum temperature, the holding time was set between 2-3 minutes as these values are used in industrial sintering [40,48].

In the current study, the oxygen partial pressure range was defined by running a pot test using 3 oxygen sensors located respectively on top, in the middle and at the bottom of the sinter bed. The results showed that the oxygen partial pressure vary between 0.02 atm to 0.21 atm.

The two levels set for each factor in the 2-full factorial experimental design are shown in Table 4.

**Table 4** Levels for different parameters

| Parameters | Low level | High level |
|---|---|---|
| Fraction of coarse ore (%) | 0 | 100 |
| Sintering temperature (°C) | 1200 | 1300 |
| Residence time (min) | 1.5 | 3.5 |
| Oxygen partial pressure (atm) | 0.02 | 0.21 |

### IV.4.3. Coding for factors and levels

Coding for factors and levels consists of transforming the scale of measurement for a factor, so that the high and the low values are respectively noted +1 and -1. More often, these values are coded "+" and "-" [65]. In addition, there can optionally be some center points, which are at the midpoint between the low and high values for each factor and are coded as "0" [65]. The coding names used in this study, for each variable or parameter at low, middle and high values are given in Table 5.

**Table 5** Coding for Factors and Factorial Levels

| Factors | Coding of factors | Coding of factorial levels | | |
|---|---|---|---|---|
| | | - | 0 | + |
| Fraction of coarse ore (%) | $X_1$ | 0 | 50 | 100 |
| Sintering temperature (°C) | $X_2$ | 1200 | 1250 | 1300 |
| Residence time (min) | $X_3$ | 1.5 | 2.5 | 3.5 |
| Oxygen partial pressure (atm) | $X_4$ | 0.02 | 0.12 | 0.21 |

### IV.4.4 Design matrix

In this study, 2-level 4-factor full factorial design with center points was used to identify the parameters that can strongly affect the formation of sinter phases. For screening purposes, to study 4 different factors, each having only two levels, the minimum number of experimental runs needed is 16. These experimental runs will be performed at least once [65]. Furthermore, 6 replicated runs referring to center points can be necessary to assess the stability of the process and the inherent variability [65].
It is also recommended to perform experimental runs in a random sequence in order to avoid having the results ruined by uncontrollable or noisy variables. The randomization of runs can effectively minimize the distortion of analysis and errors during the interpretation of the results. The design of experiment must therefore be able to ensure the accuracy of the final results as much as possible [65].

The design matrix for a full factorial experiment, which can be fractioned into 2 parts, is shown in Table 6 [65]. The first part (blue) is the 2-level factorial portion experiment and the second part (orange) refers to the centre point portion. The response for each $i^{th}$ experimental run is denoted as $R_i$.

**Table 6** Matrix of 2-level 4-factor full factorial design

| Standard order | $X_1$ | $X_2$ | $X_3$ | $X_4$ | Response |
|---|---|---|---|---|---|
| 1 | - | - | - | - | $R_1$ |
| 2 | + | - | - | - | $R_2$ |
| 3 | - | + | - | - | $R_3$ |
| 4 | + | + | - | - | $R_4$ |
| 5 | - | - | + | - | $R_5$ |
| 6 | + | - | + | - | $R_6$ |
| 7 | - | + | + | - | R7 |
| 8 | + | + | + | - | $R_8$ |
| 9 | - | - | - | + | $R_9$ |
| 10 | + | - | - | + | $R_{10}$ |
| 11 | - | + | - | + | $R_{11}$ |
| 12 | + | + | - | + | $R_{12}$ |
| 13 | - | - | + | + | $R_{13}$ |
| 14 | + | - | + | + | $R_{14}$ |
| 15 | - | + | + | + | $R_{15}$ |
| 16 | + | + | + | + | $R_{16}$ |
| 17 | 0 | 0 | 0 | 0 | $R_{17}$ |
| 18 | 0 | 0 | 0 | 0 | $R_{18}$ |
| 19 | 0 | 0 | 0 | 0 | $R_{19}$ |
| 20 | 0 | 0 | 0 | 0 | $R_{20}$ |
| 21 | 0 | 0 | 0 | 0 | $R_{21}$ |
| 22 | 0 | 0 | 0 | 0 | $R_{22}$ |

The process responses were the amount of phases formed during iron ore sintering. The considered phases were SFCA, hematite, magnetite and calcium silicates due to their significant amount in the sinter cake.

### IV.4.5 Results and discussion

The mineral compositions provided by XRD analyses of sintered pellets that were reacted in the infrared furnace is shown in Table 7. These phases are considered to be the process responses, and represent the mass percent averages of hematite, SFCA, SFCA-I, magnetite and calcium silicate formed during the sintering process.

The response data were used to determine the most important factors by computing the main effects. For each factor, the mean effect represents the average difference between response values for experimental runs performed at high level minus the ones at low level. The mean effect may be negative or positive. The negative value of the effect for a parameter indicates that the response value decreases when experimental variables increase from low to high levels. When the effect is positive, increasing the factor from the low level to the high level will result in an increase in the response value [65,66].

The greater the absolute value of the mean effect, the greater the effect on the process response, and the greater the importance of the corresponding factor. If the mean effect is zero or small, this suggests that this specific parameter has no or very little effect when the experimental values vary from a low level to a high level [65,66].

**Table 7** Response values of Experimental Design

| Standard order | $X_1$ | $X_2$ | $X_3$ | $X_4$ | Hematite | SFCA | SFCA-I | Magnetite | $C_2S$ |
|---|---|---|---|---|---|---|---|---|---|
| 1 | - | - | - | - | 61.10 | 16.44 | 15.65 | 1.58 | 5.22 |
| 2 | + | - | - | - | 79.07 | 9.81 | 7.70 | 2.45 | 4.95 |
| 3 | - | + | - | - | 45.70 | 31.62 | 9.20 | 5.10 | 8.39 |
| 4 | + | + | - | - | 66.87 | 15.27 | 7.75 | 3.48 | 6.62 |
| 5 | - | - | + | - | 50.57 | 31.17 | 9.01 | 1.61 | 7.63 |
| 6 | + | - | + | - | 72.01 | 12.05 | 5.59 | 3.69 | 6.66 |
| 7 | - | + | + | - | 40.89 | 31.86 | 10.10 | 6.86 | 10.28 |
| 8 | + | + | + | - | 67.17 | 11.47 | 5.94 | 7.73 | 7.68 |
| 9 | - | - | - | + | 54.10 | 27.85 | 12.31 | 0.00 | 5.74 |
| 10 | + | - | - | + | 80.92 | 10.98 | 4.53 | 0.00 | 4.52 |
| 11 | - | + | - | + | 48.19 | 32.86 | 14.72 | 0.00 | 4.23 |
| 12 | + | + | - | + | 79.50 | 7.05 | 8.56 | 0.00 | 4.89 |
| 13 | - | - | + | + | 45.86 | 35.63 | 8.74 | 0.00 | 9.77 |
| 14 | + | - | + | + | 76.61 | 15.28 | 4.86 | 0.00 | 3.27 |
| 15 | - | + | + | + | 44.59 | 36.80 | 6.55 | 0.00 | 12.06 |
| 16 | + | + | + | + | 77.67 | 14.05 | 3.65 | 0.00 | 4.63 |
| 17 | 0 | 0 | 0 | 0 | 55.02 | 24.38 | 16.50 | 1.32 | 4.10 |
| 18 | 0 | 0 | 0 | 0 | 56.42 | 24.26 | 13.56 | 1.28 | 4.48 |
| 19 | 0 | 0 | 0 | 0 | 57.41 | 26.35 | 11.43 | 0.00 | 4.81 |
| 20 | 0 | 0 | 0 | 0 | 54.77 | 23.30 | 17.85 | 0.00 | 4.08 |
| 21 | 0 | 0 | 0 | 0 | 57.56 | 24.91 | 14.04 | 0.00 | 3.50 |
| 22 | 0 | 0 | 0 | 0 | 56.44 | 24.74 | 14.34 | 0.00 | 4.48 |
| Average (center points) | | | | | 56.27 | 24.66 | 14.62 | 0.43 | 4.24 |
| Standard deviation | | | | | 1.17 | 1.00 | 2.27 | 0.67 | 0.45 |

$C_2S$: Calcium silicates

The results from this experiment design were used to determine the mean effects of the fraction of coarse ore and sintering temperature as well as those of residence time and oxygen partial pressure. The mean effect of different factors, which represent the difference between mass percentages of sinter phase, formed at high and low experimental settings are given in Table 8. The mean effect with the highest absolute value corresponds to the most influential factor on phase formation.

**Table 8** Mean effects for the experiment

| Phase | Factor | + | - | Mean effect |
|---|---|---|---|---|
| **Hematite** | $X_1$ | 74.98 | 48.88 | 26.10 |
| | $X_2$ | 58.82 | 65.03 | -6.21 |
| | $X_3$ | 59.42 | 64.43 | -5.01 |
| | $X_4$ | 63.43 | 60.42 | 3.01 |
| **SFCA** | $X_1$ | 12.00 | 30.53 | -18.53 |
| | $X_2$ | 22.62 | 19.90 | 2.72 |
| | $X_3$ | 23.54 | 18.99 | 4.56 |
| | $X_4$ | 22.56 | 19.96 | 2.60 |
| **SFCA-I** | $X_1$ | 6.07 | 10.78 | -4.71 |
| | $X_2$ | 8.31 | 8.55 | -0.24 |
| | $X_3$ | 6.80 | 10.05 | -3.25 |
| | $X_4$ | 7.99 | 8.87 | -0.88 |
| **Magnetite** | $X_1$ | 2.17 | 1.89 | 0.28 |
| | $X_2$ | 2.90 | 1.17 | 1.73 |
| | $X_3$ | 2.49 | 1.58 | 0.91 |
| | $X_4$ | 0.00 | 4.06 | -4.06 |
| **Ca-silicates** | $X_1$ | 4.78 | 7.92 | -3.13 |
| | $X_2$ | 7.35 | 5.35 | 2.00 |
| | $X_3$ | 7.75 | 4.95 | 2.79 |
| | $X_4$ | 6.02 | 6.68 | -1.07 |

The mean effects may also be plotted to clearly illustrate the effect of different factors on each process response. The plots of different mean effects are represented in Figures 26-30. The most important factor is the one having the biggest shift in

location of the response value. The next biggest shift is associated to the second most important factor, and so on until all factors are accounted for. The mean effects and mean plots can therefore provide the ranked list of factors from the most important to the least important.

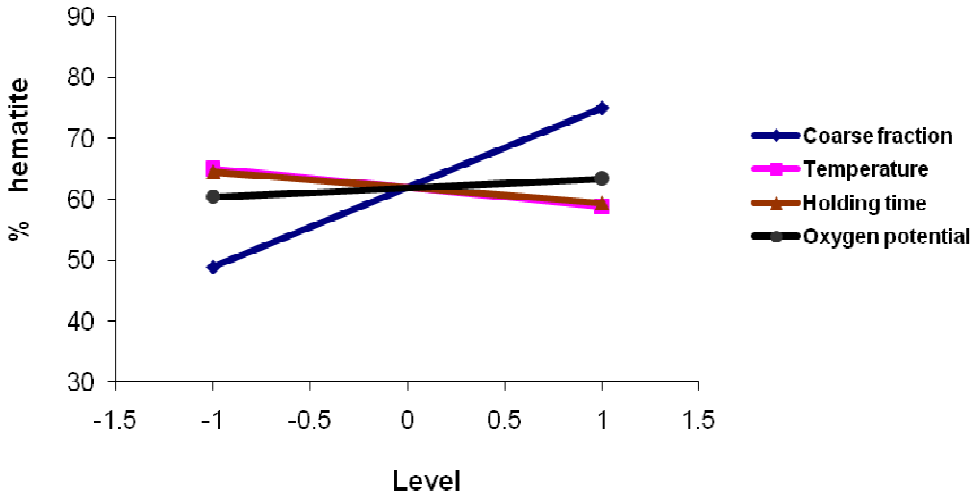


**Figure 26.** Mean effect plot of factors on assimilation of hematite

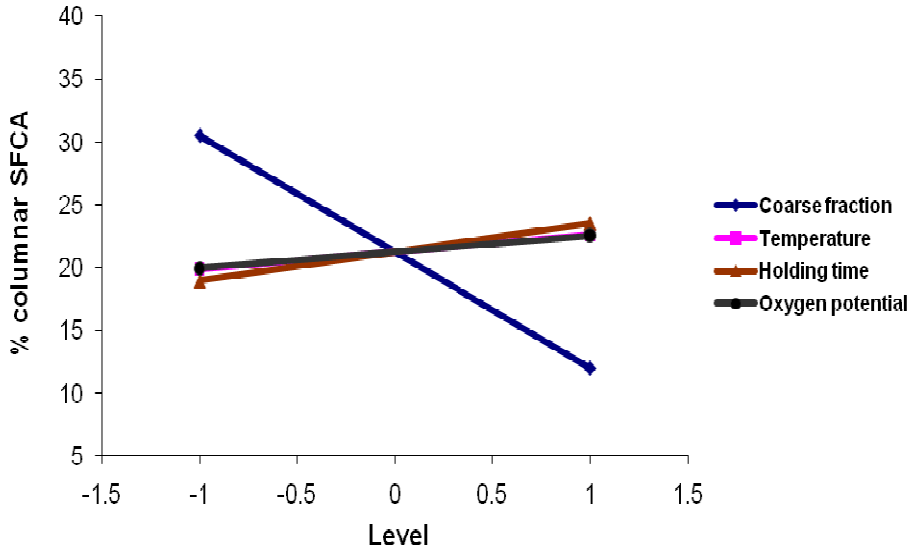


**Figure 27**. Mean effect plot of factors on formation of columnar SFCA

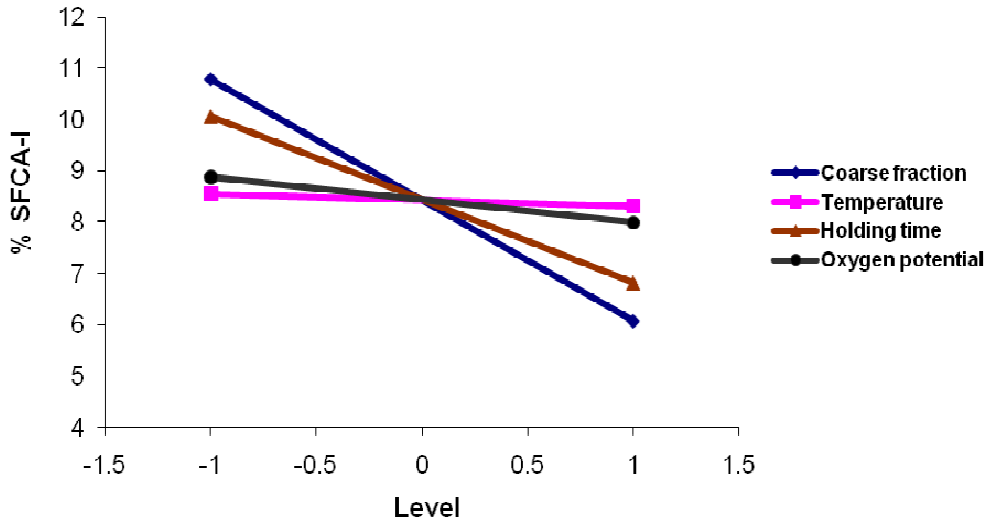


**Figure 28**. Mean effect plot of factors on formation of SFCA-I

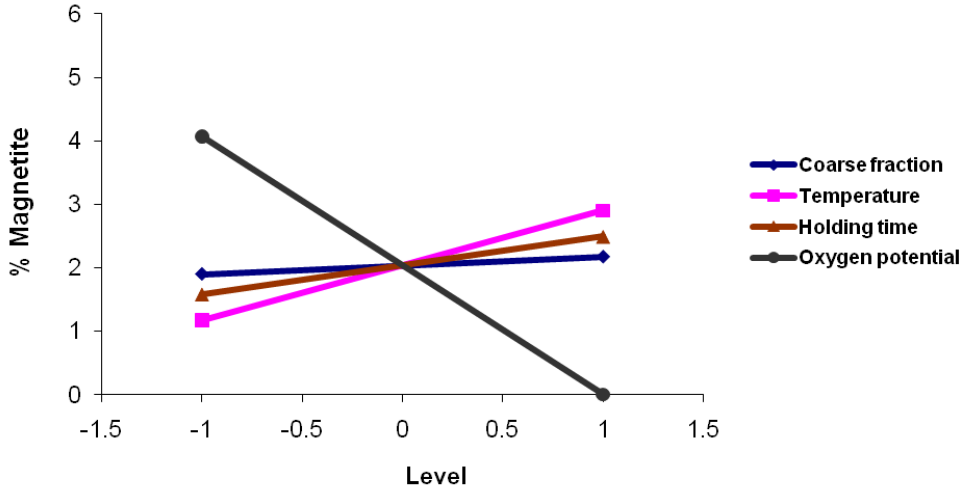


**Figure 29**. Mean effect plot of factors on formation of magnetite

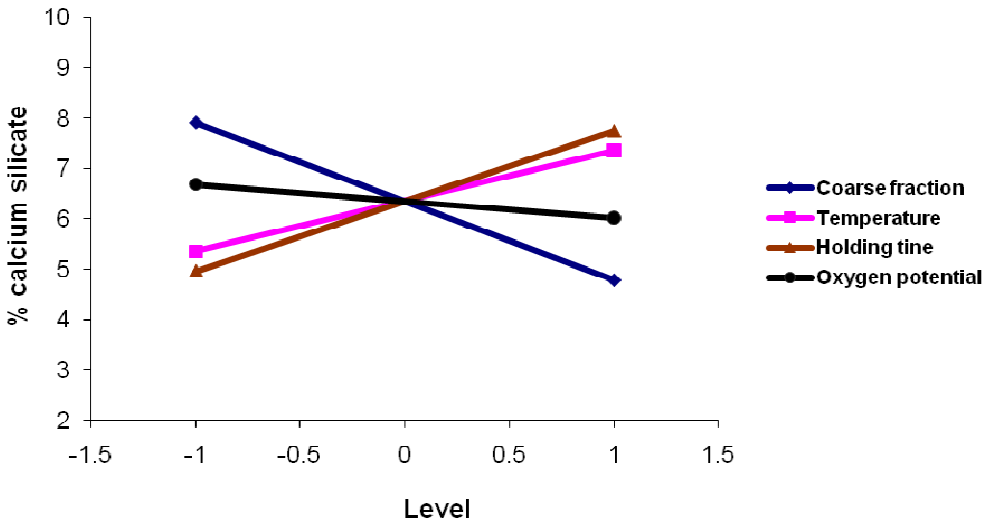


**Figure 30**. Mean effect plot of factors on formation of calcium silicates

From the mean effects and mean plots, changing the fraction of coarse ore from 0% to 100% appears to have the greatest effect on the assimilation of hematite and the formation of SFCA. When the fraction coarse ore is changed from the low level to the high level, the percentage of hematite in the sinter increases to about 26.10% and the percentage of columnar SFCA formed is decreased by 18.53%. These results can be observed in Figures 26 and 27 where the biggest shifts in response values are respectively associated with the effects of the coarse ore fraction on the assimilation of hematite and the formation of columnar SFCA. The variation of coarse ore fraction also slightly decreases the amount of SFCA-I by 4.71% (Figure28) and that of the calcium silicates by 3.13% (Figure 30), if the coarse ore fraction increases from 0% to 100%. These results are in agreement with previous studies where fine particles with high reaction area react more quickly than coarse particles [40,48].

Compared to the effects of coarse ore fraction, the variation of other factors from low to high values shows slight effects on the process. The percentage of hematite which was assimilated increases by 6.21% when the sintering temperature shifted from 1200℃ to 1300℃. It was also observed that the change of sintering temperature from 1200℃ to 1300℃ has slight shifts in the amount of SFCA (increase of 2.72%), magnetite (increase 1.73%) and calcium silicates (increase of 2.00%). However, the variation of temperature within the considered temperature range shows no effect on SFCA-I formation.

The residence time also has only a slight effect on the assimilation of hematite and the formation of SFCA. When the residence time increases from 1.5 minutes to 3.5 minutes, the percentage of hematite is decreased by 5.01%, and the percentages of columnar SFCA and calcium silicate respectively increase by 4.56% and 2.79%.
The amount of SFCA-I is decreased by 3.25% for the same variation in residence time. The effect of residence time on the formation of magnetite shows a small increase in the amount of magnetite (0.91%).

The variation of oxygen partial pressure shows a noticeable effect on the assimilation of hematite, as well as the formation of SFCA and magnetite. Changing oxygen partial pressure from 0.02 atm to 0.21 atm results in an increase in the amount of hematite compared to that of magnetite. The percentage of hematite is increased by 3.01% and the amount of magnetite is decreased by 4.06%. The increase in oxygen partial pressure during sintering also increases the amount of columnar SFCA by 2.60%. However, the effect of oxygen partial pressure on the formation of SFCA-I and calcium silicates are very small.

The results from the mean effects were also used to investigate the effect of the considered parameters on sinter phase formation or sintering reactions when fine ores were replaced by coarse ore particles.

- **Assimilation of hematite**

  The proportion of coarse ore has the greatest effect on percentage of hematite content as shown in Figure 26. The amount of hematite is increased by 23.79% with the total replacement of fine ores by coarse ore particles. This can be attributed to the reduction of surface area for sintering reactions. The study conducted by Debrincat et *al.*[6] also reported that the degree of assimilation is greater for a mixture composed of fine particles, and melt formation is enhanced due to the high reaction surface area available for sintering reactions.

  The sintering temperature and the holding time have noticeable effects on the assimilation of hematite. The hematite content is decreased with an increase in

sintering temperature and holding time. These results are similar to what was found by Loo and Matthews [48]. They reported that increasing the temperature in real systems reduces melt viscosity and increases the assimilation of large ore particles. More melt is then generated, and the amount of relict ore decreases [48].
Loo and Matthews [48] also concluded that the holding time at maximum temperature plays a significant role in assimilation of solid particles. Long holding times improve the dissolution of solid particles into the melting phase [48].

Sintering under oxidizing conditions results in more hematite. At low oxygen partial pressure, hematite can partially be reduced into magnetite, resulting in a decrease in the amount of hematite in the final sinter.
In industrial sintering, hematite is partially reduced into magnetite during the heating stage. If reducing conditions are maintained during the cooling stage, the magnetite will be preserved after the sintering process. Magnetite can be oxidized into hematite (tertiary hematite) on cooling if the oxygen partial pressure is increased.

- **Formation of columnar SFCA**

SFCA and SFCA-I are considered the main bonding phases that form during the sintering process. It is therefore of importance to understand the variation in their relative amounts when fine ores are replaced by coarse ore particles.

The effects of investigated parameters on columnar SFCA formation show a high dependence on the variation of the coarse ore fraction. The amount of columnar SFCA is decreased by 18.53% when the fraction of coarse ore is increased from 0% to 100%. This is due to the reaction area of the solid particles which is decreased, resulting in a delay of sintering reactions and decrease in the reaction rate. As columnar SFCA is identified as a high-temperature bonding phase, the decrease in reaction area and reaction rate decreases the amount of columnar SFCA in the sinter material [2,18,41,48]. The replacement of fine iron ore by coarse ore, which is associated with the reduction in reaction rate, has a negative effect on the formation of columnar SFCA during the sintering process (see Figure 27).

The effect of the holding time on formation of columnar SFCA is also noticeable. The variation of the holding time from 1.5 minutes to 3.5 minutes increases the amount SFCA by 4.56%.These results agree with those found by the studies of Scarlett *et al.* [18] where long holding times produced more columnar SFCA than SFCA-I.

The sintering temperature and oxygen partial pressure have similar effects on SFCA formation. Increasing the sintering temperature enhances the formation of columnar SFCA which is considered a "high temperature phase". Similarly, the increase in oxygen partial pressure shows an increase in columnar SFCA content due to the high amount of $Fe^{3+}$ in the melt. A decrease in oxygen partial pressure is associated with the formation of $Fe^{2+}$, which decreases the viscosity of the melt and hinders the formation of columnar SFCA [40,48].

- **Formation of SFCA-I**

Although mean plots of SFCA-I formation displayed small slopes, the fraction of Sishen coarse ore showed a noticeable effect on the formation of SFCA-I. The amount of SFCA-I decreases when the fraction of coarse ore increases from 0% to 100%. This means that the decrease in reaction area also has a negative effect on SFCA-I formation.

The holding time also negatively affected the amount of SFCA-I content when fine ores were replaced by coarse ore particles. These results are similar to what was found in previous investigations where long holding times suppresses the formation of SFCA-I [18]. Scarlett *et al.* [18] stated that long holding times at maximum temperature increased the fraction of columnar SFCA and the assimilation of hematite.

However, the effects of sintering temperature and oxygen partial pressure on the formation of SFCA-I are very small but negative. It is assumed that the amount of SFCA-I is increased for low sintering temperatures and low oxygen partial pressures.

- **Formation of magnetite**

The formation of magnetite is mainly influenced by sintering temperature and partial pressure of oxygen, and not significantly by the coarse ore fraction and holding time (Table 8 and Figure 29). The variation of the oxygen partial pressure can be associated with the variation in the ratio of $Fe^{2+}/Fe^{3+}$ in the melting phase. Decreasing the oxygen partial pressure produces more magnetite due to the formation of more $Fe^{2+}$ in the melt [16,48,57]. Higher oxygen partial pressures are associated with high concentrations of $Fe^{3+}$, resulting in the presence of more hematite in the final product [16,48,57].

The amount of magnetite is also increased by increasing the sintering temperature during the sintering process. The reduction of hematite into magnetite is an endothermic reaction with $\Delta H = +119$ kJ/mol. An increase in sintering temperature will therefore favour the formation of magnetite to the detriment of hematite.

$6\ Fe_2O_3 \rightarrow 4\ FeO.\ Fe_2O_3 + O_2 \quad \Delta H = +119$ kJ/mol

- **Formation of calcium silicates**

The effect of the different examined factors on the formation of calcium silicates is very small. However, the slight shift in the amount of calcium silicate reveals some specific trends. The amount of calcium silicates decreases with the variation of coarse ore fraction from 0% to 100% (Figure 30). The decrease of the reaction area appears to delay the formation of calcium silicates.

The increase in the holding time results in a slight increase in calcium silicate content. A very long holding time might therefore lead to the production of more calcium silicates.

The formation of calcium silicates is also affected by a change in sintering temperature. The amount of calcium silicates might be increased with high sintering temperatures.

The effect oxygen potential on the formation of calcium silicates shows a very small effect on the formation of calcium silicates, where increasing oxygen partial pressures seems to decrease the amount of calcium silicates. This complies with previous studies where sintering at low oxygen partial pressures favoured the production of magnetite and calcium silicates [4,16].

### IV.4.6 Normal probability plot of effects

The normal probability plot is a graphical technique used to determine whether or not a data set follows a normal distribution. The data are plotted against a theoretical normal distribution in such a way that the points should form a straight line [69,70].

The normal probability plots can also be used to assess the statistical significance of effects from a dispersion of data. The plotting procedure of normal probability can be summarized as follows [67,68]:

- Order the main effects from the smallest to the highest
- Assign a rank i to the $i^{th}$ smallest effect
- Compute (i - 0.5)/p; p = number of effects
- Use Appendix 1 to determine $Z_i$, where $Z_i$ is the Z value for which the area under the standard normal curve below Z is (i - 0.5)/p
- Plot $Z_i$ versus the $i^{th}$ smallest effect
- Draw a straight line through the majority of points
- Points that fall well off the line would suggest the existence of real effects.

To apply the normal probability plots, a new codification of different main effects is necessary to avoid confusion. The new codification of main effects for different phases formed during sintering is given in Table 9. The mean effects from the interactions ($X_iX_j$) between $i^{th}$ and $j^{th}$ factor were not considered due to their low values as shown in Appendix 2.

**Table 9.** Codification of main effects

| Phase | Factor | Main effect | Code |
|---|---|---|---|
| Hematite | $X_1$ | 26.10 | A |
| | $X_2$ | -6.21 | B |
| | $X_3$ | -5.01 | C |
| | $X_4$ | 3.01 | D |
| SFCA | $X_1$ | -18.53 | E |
| | $X_2$ | 2.72 | F |
| | $X_3$ | 4.56 | G |
| | $X_4$ | 2.60 | H |
| SFCA-I | $X_1$ | -4.71 | I |
| | $X_2$ | -0.24 | J |
| | $X_3$ | -3.25 | K |
| | $X_4$ | -0.88 | L |
| Magnetite | $X_1$ | 0.28 | M |
| | $X_2$ | 1.73 | N |
| | $X_3$ | 0.91 | O |
| | $X_4$ | -4.06 | P |
| Ca-silicates | $X_1$ | -3.13 | Q |
| | $X_2$ | 2.00 | R |
| | $X_3$ | 2.79 | S |
| | $X_4$ | -1.07 | T |

Afterwards, percentiles related to effects may be evaluated as shown in Table 10.

**Table 10.** Ordered mean effects and percentiles

| Code | Main effect | i | (i – 0.5)/p | $Z_i$ |
|---|---|---|---|---|
| E | -18.53 | 1 | 0.03 | -2.06 |
| B | -6.21 | 2 | 0.08 | -1.48 |
| C | -5.01 | 3 | 0.13 | -1.18 |
| I | -4.71 | 4 | 0.18 | -0.86 |
| P | -4.06 | 5 | 0.23 | -0.78 |
| K | -3.25 | 6 | 0.28 | -0.62 |
| Q | -3.13 | 7 | 0.33 | -0.47 |
| T | -1.07 | 8 | 0.38 | -0.34 |
| L | -0.88 | 9 | 0.43 | -0.21 |
| J | -0.24 | 10 | 0.48 | -0.08 |
| M | 0.28 | 11 | 0.53 | 0.08 |
| O | 0.91 | 12 | 0.58 | 0.21 |
| N | 1.73 | 13 | 0.63 | 0.34 |
| R | 2 | 14 | 0.68 | 0.47 |
| H | 2.6 | 15 | 0.73 | 0.62 |
| F | 2.72 | 16 | 0.78 | 0.78 |
| S | 2.79 | 17 | 0.83 | 0.86 |
| D | 3.01 | 18 | 0.88 | 1.18 |
| G | 4.56 | 19 | 0.93 | 1.48 |
| A | 26.1 | 20 | 0.98 | 2.06 |

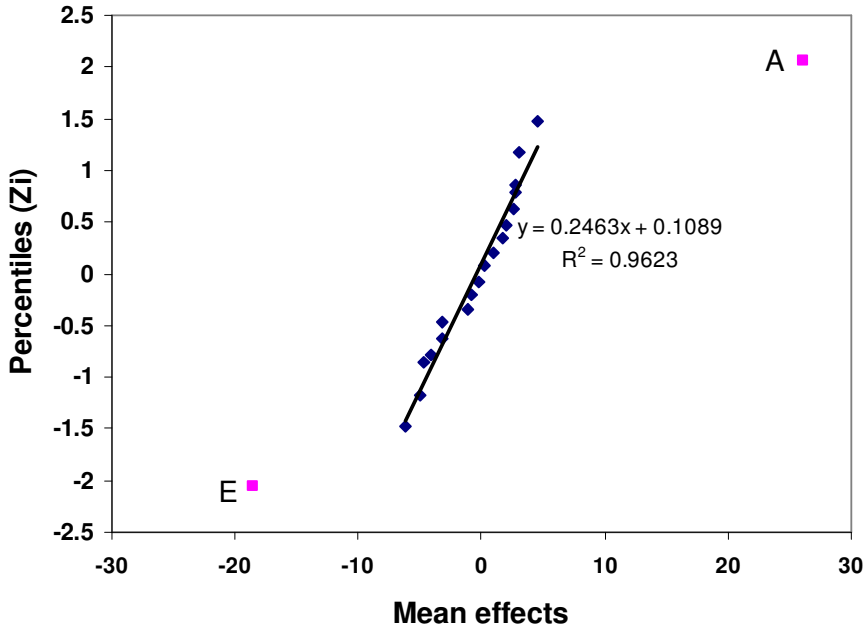


**Figure 31**. Normal probability plot of effects

The effects of coarse ore fraction on the amount of hematite (A: 26.1%) and columnar SFCA (E:-18.53%) fall far away from the straight line (Figure 31). This means that only these two effects may be statistically significant. The other points are close to a straight line with $R^2$= 96.23%. Similar results are obtained when the interactions between two factors are included (see Appendix 3).
It was therefore established that the effect of coarse particle fraction on the formation of SFCA and assimilation of hematite are the most significant during the sintering tests.

Compared to the mean effect analysis, the normal probability plot shows that the fraction of coarse ore particles strongly affects the phase formation or sintering reactions with regard to the formation of columnar SFCA. This confirms that the fraction of coarse ore is an important parameter which regulates the surface area for sintering reactions to take place, and influences the permeability of the sinter bed.
The coarse ore fraction can also influence other parameters such as sintering time, productivity and sinter quality.

### IV.4.7 Conclusions

Using a screening approach, the experimental design has shown that the fraction of coarse ore particles has the greatest effect on the assimilation of hematite and formation of SFCA during the sintering process. These results are in agreement with previous studies where the effect of changing ore particle size during iron ore sintering was examined [40,48]. It was reported that fine particles have a high reaction area, resulting in a high degree of assimilation ability. The amount of melt formed is high and can increase the sintering reactions.

As the experiment design was used to find the most important parameter (coarse ore fraction) during the sintering tests, other parameters also showed some slight effects on phase formation and sintering reactions. For instance, an increase in sintering temperature generally resulted in an increase in the amount of sinter phases.

Further analysis of the investigated effects led to the identification of the optimum experimental settings. It was established that the variation of the maximum temperature is also important because it influences other parameters such as heating rate and viscosity and fluidity of the melting phase. Scarlett *et al.* [18] as well as Loo and Matthews [48] reported that sintering with high heating rates would produce measurable amounts of both SFCA and SFCA-I only if the maximum temperature exceeds their melting point (above 1200℃). The assimilation of solid material by the melt phase is therefore considered significant at sintering temperature of about 1300℃. At higher temperatures (above 1300℃), SFCA-I can start to decompose into columnar SFCA, which in turn, can decompose into iron oxides and calcium silicates. The maximum temperature of 1300℃ corresponds to a temperature where the assimilation of hematite is high, and was selected for further investigation of sintering reactions [2,18.41.48].

In industrial sintering, the holding time at maximum temperature varies between 2 and 3 minutes [40,48]. A residence time of 2.5 minutes was assumed to be enough for the production of measurable amounts of both SFCA and SFCA-I in this study.
The sinter mix is usually heated in a reducing atmosphere and then cooled under an oxidizing atmosphere during sintering. As the heating stage with low oxygen partial

pressure is very short and the effects of oxygen partial pressure are insignificant (Table 8), it was suggested that the oxygen partial pressure could be set to 0.21 atm during laboratory experiments.

As the objective of this study was to investigate the effect of the replacement of fine iron ore by coarse ore particles on the sintering reactions, the identification of the optimum experimental settings (Table 11) led to a further investigation, where the coarse fraction was changed in 25% increments from 0% to 100%.

**Table 11** Optimum settings for a further investigation of the sintering process

| Factors | Range |
|---|---|
| Fraction of coarse ore (%) | 0 - 25 - 50 - 75 - 100 |
| Sintering temperature (°C) | 1300 |
| Residence time (min) | 2.5 |
| Oxygen Pressure (atm) | 0.21 (Air) |

## IV.5 Variation of phase formation with coarse ore fraction

The factors identified in Section IV.4.7 as optimum settings, were used in this part of the investigation to study sintering reactions when fine iron ore is progressively replaced by coarse ore. The fraction of coarse ore particles was changed from 0% to 100% in increments of 25%. The sintering temperature was set at 1300℃ in order to form a measurable amount of SFCA and prevent the decomposition of SFCA-I into SFCA. The experimental values of other sintering parameters (holding time, oxygen partial pressure, heating and cooling rate) were all kept constant and are given in Table 11.

Sintering experiments were carried out using the infrared furnace, which simulated the average sintering temperature profile recorded from sintering pot tests performed at Anglo American Kumba Iron Ore Pilot plant.

### IV.5.1. Porosity of different green pellets

As the porosity (packing density) influences the sintering rate, the compacted mixtures were subjected to porosity analysis, using a gas pycnometer Model AccuPyc II 1340. This type of pycnometer is an easy-to-use, fully automatic gas displacement pycnometer, and can determine the absolute density or volume of solid particles by measuring the pressure change of helium within calibrated chamber volumes. The current pressure and chamber temperature are displayed on the pycnometer display. An AccuPyc II 1340 pycnometer consists of a control with a built-in keypad and display area, and an analysis module, as shown in Figure 32.

**Figure 32**. Typical Micromeritics AccuPyc II 1340 gas pycnometer

Cylindrical pellets (10mm diameter) obtained by compacting 3g of different sinter mixtures under 5MPa were subjected to porosity analysis using the AccuPyc II 1340 gas pycnometer. After determining the volume of solid particles, the porosity was expressed as a percentage of total volume by comparing the volume of solid particles to the theoretical value (pellet volume). Table 12 and Figure 33 show the variation of average porosity and average length values with coarse ore fraction.

**Table 12** Porosity and length of different pellets

| | | Mix1 | Mix2 | Mix3 | Mix4 | Mix5 |
|---|---|---|---|---|---|---|
| Pellet length [mm] | A | 13.30 | 12.13 | 11.70 | 11.30 | 10.70 |
| | B | 13.21 | 12.50 | 11.60 | 11.45 | 11.01 |
| | C | 13.13 | 11.97 | 11.73 | 11.52 | 10.95 |
| | D | 12.98 | 12.10 | 11.50 | 11.45 | 10.96 |
| | Aver. | 13.16 | 12.18 | 11.63 | 11.4 | 10.91 |
| | STDEV | 0.14 | 0.23 | 0.10 | 0.10 | 0.14 |
| Pellet volume [$cm^3$] | A | 1.044 | 0.952 | 0.918 | 0.887 | 0.840 |
| | B | 1.037 | 0.981 | 0.911 | 0.899 | 0.864 |
| | C | 1.031 | 0.940 | 0.921 | 0.904 | 0.860 |
| | D | 1.019 | 0.950 | 0.903 | 0.899 | 0.860 |
| Volume of solid particles [$cm^3$] | A | 0.6805 | 0.6510 | 0.6432 | 0.6389 | 0.6123 |
| | B | 0.6870 | 0.6739 | 0.6529 | 0.6418 | 0.6366 |
| | C | 0.6784 | 0.6420 | 0.6433 | 0.6508 | 0.6269 |
| | D | 0.6798 | 0.6565 | 0.6389 | 0.6476 | 0.6304 |
| Porosity [%] | A | 34.82 | 31.63 | 28.96 | 27.98 | 27.11 |
| | B | 33.75 | 31.32 | 29.36 | 28.59 | 26.35 |
| | C | 34.18 | 31.67 | 29.09 | 28.03 | 27.07 |
| | D | 33.29 | 30.88 | 28.74 | 27.95 | 26.73 |
| | Aver | 34.01 | 31.38 | 29.04 | 28.14 | 26.81 |
| | STDEV | 0.65 | 0.36 | 0.26 | 0.30 | 0.35 |

A,B,C and D: 4 different pellets for each sinter mixture

Aver.: average

STDEV: Standard deviation

Pellet volume = $\pi(1/4)*(\text{diameter of pellet})^2 * \text{length}$

Porosity = [(pellet volume-volume of solid particles)/pellet volume]*100

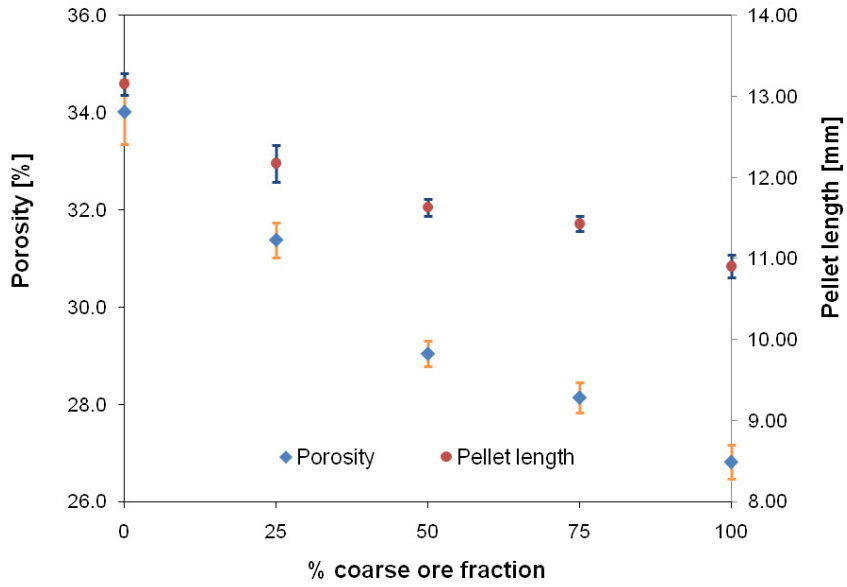


**Figure 33**. Effect of coarse ore fraction on porosity and length of pellets

It can be seen that the porosity as well as the length of pellet decrease with the replacement of fine particle by coarse particle. The particles are closer to each other in pellets consisting of more coarse particles than fine particles.

### IV.5.2 XRD, Optical microscopy and SEM results and discussion

The results presented in this chapter were obtained by using X-Ray Diffraction, reflected light optical microscopy and SEM/EDS analysis. The XRD analyses were used to quantify the mass% fraction of different phases in the sinters produced at 1300℃. Optical microscopy was only used for morphological analysis of the sinter phases, using polished sections of the samples. SEM analyses were done on the same polished sections of the sinters for identification and chemical analysis of the different phases.

#### IV.5.2.1 X-Ray Diffraction analysis

The mineral compositions of the sintered pellets produced in the sintering process at 1300℃, and for different fractions of Sishen coarse ore in the sinter mix are summarised in Table 13 and Appendix 4.

**Table 13** XRD analyses of sinters

| | Phase compositions [mass%] | | | | |
|---|---|---|---|---|---|
| | **Mix 1** | **Mix 2** | **Mix 3** | **Mix 4** | **Mix 5** |
| **Coarse ore fraction [%]** | **0%** | **25%** | **50%** | **75%** | **100%** |
| **C2S** | 9.37 | 7.59 | 6.08 | 3.01 | 4.58 |
| **Hematite** | 55.78 | 52.96 | 65.88 | 72.06 | 76.24 |
| **SFCA-I** | 5.99 | 6.13 | 4.35 | 8.41 | 10.68 |
| **SFCA** | 28.86 | 32.32 | 23.68 | 16.52 | 8.50 |
| **SFCA-I/SFCA** | 0.21 | 0.19 | 0.18 | 0.51 | 1.26 |

XRD quantification of the different sinter phases was also plotted as a function of fraction of coarse ore particles (Figures 34-37). It can be seen that the variation of the coarse ore fraction of the sinters influences the amount of the different sinter phases in the sintering process.

The variation in the fractions of the different sinter phases shows specific trends when the ratio between fines and coarse ore particles varies from 0% to 100%.

❖ **Hematite**

The amount of hematite is dependent on the fraction of coarse particles as shown in Table 13 and Figure 34. The smaller the size of the solid particles, the greater the reaction area and the greater is the amount of hematite assimilated. This complies with the DOE results (Section IV.4.5) which showed that the degree of assimilation is greater for fines that coarse particles because of the importance of available reaction surface area. For fine particles, sintering reactions are fast, and melt formation is significant. The fraction of relict particles in the sintered pellets from fine ore is therefore small compared to sinters prepared from coarse particles [6,36].

Although the reaction area of particles and volume of the melt were not specifically measured, the presence of 25% coarse ore in the sinter mix resulted in a decrease in amounts of hematite. This is presumably due to the increase in packing density,

which is associated with a decrease in porosity of the compacted pellets when fine particles are replaced by coarse particles (Table 12 and Figure 33). Pellets with 100% fine particles had an average porosity of 34.01%, while those from 25% coarse ore had an average porosity of 31.38%. The incorporation of coarse ore produced a compacted pellet with lower porosity (higher packing density). The solid particles were closer, resulting in an increase in the sintering rate, and the concentrations in hematite decreased.

Above 25% coarse particles, the level of hematite starts to increase. This is presumably due to the decrease in reaction area of the sinter mixtures with more coarse particles [40,48]. It can be established that the effect of porosity of the investigated pellets on the sintering reactions was less significant than that of the reaction surface area of solid particles, for pellets consisting of more than 25% coarse ore particles.

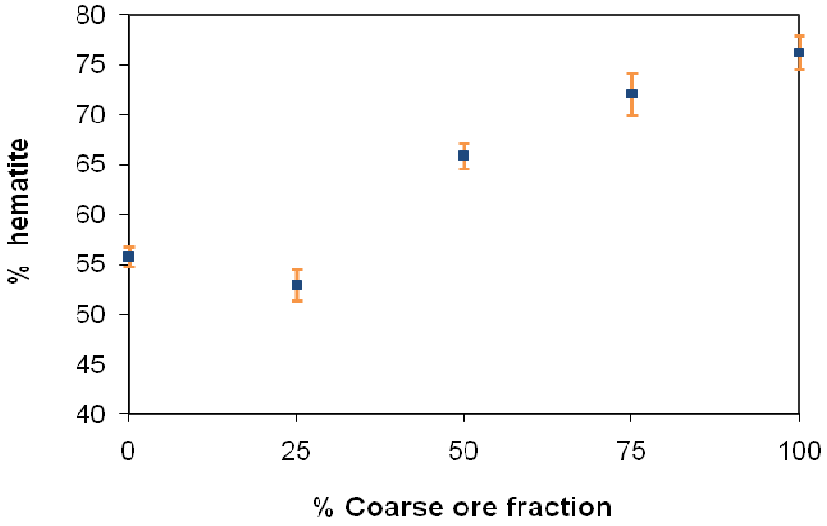


**Figure 34**. Variation of percentage hematite with coarse ore fraction

### ❖ Columnar SFCA

The sintering reactions mainly involved the formation of the melt from fine iron ore and the assimilation of coarse iron ore particles, resulting in a crystallization of SFCA as bonding phase. During sintering, different types of SFCA can form, and their concentrations depend on the sintering conditions.

The variation of columnar SFCA with the coarse ore fraction is given in Figure 35. For the sinter mix with 0% of coarse ore, fine particles can react quickly and SFCA can be formed in high concentrations. The replacement of 25% fine iron ore by coarse ore resulted in the formation of more SFCA than that from 100% fine ore. The packing density formed with only fine iron ore particles is associated with the highest porosity (34.01%), which is higher than that obtained with the introduction of 25% coarse iron ore (31.38%). Solid particles are closer in Mix 2, and can react faster and produce more SFCA.

In compacted pellets, an increase in packing density or a decrease in green porosity influence the surface contact between solid particles, resulting in an increase in sintering rate [54-56].

It can also be seen that the amount of SFCA reached a maximum and decreased for a further replacement of fine iron ore by coarse ore (Figure 35). This is presumably due to combined effects between the surface area for reaction and the porosity (packing density) of the pellet. Compacted pellets with more than 25% coarse ore fraction had low porosities (high packing density), but the surface area for reaction to take place decreased with a further increase in percentage coarse ore [40,48]. The effect of reaction area on the formation of SFCA appeared to be more significant than that of porosity for pellets consisting of more than 25% coarse ore. The assimilation of coarse ore is lower than that for fine iron ore, and the concentrations of SFCA in the final sinter are lower [40,48].

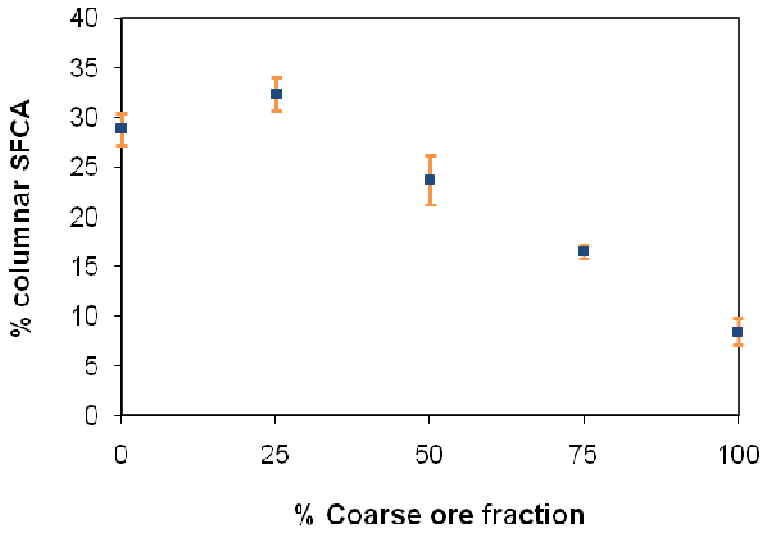


**Figure 35.** Variation of percentage SFCA with coarse ore fraction

### ❖ Acicular SFCA

The variation in SFCA-I fraction is not significant with the replacement of fine iron ore by coarse ore (Figure 36). However, it can be seen that an increase in the coarse ore fraction leads to a slight increase in SFCA-I content. The assimilation reaction is determinant for a mixture consisting of high fractions of coarse ore particles, and forms more SFCA-I than columnar SFCA. These results agree with those found by Hida *et al.* [37] where SFCA-I was reported to form by assimilation reactions, while SFCA crystallized by exsolution from the melt.

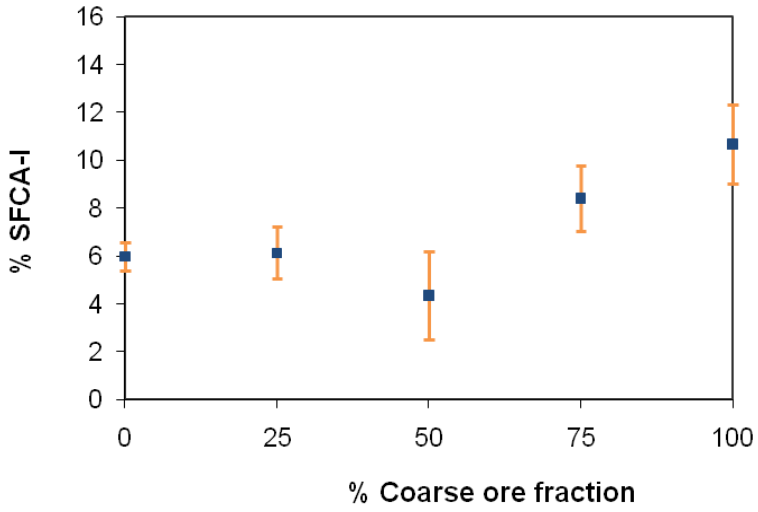


**Figure 36.** Variation of percentage SFCA-I with coarse fraction ore

### ❖ Calcium silicates

The X-ray diffraction analysis confirmed that some calcium silicate ($C_2S$) formed during experimental sintering. Figure 37 displays a trend where the amount of calcium silicates decreased with the replacement of fine iron ore by coarse particles. It can be seen that the formation of calcium silicates is dependent on the percentage $SiO_2$ in different sinter mixtures. The mixture containing only fine iron ore (Table 3) had the highest concentration of silica, and formed a sinter with the highest percentage calcium silicate. The replacement of fine iron ore by coarse ore decreased in $SiO_2$ content in the pellets, resulting in a decrease in the amounts of calcium silicates.

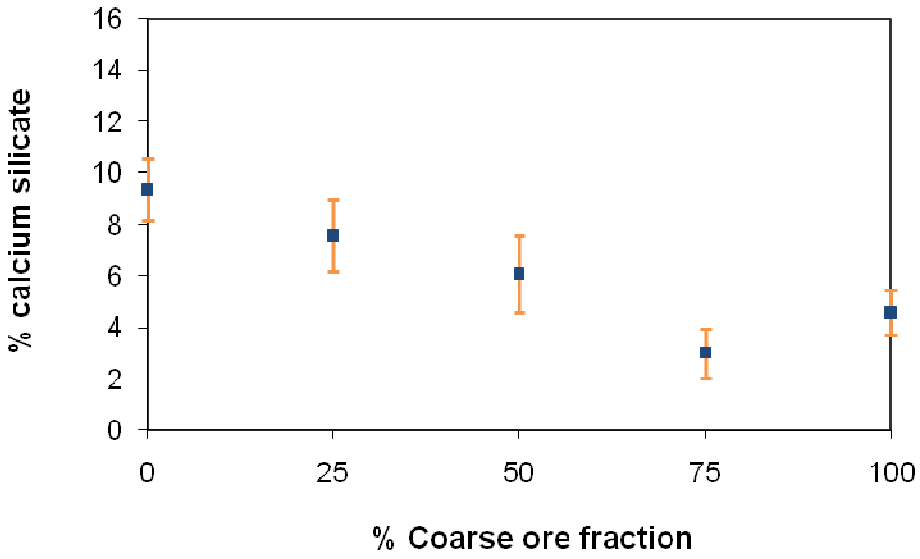


**Figure 37.** Variation of percentage calcium silicate with coarse ore fraction

### IV.5.2.2 Optical microscopy

Optical micrographs of the major sinter phases that formed at 1300℃ are shown in Figures 38-42. Based on differences in reflectance between sinter phases, optical micrographs of the sintered pellets clearly reveal two distinct phases. The bright phase is relict hematite surrounded by the grey phase of SFCA. These phases form a heterogeneous texture as is typical in industrial sinters [34].

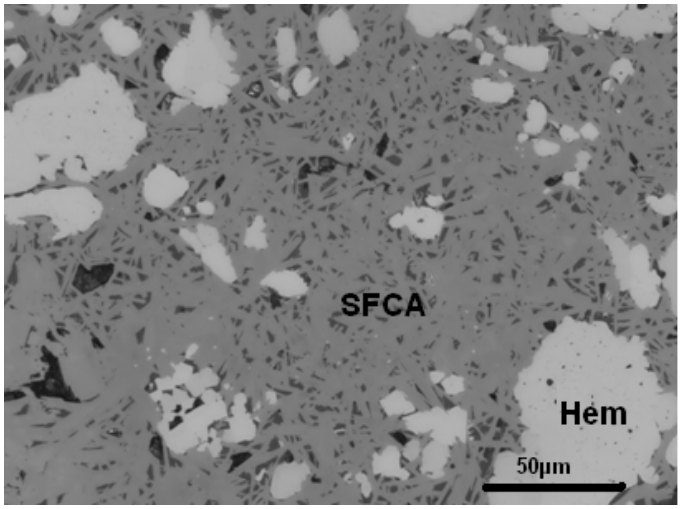


**Figure 38**. Optical micrograph of sinter with 0% coarse ore particle showing Hematite (Hem) and SFCA

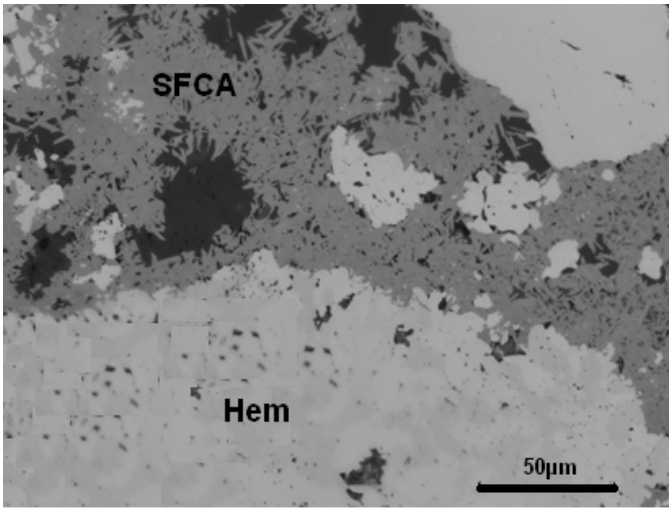


**Figure 39**. Optical micrograph of sinter with 25% coarse ore particle showing Hematite (Hem) and SFCA

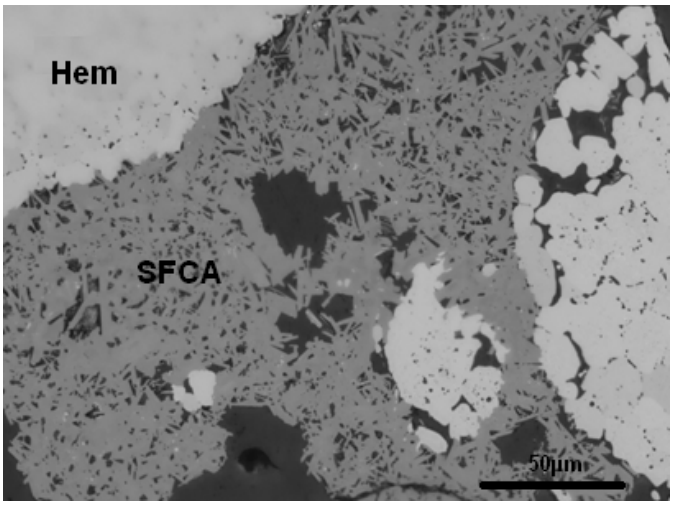


**Figure 40**. Optical micrograph of sinter with 50% coarse ore particle showing Hematite (Hem) and SFCA

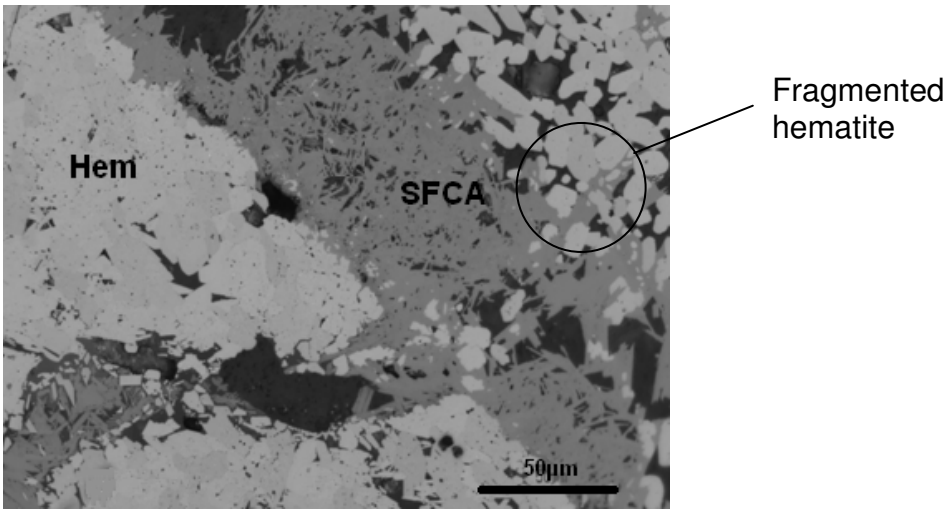


**Figure 41.** Optical micrograph of sinter with 75% coarse ore particle showing Hematite (Hem) and SFCA

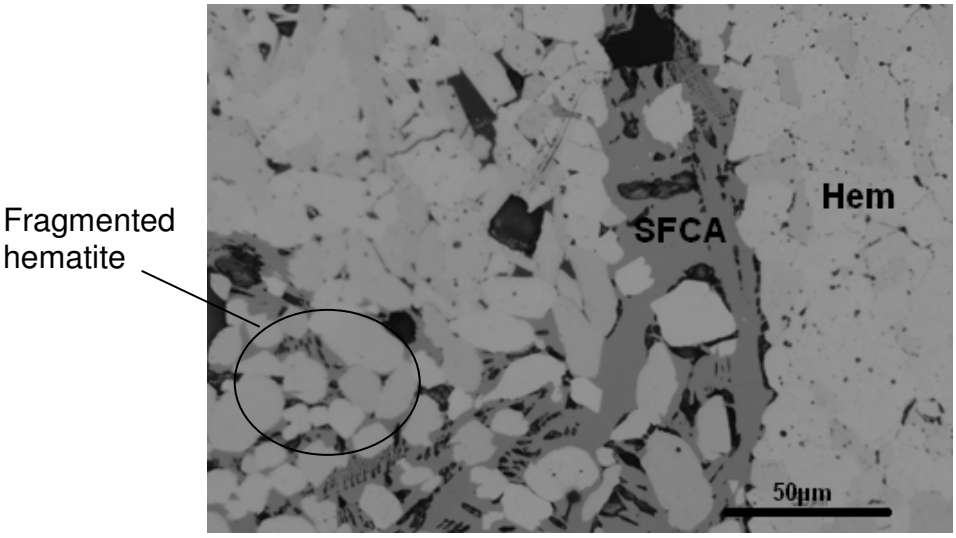


**Figure 42**. Optical micrograph of sinter with 100% coarse ore particle showing Hematite (Hem) and SFCA

The replacement of fine ore by coarse ore resulted in the formation of sinters with more hematite and less SFCA. Fines are more reactive than coarse ore and produce more melt that can promote the assimilation of solid particles into the melt.

As shown in Figures 38-42, the initial raw material has reacted although short reaction times were used. The hematite was mostly identified as relict hematite, which resulted from partial reactions between iron ores and lime, followed by slight assimilation of iron ores into the melt. Some of the relict hematite grains maintained the external forms of the original grains and some had subhedral and anhedral edges as a consequence of destabilisation by SFCA formation under prevailing sintering conditions [15,16].

For the investigated sinters, the distinction between acicular and columnar SFCA was not clear. Most of the bonding phase appeared to be columnar SFCA. This is similar to what was found in recent investigations where it was reported that acicular SFCA can appear platy and be easily confused with columnar SFCA [69]. The use of other analysis techniques therefore becomes of importance to accurately classify the different types of SFCA.

From the microstructure of sinter with 0% coarse ore shown in Figure 38, it can be seen that sintering reactions have occurred resulting in the formation of SFCA as the bonding phase. Relict hematite is still present despite the high fraction of fine iron ore in the sinter mixture.

When the fraction of coarse ore is increased above 50%, the volume of relict hematite is increased whereas the amount of SFCA is decreased as shown in Figures 41 and 42. It can also be seen that some coarse particles have been severely fragmented. This could be due to cracking and stresses generated at the contacts of coarse particles during compaction and reacting of the sinter mix. This is similar to what has been found during sintering of mixed powders consisting mostly of large particles [7]. The liquid is reported to create an attractive force between particles, putting the particle contact in compression. This generates a high dislocation density at the grain boundary and induces liquid penetration. Further, the liquid spreads through the pore (cracks) and grain structure by a combination of reaction and capillary forces. Consequently, the solid particle structure is fragmented and the uneven distribution of the liquid produces a process of clustering, resulting in closer packing of wetted particles [7].

### IV.5.2.3 Scanning Electron Microscopy

The polished sections of the sinter pellets were gold coated and examined using a JOEL JSM-6300 scanning electron microscope (SEM), with an acceleration voltage of 20kV. Energy dispersive X-ray spectrometry (EDS) was used to determine the chemical composition of the SFCA phase. The points that were analysed with EDS are marked on the backscattered electron images in Figures 43-47, and their chemical compositions given in Table 14.

The morphology of the different phases in the sinter pellets are given in Figures 43-47. It can be seen that the sinter phases which are clearly distinguishable are hematite (bright) and SFCA (grey). The distinction between different types of SFCA was not evident. This can be due to slight chemical differences between the types of SFCA.

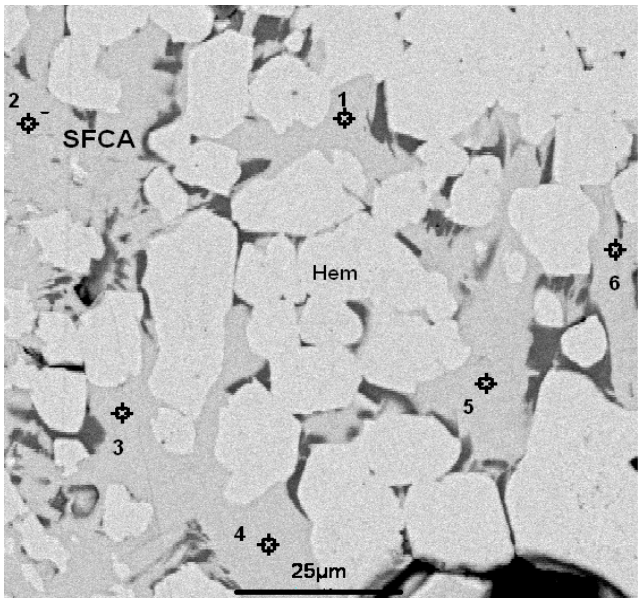


**Figure 43**. Backscattered electron image of sinter with 0% coarse ore particle, showing Hematite (Hem) and SFCA

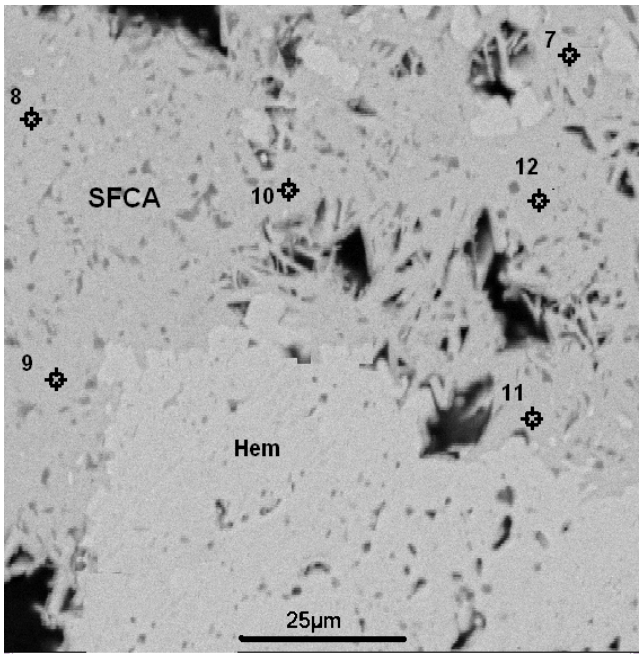


**Figure 44.** Backscattered electron image of sinter with 25% coarse ore particle showing Hematite (Hem) and SFCA

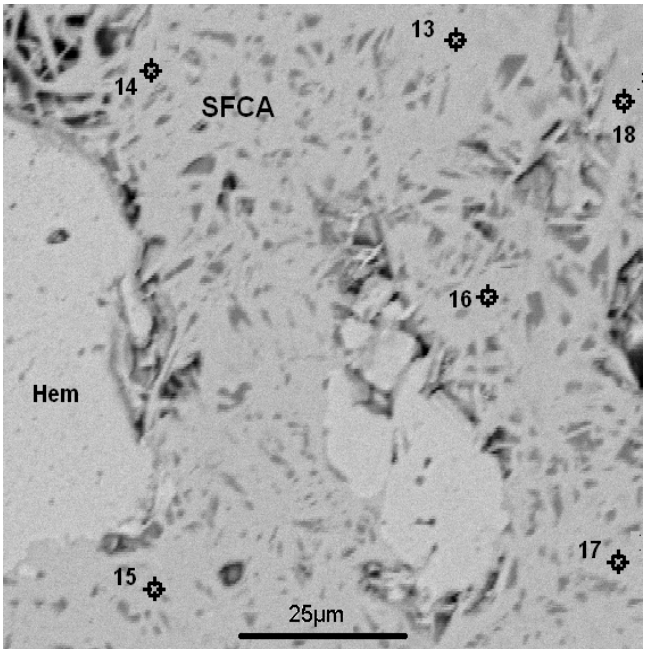


**Figure 45**. Backscattered electron image of sinter with 50% coarse ore particle, showing Hematite (Hem) and SFCA

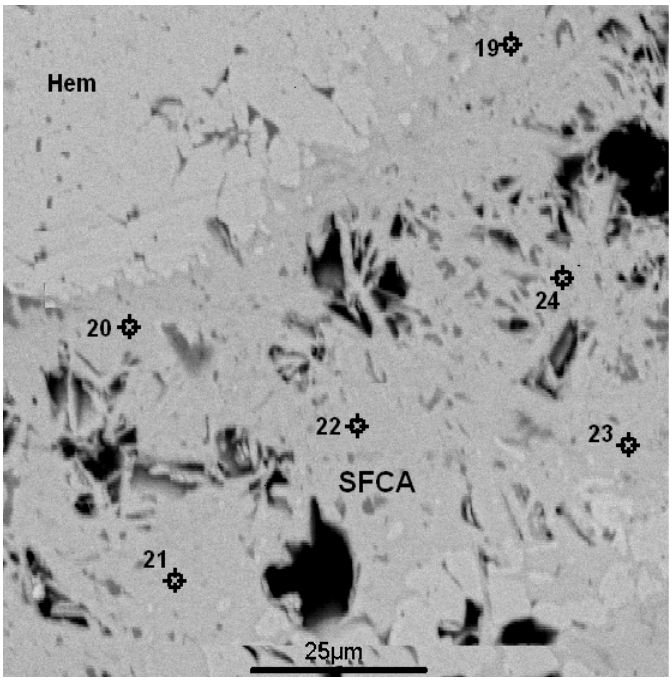


**Figure 46**. Backscattered electron image of sinter with 75% coarse ore particle, showing Hematite (Hem) and SFCA

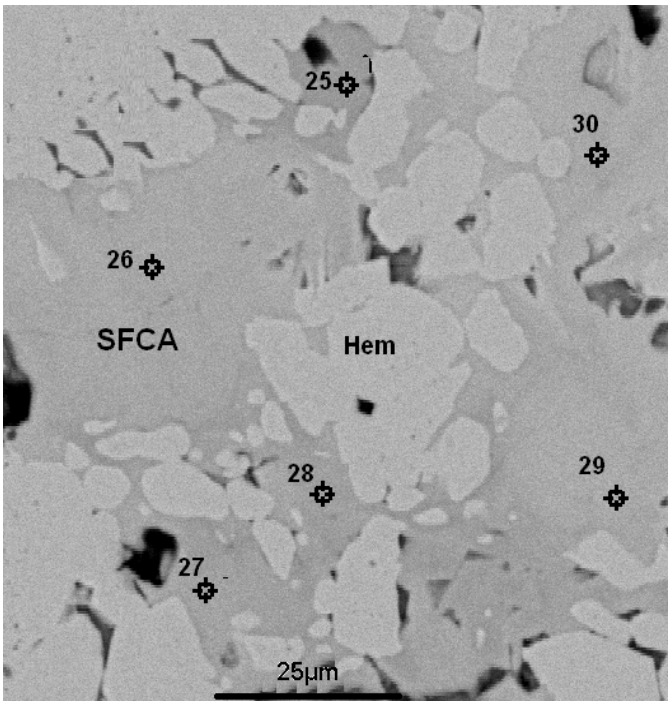


**Figure 47**. Backscattered electron image of sinter with 100% coarse ore particle, showing Hematite (Hem) and SFCA

**Table 14** Chemical compositions of SFCA phase using EDS analysis.

| Sample | Points | Chemical composition (wt%) | | | | | | | | Stoichiometry | |
|---|---|---|---|---|---|---|---|---|---|---|---|
| | | $Fe_2O_3$ | $SiO_2$ | $Al_2O_3$ | MnO | CaO | $K_2O$ | MgO | Total | $M_{14}O_{20}$ (SFCA) | $M_{20}O_{28}$ (SFCA-I) |
| Mix 1 | 1 | 83.5 | 1.8 | 2.5 | 1 | 10 | 0 | 1.1 | 99.9 | $M_{13.98}O_{20}$ | $M_{19.57}O_{28}$ |
| | 2 | 84.6 | 2.3 | 2.5 | 0.7 | 9.3 | 0 | 0.5 | 99.9 | $M_{13.84}O_{20}$ | $M_{19.38}O_{28}$ |
| | 3 | 82.3 | 2.2 | 2.3 | 0.8 | 11.8 | 0 | 0.5 | 99.9 | $M_{14.01}O_{20}$ | $M_{19.62}O_{28}$ |
| | 4 | 79.9 | 4 | 2 | 0.5 | 13.3 | 0 | 0.3 | 100.0 | $M_{13.96}O_{20}$ | $M_{19.54}O_{28}$ |
| | 5 | 80.6 | 3.9 | 1.7 | 0 | 13.3 | 0.1 | 0.3 | 99.9 | $M_{14.01}O_{20}$ | $M_{19.62}O_{28}$ |
| | 6 | 80.3 | 3.9 | 1.5 | 0.4 | 13.7 | 0.1 | 0.1 | 100.0 | $M_{14.05}O_{20}$ | $M_{19.67}O_{28}$ |
| Mix 2 | 7 | 82.7 | 3 | 0.7 | 0.3 | 13.1 | 0.1 | 0.1 | 100.0 | $M_{13.95}O_{20}$ | $M_{19.52}O_{28}$ |
| | 8 | 79 | 4.1 | 1.6 | 0.3 | 14.7 | 0.1 | 0.2 | 100.0 | $M_{14.00}O_{20}$ | $M_{19.60}O_{28}$ |
| | 9 | 81.8 | 3.3 | 1.1 | 0.3 | 13.2 | 0.1 | 0.2 | 100.0 | $M_{14.05}O_{20}$ | $M_{19.67}O_{28}$ |
| | 10 | 81.9 | 3.4 | 1.5 | 0.3 | 12.7 | 0 | 0.2 | 100.0 | $M_{13.92}O_{20}$ | $M_{19.49}O_{28}$ |
| | 11 | 79.2 | 4.8 | 1.8 | 0.5 | 13.2 | 0.3 | 0.2 | 100.0 | $M_{13.96}O_{20}$ | $M_{19.54}O_{28}$ |
| | 12 | 80 | 5.1 | 1.8 | 0.4 | 12.2 | 0.2 | 0.3 | 100.0 | $M_{13.84}O_{20}$ | $M_{19.38}O_{28}$ |
| Mix 3 | 13 | 79.3 | 4 | 2.8 | 0.4 | 13.2 | 0 | 0.3 | 100.0 | $M_{13.96}O_{20}$ | $M_{19.54}O_{28}$ |
| | 14 | 80.3 | 3.8 | 2.2 | 0.3 | 13 | 0 | 0.3 | 99.9 | $M_{13.96}O_{20}$ | $M_{19.54}O_{28}$ |
| | 15 | 81 | 3.6 | 1.9 | 0.4 | 12.8 | 0 | 0.3 | 100.0 | $M_{13.96}O_{20}$ | $M_{19.54}O_{28}$ |
| | 16 | 79.5 | 4.4 | 1.1 | 0.3 | 14.5 | 0.1 | 0.1 | 100.0 | $M_{14.05}O_{20}$ | $M_{19.67}O_{28}$ |
| | 17 | 78.6 | 4.2 | 1.4 | 0.4 | 15.2 | 0.1 | 0.1 | 100.0 | $M_{14.04}O_{20}$ | $M_{19.65}O_{28}$ |
| | 18 | 80.1 | 3.4 | 1.4 | 0.4 | 14.4 | 0 | 0.4 | 100.1 | $M_{14.07}O_{20}$ | $M_{19.70}O_{28}$ |
| Mix 4 | 19 | 82.5 | 2.5 | 1.5 | 0.2 | 13.1 | 0.1 | 0.2 | 100.1 | $M_{14.05}O_{20}$ | $M_{19.67}O_{28}$ |
| | 20 | 81.9 | 2.9 | 1.8 | 0.2 | 13.1 | 0 | 0.1 | 100.0 | $M_{14.01}O_{20}$ | $M_{19.62}O_{28}$ |
| | 21 | 84.6 | 1.7 | 0.9 | 0.1 | 12.7 | 0 | 0 | 100.0 | $M_{14.01}O_{20}$ | $M_{19.62}O_{28}$ |
| | 22 | 82.2 | 2.1 | 1.3 | 0.1 | 14.3 | 0 | 0 | 100.0 | $M_{14.10}O_{20}$ | $M_{19.73}O_{28}$ |
| | 23 | 83.7 | 1.7 | 0.9 | 0.2 | 13.5 | 0 | 0 | 100.0 | $M_{14.07}O_{20}$ | $M_{19.70}O_{28}$ |
| | 24 | 80 | 2.9 | 2.1 | 0.2 | 14.5 | 0 | 0.2 | 99.9 | $M_{14.00}O_{20}$ | $M_{19.60}O_{28}$ |
| Mix 5 | 25 | 84.7 | 2.1 | 1.4 | 0.1 | 11.6 | 0 | 0.1 | 100.0 | $M_{13.96}O_{20}$ | $M_{19.54}O_{28}$ |
| | 26 | 80.3 | 3.7 | 2.9 | 0.1 | 12.7 | 0 | 0.3 | 100.0 | $M_{13.92}O_{20}$ | $M_{19.49}O_{28}$ |
| | 27 | 80 | 3.2 | 2.9 | 0.2 | 13.2 | 0.1 | 0.3 | 99.9 | $M_{13.98}O_{20}$ | $M_{19.57}O_{28}$ |
| | 28 | 80.3 | 3.4 | 3.4 | 0.1 | 12.4 | 0 | 0.3 | 99.9 | $M_{13.93}O_{20}$ | $M_{19.51}O_{28}$ |
| | 29 | 81.4 | 2.8 | 2.7 | 0.1 | 12.6 | 0.1 | 0.3 | 100.0 | $M_{13.96}O_{20}$ | $M_{19.54}O_{28}$ |
| | 30 | 82.1 | 2.6 | 2.7 | 0.1 | 12.1 | 0 | 0.3 | 99.9 | $M_{13.96}O_{20}$ | $M_{19.54}O_{28}$ |

Calculations of stoichiometries of the analysed SFCA phases from the EDS analyses did not permit a clear distinction between the two types of SFCA, based on the $M_{14}O_{20}$ (SFCA) and $M_{20}O_{28}$ (SFCA-I) structures that Mumme *et al.*[20] and Mumme [21] identified.

The EDS analyses of the SFCA phases were plotted on the (0-5)wt% $Al_2O_3$ - $SiO_2$ - CaO - $Fe_2O_3$ plane, which was proposed by Pownceby and Clout [24] (Figures 48-52). Chemical compositions of the SFCA phases were close to the regions of SFCA and SFCA-I. It can also be seen that the replacement of fine iron ore by coarse ore slightly moves most of the chemical compositions of SFCA towards the area that is referred to as SFCA-I (Figures 50-52). This can confirm the XRD results, which reported that high fractions of coarse ore in pellets favour the formation of SFCA-I more than that of columnar SFCA.

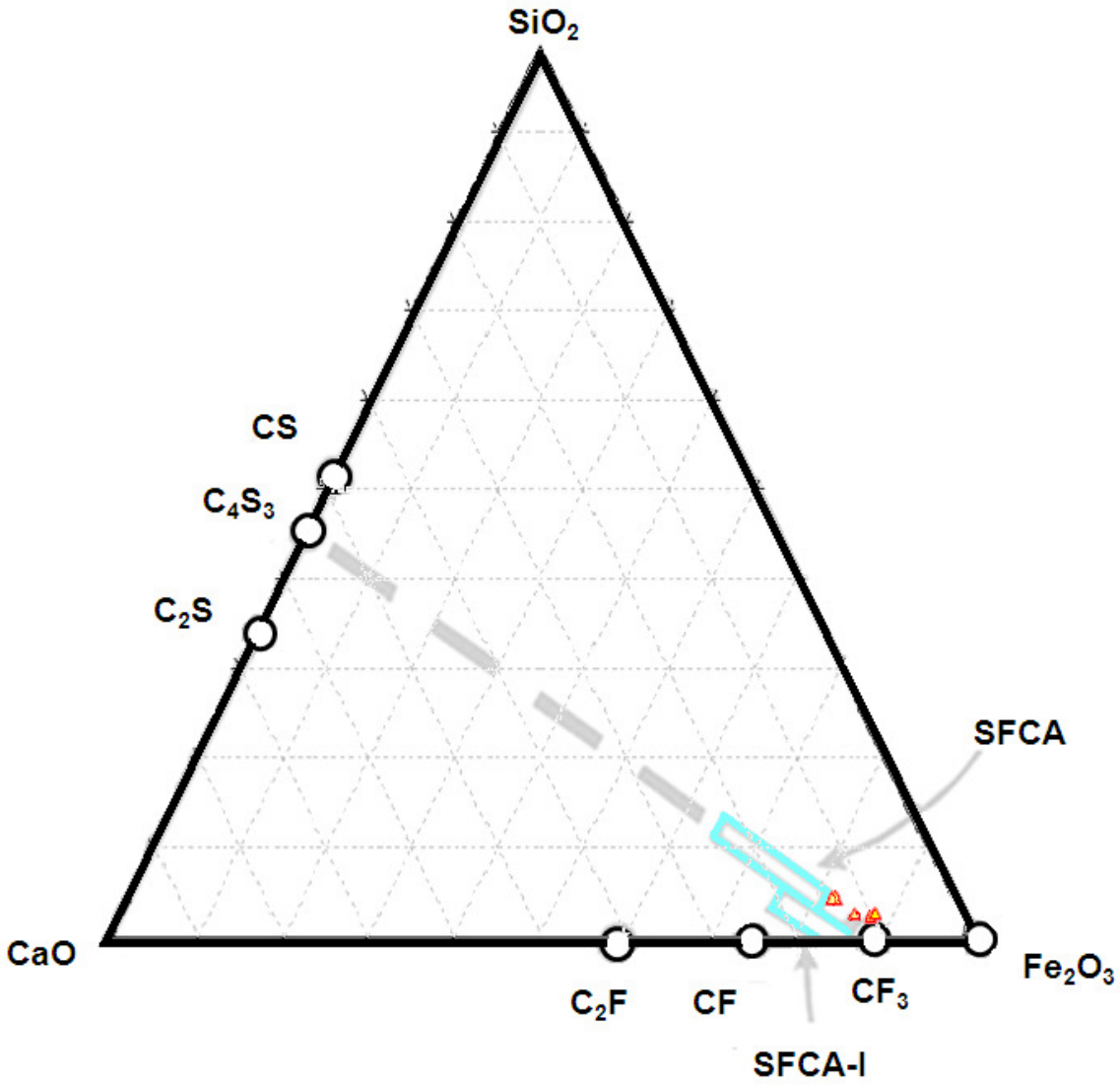


**Figure 48**. Chemical compositions of the SFCA phases in the sintered pellets with 0% coarse ore plotted on the (0-5)wt% $Al_2O_3$ - $SiO_2$ - CaO - $Fe_2O_3$ plane described by Pownceby and Clout [24]

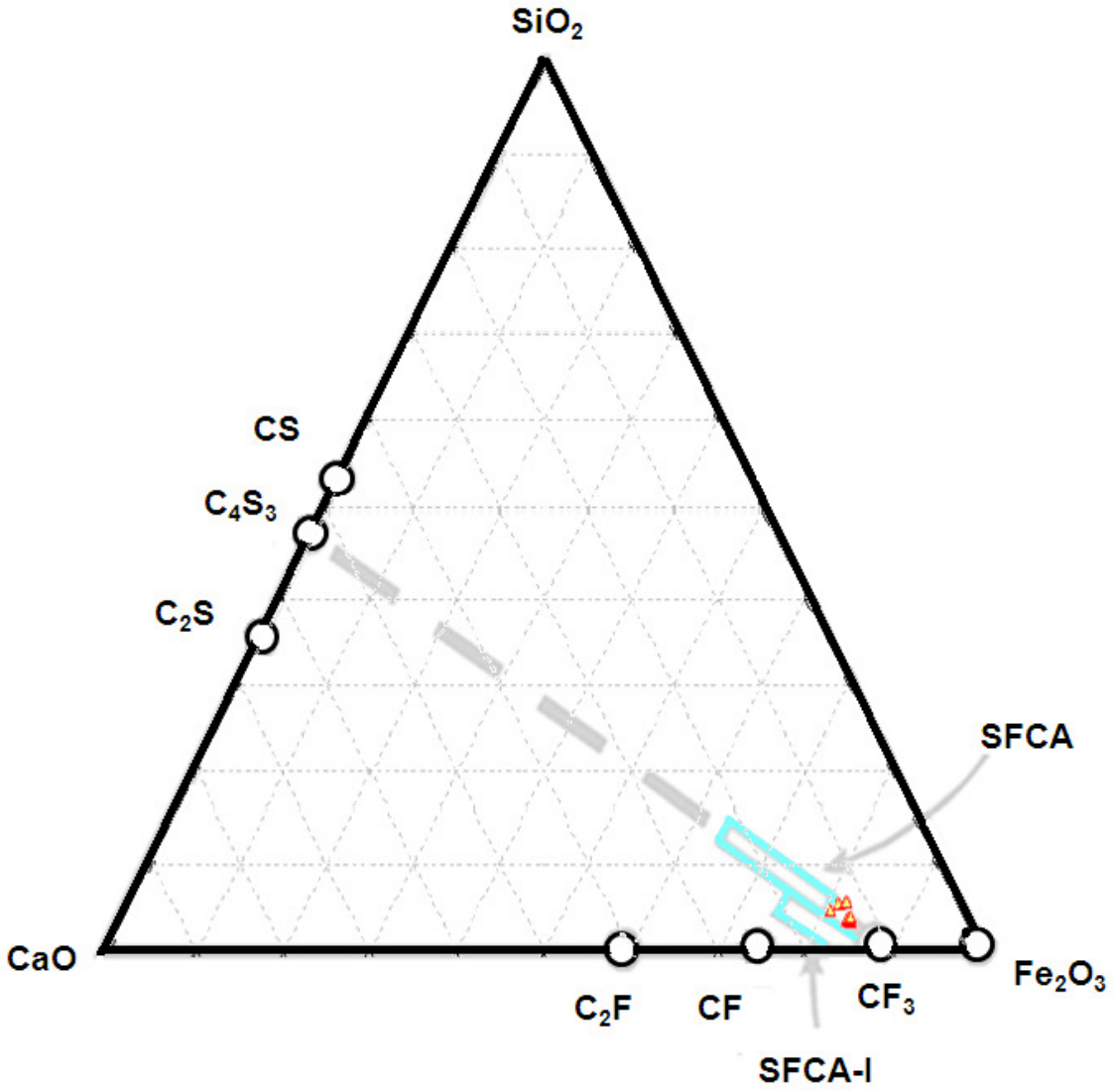


**Figure 49**. Chemical compositions of the SFCA phases in the sintered pellets with 25% coarse ore plotted on the (0-5)wt% $Al_2O_3$ - $SiO_2$ - CaO - $Fe_2O_3$ plane described by Pownceby and Clout [24]

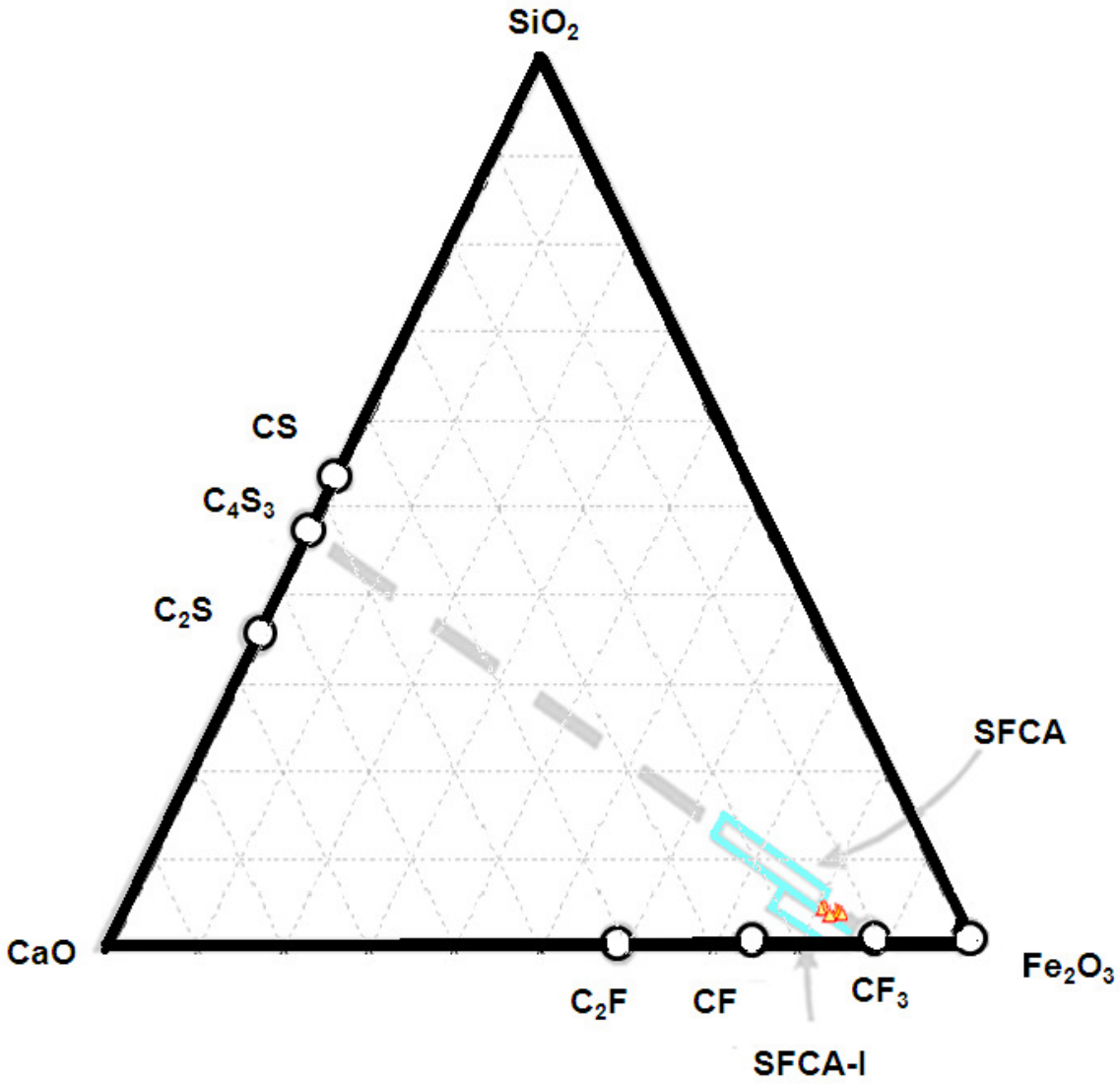


**Figure 50.** Chemical compositions of the SFCA phases in the sintered pellets with 50% coarse ore plotted on the (0-5)wt% $Al_2O_3$ - $SiO_2$ - CaO - $Fe_2O_3$ plane described by Pownceby and Clout [24]

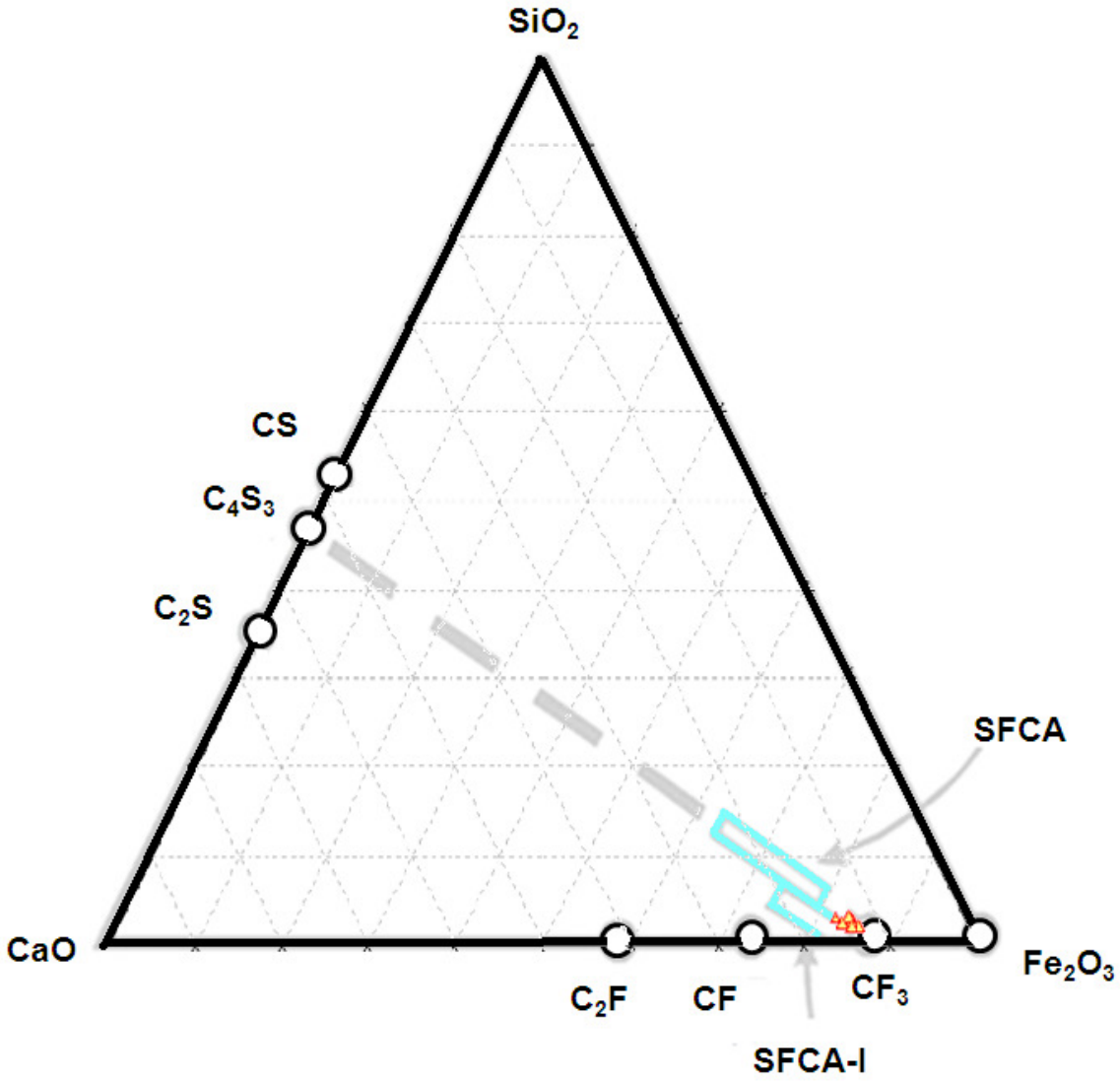


**Figure 51.** Chemical compositions of the SFCA phases in the sintered pellets with 75% coarse ore plotted on the (0-5)wt% $Al_2O_3$ - $SiO_2$ - CaO - $Fe_2O_3$ plane described by Pownceby and Clout [24]

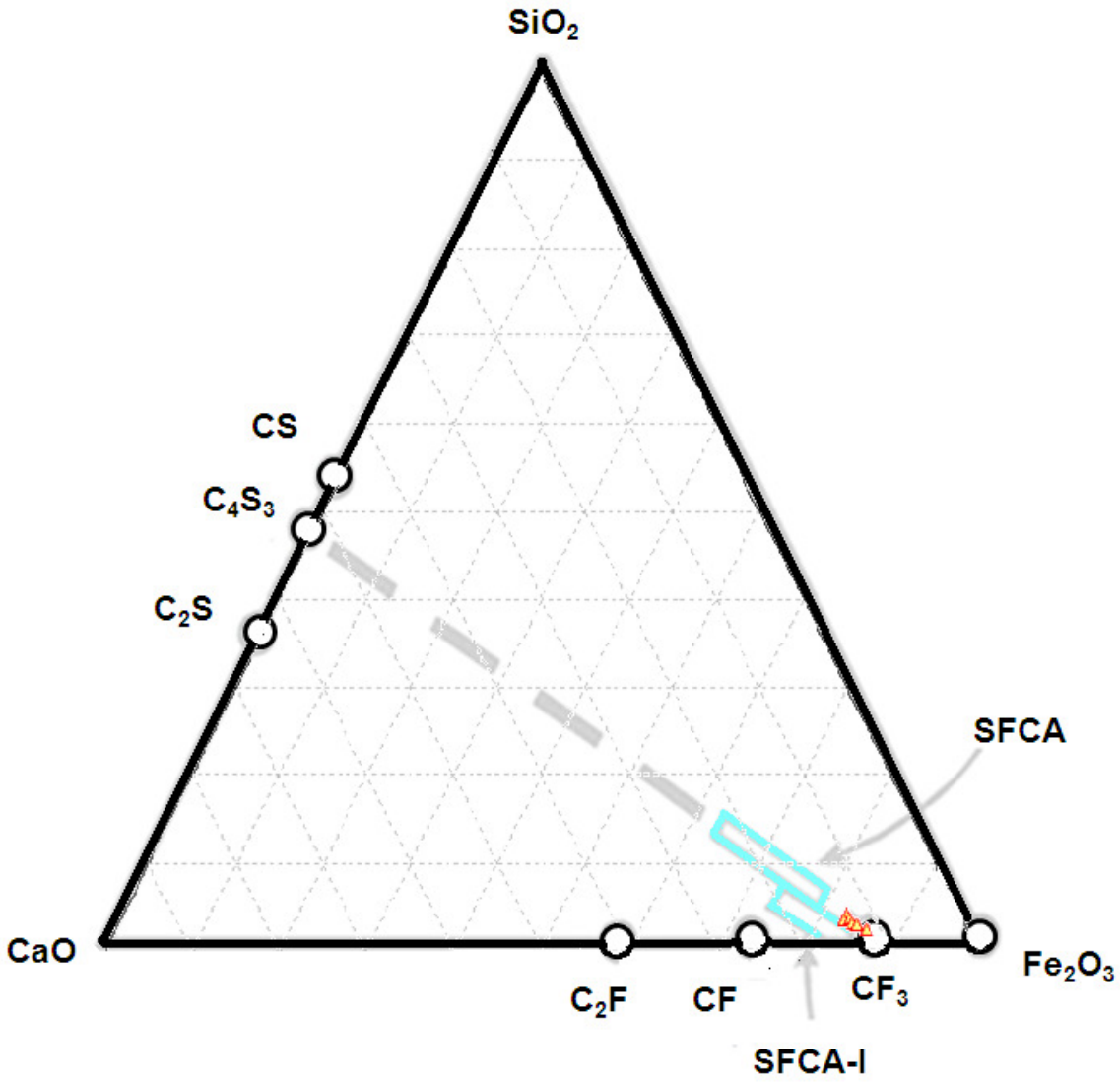


**Figure 52.** Chemical compositions of the SFCA phases in the sintered pellets with 100% coarse ore plotted on the (0-5)wt% $Al_2O_3$ - $SiO_2$ - CaO - $Fe_2O_3$ plane described by Pownceby and Clout [24]

### IV.5.2.4 Conclusions on XRD, Optical microscopy and SEM analyses

The replacement of fine iron ore by coarse ore in the sinter mix influenced the formation of both acicular SFCA (SFCA-I) and columnar SFCA (SFCA).

From XRD analysis, the proportions of SFCA in sinter pellets are slightly increased when the fraction of coarse ore varies from 0% to 25%, but decreases with a further increase in percentage coarse ore. Compacted pellets with 0% coarse ore had a higher porosity than those that were formed with the incorporation of coarse ore. At 25% coarse ore fraction, the porosity of the compacted pellets decreased, resulting in an increase in packing density and sintering rate. More hematite reacted, resulting in the formation of high amounts of SFCA. Above 25% coarse ore fraction, the amount of hematite increased, and the concentrations of columnar SFCA decreased despite a further decrease in porosity (increase in packing density). This was attributed to the decrease in reaction surface area for coarse ore, and the short reaction time, which limited the extent of reaction of the coarse particles. The formation of SFCA-I was slightly dependent on the replacement of fine iron ore by coarse ore. Increasing the coarse ore fraction slightly favoured the formation of SFCA-I under laboratory conditions.

Two major sinter phases could easily be identified by optical microscopy and SEM analysis: hematite and SFCA. A clear distinction between the different types of SFCA could not be made using EDS analysis.
The chemical compositions of the analysed SFCA phases were subsequently plotted on the (0-5)wt% $Al_2O_3$ - $SiO_2$ - CaO - $Fe_2O_3$ plane. These compositions of SFCA were close to the regions of SFCA and SFCA-I. For pellets with more than 50% coarse ore, the chemical compositions of the SFCA phases tend to be concentrated in the SFCA-I region.

## V. Grate pot tests

The main purpose of this chapter was to generate pilot plant scale data in order to assess the quality of the sinter when some of the fine iron ore is replaced with coarse ore. These results were used to compare the physical and mineralogical characteristics of these different sinter cakes.

As discussed previously, the proportion of coarse particles is the key parameter which is used to control the permeability of the sinter bed. A mixture with only fine ore forms a sinter bed with low permeability, which directly affects the sinter productivity and quality. The replacement of fine iron ore by coarse ore increases the permeability of the sinter bed, resulting in a more stable gas flow in the sinter bed, and increases sinter productivity. However, a sinter mix with a high fraction of coarse ore might produce a sinter with low strength [13,14,15]. The amount of coarse particles must therefore be optimised to produce a sinter with the best possible properties.

### V.1 Preparation of sinter mixtures

Sinter mixtures were prepared using the same ratios of iron ores as those used in the laboratory tests. The particle size distributions for different iron ores is given in Table 15. The average particle sizes of Thabazimbi and Sishen fine iron ore are respectively 2.94 mm and 2.76 mm and that of Sishen coarse ore is 6.72 mm.

**Table 15** Particle size distributions of the ores

| | Sieve size (mm) | | | | | | | $D_{50}$ |
|---|---|---|---|---|---|---|---|---|
| | +8 | +5 | +3.35 | +1 | +0.106 | +0.045 | -0.045 | |
| **Thabazimbi fine ore** | 1 | 21 | 20 | 27 | 25 | 5 | 1 | 2.94 |
| **Sishen fine ore** | 0 | 10 | 30 | 42 | 18 | 0 | 0 | 2.76 |
| **Sishen coarse ore** | 15 | 73 | 10 | 10 | 1 | 0 | 0 | 6.72 |

Referring to laboratory tests and Anglo American Kumba Iron Ore specifications, five mixtures were prepared, using the coarse ore in fractions ranging from 0% to 100%,

with increments of 25%. Tables 16 and 17 respectively display the Anglo American Kumba Iron Ore specifications and the compositions of the different sinter mixtures.

**Table 16** Kumba Iron Ore Specifications

| Parameters | Range |
|---|---|
| Basicity CaO/SiO2 | 2.00 |
| FeO | 7.00 % |
| MgO | 2.00 % |

**Table 17** Proportions of raw materials in sinter mixtures

| Raw materials | Mass percent (mass %) | | | | |
|---|---|---|---|---|---|
| | **Mix1** | **Mix2** | **Mix3** | **Mix4** | **Mix5** |
| Thabazimbi fine ore | 35.59 | 29.12 | 17.74 | 8.85 | 0.00 |
| Sishen fine ore | 35.59 | 29.12 | 17.74 | 8.85 | 0.00 |
| Sishen coarse ore | 0.00 | 12.85 | 35.47 | 53.12 | 70.71 |
| Coke breeze | 3.43 | 3.43 | 3.43 | 3.43 | 3.43 |
| Anthracite | 1.47 | 1.47 | 1.47 | 1.47 | 1.47 |
| Limestone | 11.11 | 11.07 | 11.01 | 10.97 | 10.92 |
| Dolomite | 7.37 | 7.43 | 7.52 | 7.59 | 7.66 |
| Silica | 0.84 | 0.90 | 1.02 | 1.11 | 1.20 |
| Water | 4.60 | 4.60 | 4.60 | 4.60 | 4.60 |
| **Total** | **100** | **100** | **100** | **100** | **100** |

### V.2 Sintering procedure

All sintering tests were performed in sinter pots at Anglo American Kumba Iron Ore Pilot Plant. This pot is 516 m height, with a 0.160 $m^2$ grate area, and can treat approximately 150 kg of the sinter mixture. The raw materials were mixed for 30 seconds in a mixer, after which water was sprinkled over the mixture for 2 minutes. The fine particles immediately started adhering to coarse ore particles, pseudo-particles formed and were fed into the sinter pot via a conveyor belt. The sinter

mixture was ignited for one and a half minutes at approximately 1050℃ with a LP gas burner. During the ignition stage, a differential pressure of 180 mm water was maintained for the first 30 seconds and was then increased to 540 mm water for the last 60 seconds. Once the ignition was complete, the differential pressure was increased to 1200 mm water and kept constant for the rest of the test. The test was complete once the off gas reached a peak temperature indicating that the flame front had reached the bottom of the bed. The sinter cake was then taken out of the pot and subjected to a break down simulation [70]. Figure 53 shows a schematic sinter pot**.**

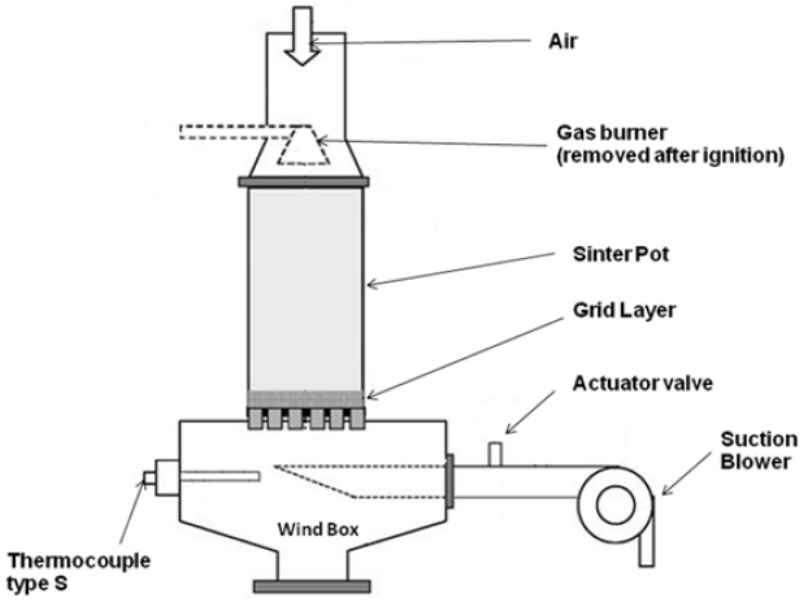


**Figure 53**. Sinter pot test equipment

## V.3 Results and discussion

The sinter samples were collected and subjected to several tests for the evaluation of physical and metallurgical properties of the sinter such as cold strength index, reducibility index and reduction disintegration index. Sinter samples were also taken for chemical and mineralogical analyses in order to determine the influence of sinter phases on sinter quality.

### V.3.1 Influence of coarse ore fraction on sinter production and mean particle size ($D_{50}$)

The results from different sinter pot tests are summarized in Table 18.

**Table 18** Production and particle size distribution of sinter

| | Mix 1 | Mix 2 | Mix 3 | Mix 4 | Mix 5 |
|---|---|---|---|---|---|
| **Production** | | | | | |
| Production rate [t/m$^2$/h] | 24.9 | 27.1 | 32.7 | 36.1 | 41.4 |
| Sintering time [min] | 29.4 | 29.2 | 25.1 | 22.6 | 21.0 |
| Sintering rate [mm/min] | 17.0 | 17.1 | 19.9 | 22.1 | 23.9 |
| Total fuel [kg/ton sinter] | 80.5 | 75.8 | 76.4 | 77.8 | 73.9 |
| Yield | 82.5 | 83.4 | 81.3 | 81.2 | 82.9 |
| Shrinkage of sinter cake [%] | 13.0 | 12.0 | 9.0 | 9.5 | 9.0 |
| **Sinter sieve analysis [mass%]** | | | | | |
| Fraction [mm] | | | | | |
| +40 | 7.4 | 2.7 | 1.3 | 1.6 | 0.9 |
| - 40 +25 | 12.1 | 9.4 | 7.0 | 3.6 | 3.4 |
| - 25 +16 | 18.3 | 19.3 | 16.0 | 9.8 | 8.1 |
| - 16 +12.5 | 10.0 | 12.1 | 13.5 | 11.6 | 10.2 |
| - 12.5 +10 | 7.4 | 11.0 | 12.3 | 13.5 | 12.0 |
| - 10 + 5 | 21.1 | 25.0 | 30.7 | 39.6 | 47.5 |
| - 5 (return fines) | 23.8 | 20.5 | 19.2 | 20.3 | 17.9 |
| Total | 100 | 100 | 100 | 100 | 100 |
| **$D_{50}$ (excluding the - 5 mm sinter)** | 20.0 | 16.6 | 14.6 | 12.7 | 11.7 |

#### V.3.1.1 Productivity and sintering rate

The production rate is a measure of the productivity or capacity of a sinter plant and strongly depends on the permeability of the sinter. It was found that the sinter productivity is increased with the increase in coarse ore fraction (Table 18 and Figure 54). The sinter mix with 0% coarse ore fraction has the lowest productivity (24.9t/m$^2$/h) whereas the productivity of the sinter from the mixture of 100% coarse

ore corresponds to the highest value (41.4t/m$^2$/h). This means that the replacement of fine iron ore by coarse ore results in an increase in the airflow rate and the speed of the flame front through the sinter bed.

The variation of the sintering rate or the flame front speed (FFS) was also plotted in Figure 54. The replacement of fine iron ore by coarse ore particles also enhanced the sintering rate.

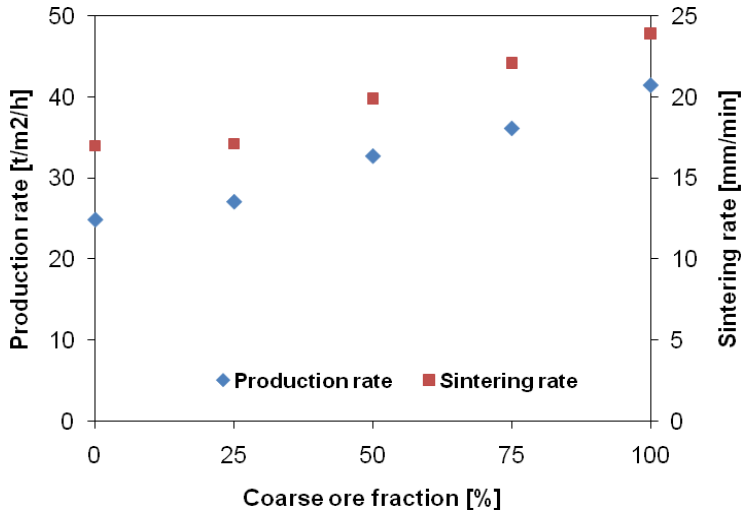


**Figure 54.** Influence of coarse ore fraction on production and sintering rates

Umadevi *et al.*[36] also found that sinter productivity and sintering rate decrease with a decrease in iron ore mean particle size due to the decrease in the airflow rate. Sintering time increases. The greater the proportion of coarse ore in the sinter bed, the greater the sintering rate.

### V.3.1.2 Consumption of fuel

The fuel consumption for the production of 1 ton of sinter decreased when fine iron ore was replaced with coarse ore (Table 18 and Figure 55). This means that sintering of the mixture with 0% of coarse ore requires more energy (80.5 kg fuel/ton sinter) than when more coarse ore is used to produce 1 ton of sinter. A mixture with 100% coarse ore had the lowest fuel consumption (73.9 kg fuel/ton sinter). This is presumably due to the high permeability of the sinter bed, resulting in a high sintering

rate and low contact time between hot gas and solid particles. The reaction time is short, and the assimilation reactions are low.

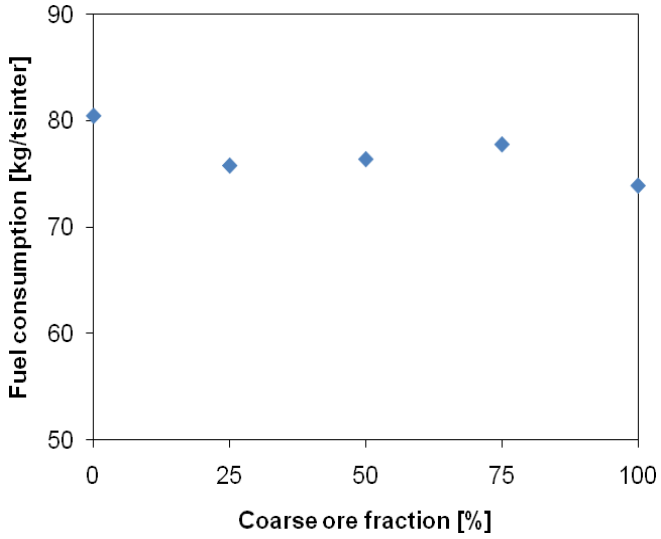


**Figure 55.** Influence of coarse ore fraction on fuel consumption

### V.3.1.3 Sinter yield

The yield is defined as the ratio of the mass of sinter produced to the total mass of the raw materials fed in the process. The sinter yield is not strongly affected by the replacement of fine iron ore by coarse ore as shown in Figure 56.

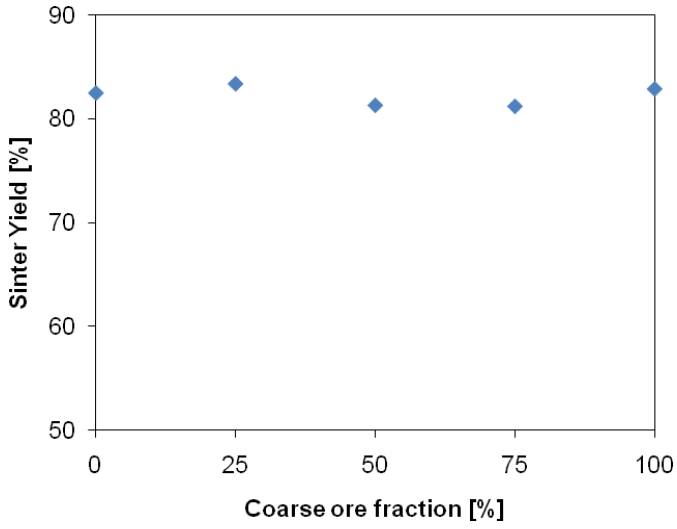


**Figure 56.** Influence of coarse ore fraction on sinter yield

### V.3.1.4 Particle size distribution of sinters

The average particle size ($D_{50}$) of the different sinters decreases with the replacement of the fine iron ore by coarse ore (Table 18 and Figure 57). The sinter mix with 0% coarse ore fraction has the highest average particle size (20mm) whereas the sinter produced with a mixture of 100% coarse ore has the lowest average particle size value (11.7mm).

It was also observed that the return fines (the -5 mm fraction) decreases with the increase in coarse ore fraction in the sinter mix. The sinter made with only fine iron ore has the highest proportion of return fines (23.8%). The replacement of fine iron ore by coarse ore decreased the amount of return fines (17.9%).

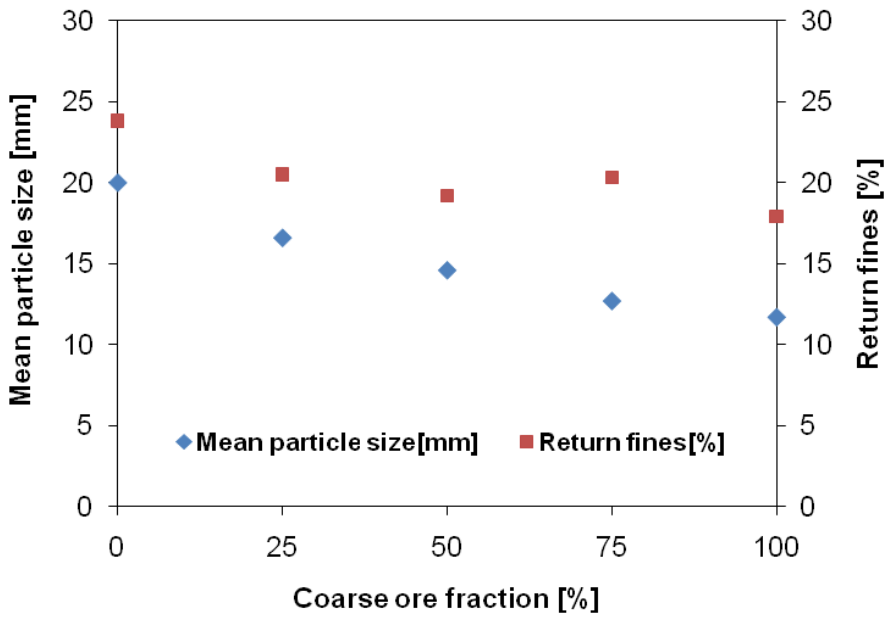


**Figure 57.** Influence of coarse ore fraction on average particle size and percentage return fines

### V.3.2 Influence of coarse ore fraction on mineral composition of sinters

The quantification of sinter phases was done by the powder diffraction technique (Rietveld method). The phase compositions of the different sinters that were produced are given in Table 19. The relationship of coarse ore fraction and formation of the sinter phases during pot tests is also given in Figures 58 and 59.

**Table 19** Quantitative XRD analysis of the sinters produced in the pot tests.

| Sinter phases | Proportions of phases [wt%] | | | | |
|---|---|---|---|---|---|
| | Mix1 | Mix2 | Mix 3 | Mix4 | Mix5 |
| Calcium silicates | 3.28 | 5.73 | 4.47 | 5.82 | 4.80 |
| Hematite | 40.32 | 42.95 | 51.81 | 54.80 | 64.39 |
| Magnetite/magnesioferrite | 25.80 | 23.15 | 19.67 | 16.59 | 10.45 |
| SFCA | 15.63 | 10.07 | 8.94 | 10.85 | 6.10 |
| SFCA-I | 14.97 | 18.11 | 15.11 | 11.94 | 14.26 |
| SFCA total | 30.60 | 28.18 | 24.04 | 22.80 | 20.36 |
| SFCA-I/SFCA | 0.96 | 1.80 | 1.69 | 1.10 | 2.34 |

The replacement of fine iron ore by coarse ore resulted in an increase in the amount of hematite (Figure 58). The increase in coarse ore fraction in the sinter bed results in a decrease in sintering time. This can explain the increase in hematite content when fine iron ore are replaced by coarse ore. The variation in hematite content is similar to that obtained on the laboratory scale. Coarse ore provides a small reaction area and low assimilation rate, which results in an increase in hematite.

During sintering, higher oxides are reduced to lower oxides in the heating stage, whereas lower oxides are oxidized on cooling. The increase in the sinter permeability delays the reduction reaction of hematite into magnetite to occur during the heating stage, resulting in a lower amount of magnetite in the final sinter [36].

The replacement of fine iron ore by coarse ore did not influence the amounts of calcium silicates formed during the sintering process.

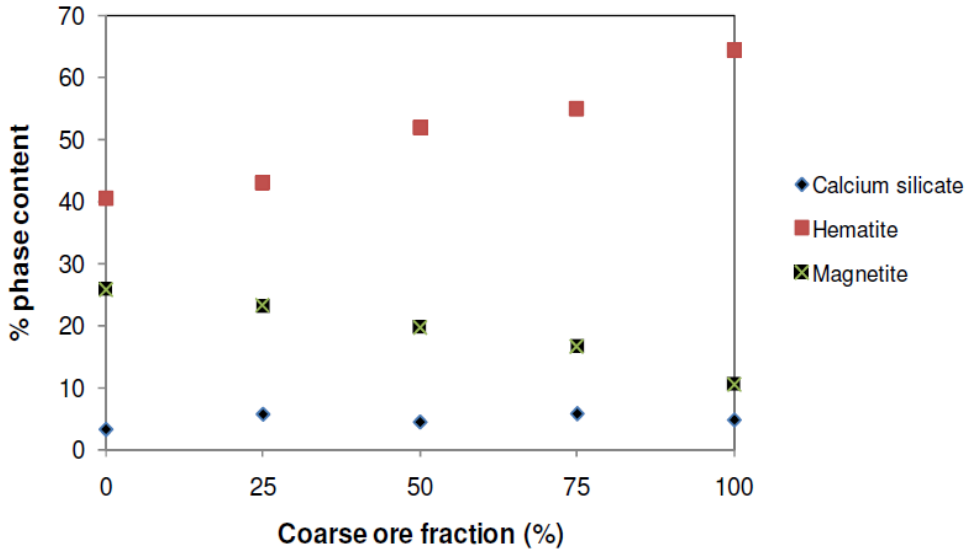


**Figure 58.** Variation in the amounts of hematite, magnetite and calcium silicate contents in the sinter with coarse ore fraction

The amount of SFCA-I produced in the sinter pots is higher than that obtained on a laboratory scale. This is presumably due to the reducing conditions provided by the combustion of coke during the heating stage. The oxygen partial pressure is initially low (reducing conditions) and continues to increase throughout the process up to 0.21 atm. Hsieh and Whiteman [57] reported that the SFCA-I phase easily forms under reducing conditions during the sintering process. Columnar SFCA is favoured by oxidizing conditions.

The acicular SFCA phase (SFCA-I) in the sinter slightly increased and reached a maximum at 25% coarse ore and decreased with a further replacement of fine iron ore by coarse ore particles (Figure 59). The presence of coarse ore particles in the sinter bed created low-density areas around the coarse ore particles, resulting in a higher assimilation ability [6]. It can be established that the sinter mix with 25% coarse ore presumably reached the maximum assimilation reaction rate, and formed higher amounts of SFCA-I. Above 25% coarse ore fraction, the decrease of reaction area becomes determinant, resulting in low assimilation reactions, and low amounts of SFCA-I that form.

The amount of columnar SFCA is decreased with an increase in coarse ore fraction. The increase in the airflow rate decreased the sintering time. The contact time of hot gas and solid particles is small, and the sinter bed could not reach high temperatures (>1300℃), which favours the formation of columnar SFCA [40,48].

By comparing the SFCA-I/SFCA ratios obtained on laboratory and pilot plant scales, it can be seen that this ratio is very significant for sinter produced from 100% coarse ore. This confirms that SFCA-I easily forms by assimilation of coarse ore particles. Hida et al. [37] also reported that acicular SFCA is formed by assimilation reactions, while other forms of SFCA are produced by exsolution from the melting phase.

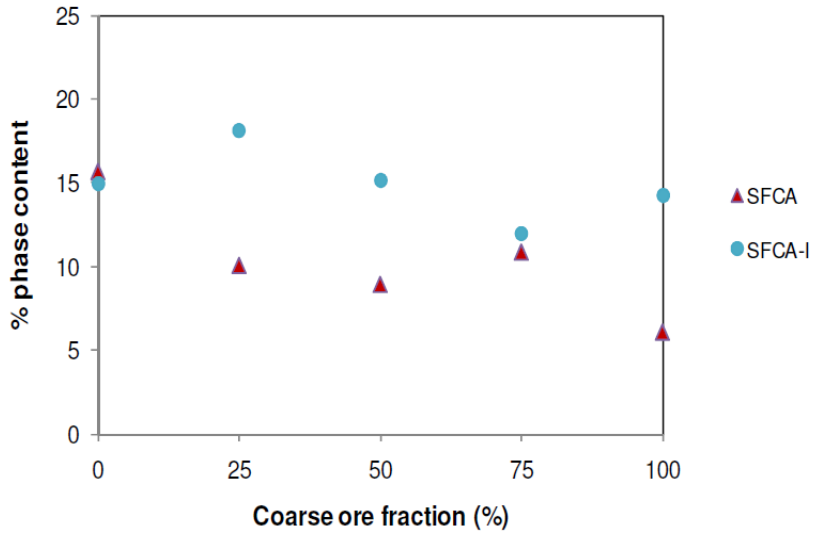


**Figure 59.** Variation in the amounts of SFCA and SFCA-I with coarse ore fraction

### V.3.3. Influence of coarse ore fraction on sinter quality

The sinters resulting from the sinter pot tests were evaluated with respect to their physical and metallurgical properties, namely tumbler index (TI), reducibility index (RI) and reduction disintegration index (RDI). These different indices of the investigated sinters are given in Table 20.

**Table 20** Physical and metallurgical properties of the produced sinters

| | Mix 1 | Mix 2 | Mix 3 | Mix 4 | Mix 5 |
|---|---|---|---|---|---|
| **Physical properties** | | | | | |
| Tumbler index (+6.3mm),% | 77.8 | 78.5 | 81.6 | 81.1 | 82.6 |
| Abrasion index (-0.5mm),% | 5.9 | 5.2 | 4.7 | 4.1 | 3.9 |
| **Metallurgical properties** | | | | | |
| RDI (-3.15mm), % | 28.4 | 17.5 | 11.2 | 7.4 | 6.6 |
| RDI (-0.5mm),% | 5.6 | 3.9 | 2.9 | 1.9 | 2.0 |
| RI ,%/min | 1.2 | 1.0 | 0.8 | 0.8 | 0.7 |

### V.3.3.1 Tumbler index and abrasion index of sinters

The effects of coarse ore fraction on the tumbler index and abrasion index are given in Figure 60. It can be seen that the replacement of fine iron ore by coarse ore particles slightly improves the cold strength from 77.8% to 82.6%. The tumbler index of all the investigated sinters reached the acceptable requirement of TI > 70%.

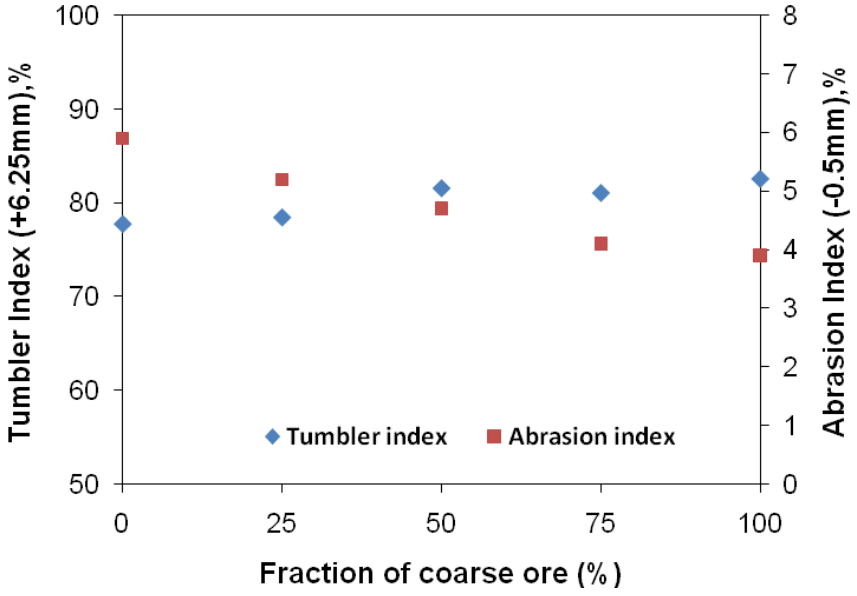


**Figure 60**. Effect of coarse ore fraction on tumbler and abrasion indexes

The abrasion index decreases with the replacement of fine iron ore by coarse ore as shown in Figure 60. Referring to the industrial requirement of an abrasion index of

less than 5%, only sinters produced from mixtures of 50%, 75% and 100% of coarse ore have acceptable abrasion index.

### V.3.3.2 Reduction disintegration of sinter

According to the ISO 4696-1 test, the reduction disintegration index (RDI) is evaluated from the test portions sieved to -3.15 mm and -0.5 mm. The RDI (-3.15 mm) and RDI (-0.5 mm) represent respectively the tendency of the sinter to generate fines and dust during reduction at low temperature. In practice, the blast furnace operators recommend that sinters should have a value for RDI (-3.15mm) lower than 30%, and a RDI (-0.5mm) lower than 5% [38,70].

The influence of coarse ore fraction on the reduction disintegration of the sinter is given in Figure 61. It can be seen that the value of RDI (-3.15mm) is decreased with an increase in coarse ore fraction in the sinter mix. This agrees with previous results where an increase in coarse ore fraction resulted in a decrease in the sinter disintegration [36-38].

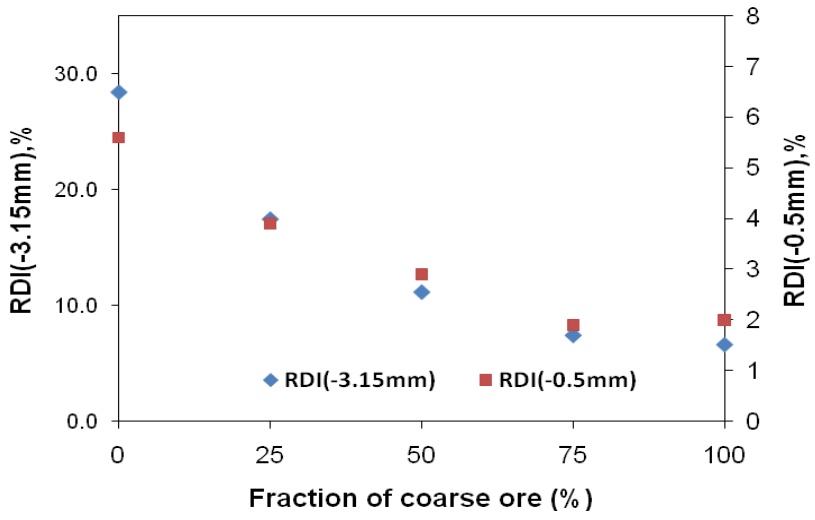


**Figure 61.** Effect of coarse ore fraction on reduction disintegration

Increasing the coarse ore fraction decreases the formation of dust (Figure 61). Sinter with the highest $RDI_{-0.5}$ value would therefore form more dust in the upper zone of the blast furnace, than the other sinters. From the experimental data in Table 20, all

sinters made with addition of coarse ore meet industrial requirements of RDI (-0.5mm) values of less than 5% except Mix 1.

### V.3.3.3 Reducibility of sinter

The reducibility of the produced sinters was determined using the ISO 4695 test procedure. The experimental data (Table 20 and Figure 62) show that the replacement of fine iron ore by coarse ore decreases the reducibility of the sinter from 1.2 %/min to 0.7%/min. From Tables 19 and 20, sinter made with fine iron ore consisted of a low hematite, high SFCA (total) and high magnetite content, and had the highest reducibility index. This seems to contradict the investigations conducted by Umadevi *et al.* [36], who stated that the high reducibility of the sinter is a result of increasing hematite and SFCA contents, and decreasing magnetite. However, the study by Hida *et al.*[37] showed that the reducibility of sinter is directly related to the internal pore volume and the surface area of the ore particles. Since Sishen ore is dense, the Sishen coarse ore particles will definitely affect the reducibility of the sinter product. This can explain the decrease in reducibility with an increase in coarse ore fraction.

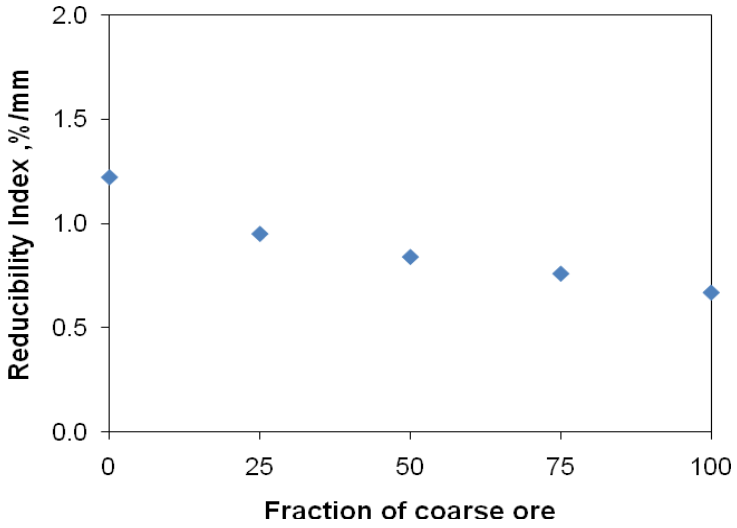


**Figure 62.** Effect of coarse ore fraction on reducibility index

Generally, the industry accepts a reducibility index (RI) of between 1%/min and 1.2%/min.

### V.3.3.4 Conclusions

Analysis of the sinters produced in the sinter pot tests confirmed that the replacement of fine iron ore by coarse ore affect the mineral compositions and physical and metallurgical properties of the sinters.

The hematite concentrations increased with an increase in coarse ore fraction in the sinter mix. The short reaction time did not allow more coarse ore particles to react during the sintering process. It was established that the magnetite and SFCA concentrations decreased with replacement of fine iron ore by coarse ore.

Sinters produced from sinter pot tests consisted of more SFCA-I than SFCA compared to those formed on laboratory scale. This is presumably due to the difference in sintering conditions. During laboratory tests, only oxidizing conditions were used, while reducing and oxidizing conditions prevail in the heating and cooling stages during sinter pot tests. It was established that the SFCA-I/SFCA ratio increased with an increase in coarse ore fraction for sintering tests on laboratory and pilot plant scale. This confirms that SFCA-I is mainly formed by assimilation reactions, while columnar SFCA is produced by exsolution from the melt.

The amount of SFCA-I content slightly increased with the increase in coarse ore fraction and reached a maximum at 25% coarse ore and decreased for further replacement of fine iron ore by coarse ore. The incorporation of 25% coarse ore in the sinter bed is assumed to form low-density areas around the coarse ore, resulting in an improvement in assimilation reactions. A further replacement of fine iron ore by coarse ore resulted in a decrease in the amounts of SFCA-I, presumably due to a decrease in surface area available for sintering reactions.

The tumbler index increased with an increase in proportions of coarse ore in the sinter mix. This trend is associated with the presence of high hematite content as well as low amount of spinel (magnetite/magnesioferrite) formed during sintering. The

replacement of fine iron ore by coarse ore from 0% to 100% showed a decrease in abrasion index.

The reduction disintegration of sinters increased with the increase in hematite content and decrease in spinel phase content. Sintering time decreased with an increase in coarse ore fraction, resulting in a decrease in contact time between the reducing gas and the coarse ore. The reduction of hematite to magnetite is therefore less likely to occur.

The reducibility of sinter decreased with an increase in the proportion of coarse ore. This could be explained by the presence of the denser coarse ore particles which provided small surface areas for the reduction reaction to occur and lower internal pore volumes.

The values of the tumbler index for all sinters meet the requirements of more than 70%. The abrasion index varies between 5.9% and 3.9%. Sinters with 0% and 25% coarse ore do not meet the industrial requirements of an abrasion index of less than 5%.

The reduction disintegration index of the different sinters is less than 30%. This meets the requirements of the blast furnace operators.

The reducibility index changes from 1.2 to 0.7 %/min as the proportion of coarse ore increases. Only sinters prepared from 0% and 25% coarse ore have reducibility indexes in excess of 1.0 %/min as required by the blast furnace users.

In practice, it is important to find an optimum between mineral compositions and sinter quality which complies with the generally accepted specifications. Sinter made with 25% coarse ore fraction has the optimum properties which meet the specifications required by the blast furnace operators on its TI, RDI(-3.15), RDI(-0.5) and RI. Only its abrasion index is slightly high at 5.2%, compared to the required maximum value of 5% (Table 21). This sinter is also characterised by a low fuel consumption of 75.8 kg/ton sinter and the highest sinter yield of 83.4%.

**Table 21** Properties of the studied sinters and industrial requirements

| | Average particle size $D_{50}$ [mm] | Physical and mechanical properties of sinter | | | | |
|---|---|---|---|---|---|---|
| | | TI (+6.3mm) [%] | AI (-0.5mm) [%] | RDI (-3.15mm) [%] | RDI (-0.5mm) [%] | RI [%/min] |
| **Industrial requirements** | ≥ 16 | ≥ 70 | ≤ 5 | ≤30 | ≤ 5 | ≥ 1.0 |
| **Sinter with 0% coarse ore** | 20 | 77.8 | 5.9 | 28.4 | 5.6 | 1.2 |
| **Sinter with 25% coarse ore** | 16.6 | 78.5 | 5.2 | 17.5 | 3.9 | 1.0 |
| **Sinter with 50% coarse ore** | 14.6 | 81.6 | 4.7 | 11.2 | 2.9 | 0.8 |
| **Sinter with 75% coarse ore** | 12.7 | 81.1 | 4.1 | 7.4 | 1.9 | 0.8 |
| **Sinter with 100% coarse ore** | 11.7 | 82.6 | 3.9 | 6.6 | 2.0 | 0.7 |

# VI Conclusions

The effect of replacement of fine iron ore by coarse ore on sintering reactions was investigated by performing experimental tests using an infrared furnace and sinter pot tests. In all sinter mixtures, the basicity ($CaO/SiO_2$) was kept constant at 2. The following conclusions can be drawn from the test results:

## VI.1. Laboratory tests

Sintering tests on laboratory scale were carried out using an infrared furnace, which enables the simulation of a sintering temperature profile at fast heating rate and controlled cooling. The heating rate and cooling rate were respectively set to 15℃/s and 2℃/s, and resulted in a temperature profile close to that used in the Anglo American Kumba Iron Ore (Value-in-Use) pilot plant.

Since a large number of parameters are involved in the sintering process, it was important to determine the ranking of effects of some sintering parameters on SFCA formation. In this study, the selected parameters were coarse ore fraction, maximum temperature, holding time and oxygen partial pressure. From the XRD analysis, sintered pellets mainly consisted of hematite, magnetite, SFCA, SFCA-I and calcium silicates.
The experiment design has shown that the proportion of coarse ore in the sinter mix strongly influences the formation of SFCA phase and assimilation of hematite. The other parameters have small effects on the formation of sinter phases as well as the assimilation of hematite. This therefore leads to a compromise in optimum conditions (sintering temperature, holding time and oxygen partial pressure) which should result in acceptable amounts of SFCA, SFCA-I, magnetite and calcium silicate in the produced sinters.

The variation of coarse ore fraction from 25%, 50%, 75% to 100% showed that sintering reactions were dependent on the porosity of the green pellets. The porosity of the compacted pellets decreased with the incorporation of coarse ore. The

compacted pellet prepared from 0% coarse ore had the highest porosity value of 34.01%, while those from 100% coarse ore had the lowest value of 26.81%.

XRD results indicated that the proportions of SFCA in sinter pellets are slightly increased when the fraction of coarse ore varies from 0% to 25%, but decreases with a further increase in percentage coarse ore. At 25% coarse ore fraction, the porosity of the compacted pellets decreased, resulting in an increase in packing density and sintering rate. More hematite reacted, resulting in the formation of high amounts of SFCA. Above 25% coarse ore fraction, the amount of hematite increased, and the concentrations of columnar SFCA decreased despite a further decrease in porosity (increase in packing density). This could be due to the decrease in reaction surface area for coarse ore, and the short reaction time, which limited the extent of reaction of the coarse particles. The variation of SFCA-I content was slightly increased with the replacement of fine iron ore by coarse ore.

Reflected light microscopy and SEM analysis revealed the existence of two major sinter phases: hematite surrounded by SFCA phase. The acicular and columnar SFCA could not be distinguished using EDS analysis and calculating the $M_{14}O_{20}$ and $M_{20}O_{28}$ stoichiometries of the phases. Chemical compositions of the SFCA phases fell in both phase fields of SFCA and SFCA-I, defined in the (0-5)%wt $Al_2O_3$ - $Fe_2O_3$-CaO-$SiO_2$ pseudo ternary system. Chemical compositions of the SFCA phases moved towards the region of SFCA-I on this diagram, as the proportion of coarse ore increases.

**VI.2. Grate pot tests**

Compared to laboratory experiments, XRD results revealed that more acicular SFCA (SFCA-I) was produced in sinter pot tests due to the lower oxygen partial pressures during the heating stage. During sinter pot tests, reducing and oxidizing conditions prevail in the heating and cooling stages, while only oxidizing conditions were used during laboratory tests. It was established that the replacement of fine ore by coarse ore resulted in an increase in the SFCA-I/SFCA ratio for sintering tests on laboratory and pilot plant scale. This confirms that SFCA-I is mainly formed by assimilation reactions, while columnar SFCA is produced by exsolution from the melt.

The amount of SFCA-I content slightly increased with the increase in coarse ore fraction and reached a maximum at 25% coarse ore and decreased for further replacement of fine iron ore by coarse ore. The incorporation of 25% coarse ore in the sinter bed is assumed to form low-density areas around the coarse ore, resulting in an improvement in assimilation reactions. A further replacement of fine iron ore by coarse ore resulted in a decrease in the amounts of SFCA-I, presumably due to a decrease in sintering time and surface area available for sintering reactions to take place.

The concentrations in hematite increased with an increase in coarse ore fraction in the sinter mix. The short reaction time and decrease in reaction area did not enable more coarse ore particles to react during the sintering process. XRD results confirmed the formation of spinel (magnetite/magnesioferrite) due to the reducing conditions during the heating stage. An increase in percentage coarse ore resulted in a decrease in spinel and SFCA concentrations. It was established that the formation of SFCA and spinel resulted from exsolution reactions rather than assimilation reactions.

The tumbler index of sinters increased with an increase in proportions of coarse ore in the sinter mix. The increase in sinter strength is associated with the presence of high hematite content as well as low amount of spinel (magnetite/magnesioferrite) formed during sintering. The replacement of fine iron ore by coarse ore from 0% to 100% showed a decrease in abrasion index.

The reduction disintegration increased with the percentage coarse ore increases. This could be assumed due to a decrease in sintering time and reaction area when fine ore is replaced by coarse particle.

The reducibility of sinter decreased with an increase in the proportion of coarse ore. This could be explained by the presence of the coarse ore particles which provided small surface areas and lower internal pore volumes for the reduction reaction to occur.

Sinter properties were assessed based on industrial norms. The replacement of 25% fine iron ore by coarse ore produced sinters with optimum properties, namely low $RDI_{-3,15}$, RI>1.00%/min and good cold strength. This sinter was also associated with a low coke consumption and an acceptable average particle size of 16.6 mm.

# VII Recommendations for future work

The replacement of fine iron ore with coarse ore influences sintering reactions with regard to the formation of acicular and columnar SFCA. In this investigation, the fraction of coarse ore was varied from 0% to 100% in 25% increments. However, sintering of mixtures with coarse particles in excess of 50% is not meaningful due to a significant decrease in reducibility of the produced sinters. The 0% - 50% coarse ore interval should be used for further study of the sintering reactions.

The influence of the permeability of the sinter bed and reaction surface area of solid particles on sintering reactions should further be investigated.

In order to characterise both acicular and columnar SFCA by SEM/EDS more accurately, more points on the polished sections should be analysed, followed by clustering of the compositions on the relevant phase diagrams.

## References

1. Yang, L.X. & Davis, L. 1999. Assimilation and mineral formation during sintering for blends containing magnetite concentrate and hematite/pisolite sintering fines, *ISIJ International*, vol. 39, no. 3, p. 239-245.

2. Scarlett, N.V.Y., Pownceby, M.I., Madsen, I.C, & Christensen, A.N. 2004. In situ X-ray diffraction analysis of iron ore sinter, *Journal of Applied crystallography*, vol. 37, no. 3, p. 362-368.

3. LV, X., Bai, C., Deng, Q., Huang, X. & Qiu, G. 2011. Behaviour of liquid phase formation during iron ores sintering, *ISIJ International*, vol. 5, no. 5, p. 722-727.

4. Yang, L.X. & Matthews, E. 1997. Sintering reactions of magnetite concentrates under various atmospheres, *ISIJ International*, vol. 37, no. 11, p. 1057-1065.

5. Mitra, K. & Nath, N.K. 2005. Analysis of two-layer sintering process for different bed heights by genetic algorithm, *Process Modelling and CFD*, *Tata Research Development & Design Centre*, p. 335-349.

6. Debrincat, D., Loo, C. E. & Hutchens, M. F. 2004. Effect of iron ore particle assimilation on sinter structure, *ISIJ International*, vol. 44, no. 8, p. 1308-1317.

7. Kamijo, C., Matsumura, M. & Kawaguchi, T. 2005. Sintering behaviour of raw material bed placing large particles, *ISIJ International*, vol. 45, no. 4, p. 544-550.

8. German, R.M. 1996. Sintering theory and practice, *Wiley-Interscience Publication*, New York, p.178-312.

9. Rahaman, M.N. 2003. Ceramic processing and sintering 2nd Edition, *CRC Press*, USA, p 620-757.

10. Formoso, A., Moro, A., Pello, G.F., Menendez, J.L., Muniz, M. & Cores, A. 2003. Influence of nature and particle size distribution on granulation of iron ore mixtures used in a sinter strand, *Ironmaking and Steelmaking*, 2003, vol. 30, no. 6, p. 447- 460.

11. McCann, G., Strevov, V., Lucas, J.A, Evans, T. & Strevov, L. 2004. Iron ore characterization during high temperature thermal processing, 2004, *Dev. Chem. Eng. Mineral Process*. 12(3/4), p. 1-14.

12. Fisher, R. 2010. Does the handling of iron sinter present a potential health hazard from the release of respirable crystalline silica*? Technical Working Group, The Iron Platform*.

13. Yang, W., Choi, S., Choi, E.S., Ri, D.W. & Kim, S. 2006, Combustion characteristics in an iron ore sintering bed-evaluation of fuel substitution, *The Combustion Institute*, *Elsevier Inc*, vol. 145, p. 447-463.

14. Yang, W., Ryu, C., Choi, S., Choi, E.S., Ri, D.W. & Huh, W. 2004. Mathematical model of thermal processes in an iron ore sintering bed, *Metals and Materials International*, vol. 10, no. 5, p. 493-500.

15. De Magalhaes, M.S. & Brandao, P.R.G. 2003. Microstructures of industrial sinters from Quadrilatero Ferrifero's iron ores, *Minerals Engineering*, *Elsevier*, p.1251.

16. Chaigneau, R. 1994. *Fluxed sinter formation and SFCA reduction under Simulated Conditions*, PhD Thesis, Delft University Press, p. 12-28.

17. Patrick, R.C. & Lovel, R.R. 2001, Leaching dicalcium silicates from iron ore sinter to remove phosphorus and other contaminants, *ISIJ International*, vol. 41, no. 2, p. 128-135.

18. Scarlett, N.V.Y., Pownceby, M.I., Madsen, I.C. & Christensen, A.N. 2004. Reaction sequences in the formation of silico-ferrites of calcium and aluminum in iron ore sinter, *Metallurgical and materials transactions B*, vol. 35B, p. 929-936.

19. Loo, C. E. & Leung, W. 2003. Factors influencing the bonding phase structure of iron ore sinters, *ISIJ International*, vol. 43, no. 9, p. 1393-1402.

20. Mumme, W.G., Clout, J.M.F. & Gable, R.W. 1988. The crystal structure of SFCA-I $Ca_{3.18}Fe^{3+}_{14.66}Al_{1.34}Fe^{2+}_{0.82}O_{28}$, a homologue of the aenigmatite structure type, and new structure type, and new crystal refinements of β-CCF, $Ca_{2.99}Fe^{3+}_{14.30}Fe^{2+}_{0.55}O_{25}$ and Mg-free SFCA, $Ca_{2.45}Fe^{3+}_{9.04}Al_{1.74}Fe^{2+}_{0.16}Si_{0.6}O_{20}$. *Neues Jahrbuch Miner. Abh*, vol. 173, no. 1, p. 93-117.

21. Mumme W.G. 2003. The crystal structure of SFCA-II, $Ca_{5.1}Al_{9.3}Fe^{3+}_{14.30}Fe^{2+}_{0.55}O_{48}$, a homologue of the aenigmatite structure type, and new structure type, and new crystal refinement of SFCA, $Ca_2Al_5Fe_7O_{20}$. Implications for the nature of the "ternary-phase solid-solution previously reported in the $CaO$-$Al_2O_3$-iron oxide system. *Neues Jahrbuch Miner. Abh.*, vol. 178, no. 3, p.307-335.

22. Hancart, J., Leroy, V. & Bragard, A. 1967. CNRM Metall. Report, DS 24/67, p. 3-7.

23. Dawson, P.R, Ostwald, J. & Hayes, K.M. 1984. The influence of sintering temperature profile on the mineralogy and properties of iron ore sinters, *Proc. Aust. Inst. of Mining and Metallurgy*, p. 103-169.

24. Pownceby, M.I. & Clout, J.M.F. 2003. Importance of fine iron ore chemical composition and high temperature phase relations, applications to iron ore sintering and pelletizing. *Mineral Processing and Extractive Metallurgy*, vol. 112, p. 44-51.

25. Bhagat R.P., Chattoray, U. & SIL, S.K. 2006. Porosity of sinter and its relation with the sintering indices, *ISIJ International*, vol. 46, no. 11, p. 1728-1730.

26. Yang Y. H. & Standis N. 1991. Fundamental mechanisms of pore formation in iron ore sinter and pellets, *ISIJ International*, vol. 31, no. 5, p. 468-477.

27. I.S.O. 3271. 1995. Iron ores - Determination of tumble strength, I.S.O. Standard.

28. I.S.O. 4695. 1996. Iron ores - Determination of reducibility, I.S.O. Standard.

29. I.S.O. 4696-1. 1996. Static Test for low temperature reduction - disintegration, I.S.O. Standard.

30. Cores, A., Babich, A., Muñiz, M., Ferreira, S & Mochon, J. 2010. The influence of different iron ores mixtures composition on the quality of sinter, *ISIJ International*, vol. 50 , no. 8, p. 1089-1098.

31. Husslage, W.M., Bakker, T., Kock. M.E. & Heerema, R.H. 1999. Influence of reduction conditions on the expansion and microstructure of sintered hematite compacts during the transition to magnetite, *Minerals & Metallurgical Processing*, vol.16, no. 3, p.23-33.

32. Zi-wei, Y., Mao-fa, J. & Li-xian, X. 2006. Effects of mineral composition and microstructure on crack resistance of sintered ore, *Journal of Iron and Steel Research, International*, vol. 13, no. 4, p. 9-12.

33. Higuchi, K., Orimoto, T., Koizumi, F., Furuta, H., Takamoto, Y., Sato, T. & Shinagawa, K. 2006. Quality improvement of sintered ore in relation to blast furnace operation, *Nippon Steel Technical Report No.94*, p. 36-41.

34. Dawson, P.R. 1993. Research studies on sintering and sinter quality. Ironmaking and Steelmaking, vol. 20, no. 2, p. 17-143.

35. Sasaki, M. & Hida, Y. 1982. Considerations on the properties of sinter from the point of sintering reactions, *Tetsu-to-Hagane*, vol. 68, p. 563-598.

36. Umadevi, T., Brahmacharyulu, A., Roy, A.K., Mahapatra, P.C., Prabhu, M. & Ranjan, M. 2011. Influence of fines feed size on microstructure, productivity and quality of iron ore sinter, *ISJ International*, vol. 51, no. 6, p. 922-929.

37. Hida, Y., Ito, K., Sasaki, M. & Umezu, Y. 1983. Effect of the mineralogical properties of coarse ores on the reducibility and the productivity of sinter, *Transactions ISIJ*, vol. 23, p. B-3.

38. Ghost, A. & Chatterjee, A. 2008. Ironmaking and steelmaking: Theory and Practice, *Prentice Hall of India Private Limited*, New Delhi, p.157-178.

39. Malysheva, Y. & Mansurova, N.R. 2008. Use of phase diagrams for the prediction of ferrite and silicate-binder compositions of fluxed sinters, *Russian Metallurgy, Pleiades Publishing*, p. 93-98.

40. Loo, C. E., Williams, R. P. & Matthews, L. T. 1992. Influence of material properties on high temperature zone reactions in sintering of iron ore, Trans. Inst. Min. Metall. C, vol.101, p. 7-15.

41. Chakraborti, N., Deb, K. & Jha, A. 2000. A genetic algorithm based heat transfer analysis of a bloom re-heating furnace. *Steel Res.*, vol. 71, no. 10, p. 396-402.

42. Levin, E.M, Robbins, C.R & Mc Murdie, H.F. 1969. Phase diagrams for ceramists, 2nd edition, *The American Ceramic Society Inc.*, Columbus, p. 49.

43. Boyanov, B.S. 2005. Solid state interactions in the systems $CaO(CaCO_3)$-$Fe_2O_3$ and $CuFe_2O_4$-CaO, *Journal of Mining and Metallurgy*, 41 B, p. 67-77.

44. Lu, L., Holmes, R. J. & Manuel, J. R. 2007. Effects of alumina on sintering performance of hematite iron ores, *ISIJ International*, vol. 47, No. 3, p. 349-358.

45. Levin, E.M, Robbins, C.R & Mc Murdie, H.F. 1969. Phase diagrams for ceramists, 2nd edition, *The American Ceramic Society Inc.*, Columbus, p.228

46. Lister, D.H. & Glasser, F.P. 1967. Phase relations in the system $CaO$-$Al_2O_3$ – Iron oxide, *Trans. Brit. Ceram. Soc.*, 66, p.293-305.

47. Muan, A. & Osborn, E.F. 1965. Phase equilibria among oxides in steelmaking, *Addison-Wesley Publishing Comp. Inc*, Massachusetts, p.113.

48. Loo, C.E. & Matthews, L.T. 1992. Assimilation of large ore and flux particles in iron ore sintering, *Trans. Inst. Min. Metall. Section C*, *Mineral processing and Extractive Metallurgy*, vol. 101, p.105-118.

49. Perry R. H. & Green D. 1984. *Perry's chemical engineer's handbook 6th edition*, *McGraw-Hill*.

50. Matsuno, F. & Harada, T. 1981. Changes of mineral phases during the sintering of iron ore-lime stone systems, *Transactions of the Iron and Steel Institute of Japan,* vol. 21, no. 5, p. 318-325.

51. Hida, Y., Sasaki, M., Sato, K., Kagawa, M., Takeshi, M., Soma, H., Naito, H., & Taniguchi, M. 1987, *Nippon Steel Tech. Rep.35*, p. 59-67.

52. Kalenga, M.K. 2007. *Investigation into the influence of magnesia content, alumina content, basicity and ignition temperature on the mineralogy and properties of iron sinter*, MSc Thesis, University of Pretoria, p.25-27.

53. Cumberland, D.J. & Crawford, R.J. 1987. The packing of particles, Handbook of powder technology series, vol. 6, *Elsevier*, Amsterdam.

54. Zou, R.P., Feng, C.L. & Yu, A.B. 2001. Packing density of binary mixtures of wet spheres, *Journal of American Ceramic*. Society, 84 [3], p. 504-508.

55. Loo, C. E., Matthews, L. T. & Ostwald, J. 1992. Sintering mechanism of Western Australian pisolitic limonite, *Mineral processing and extractive metallurgy*, vol. 101, p.70-80.

56. Yang, L.X. 2005. Sintering fundamentals of magnetite alone and blended with hematite/goethite ore, *ISIJ International*, vol.45, p. 469-476.

57. Hsieh, L.H., & Whiteman, J.A. 1989. Effect of oxygen potential on mineral formation in lime-fluxed iron ore sinter, *ISIJ International*, vol. 29, no. 8, p. 625-634.

58. Pownceby, M.I. & Clout, J.M.F. 2000. Phase relations in the Fe-rich portion of the system Fe2O3(-Fe3O4)-CaO-SiO2 (FCS) at 1240°C-1300°C and oxygen partial pressure of $5x10^{-3}$ atm, implications for iron ore sinter, *Trans. Inst. Min. Metall. C*, vol.109, p.36-47.

59. Van der Berg, T. 2008. *Assessment of production of fine material in iron ore sinter*, MSc Thesis, University of Pretoria University of Pretoria, p. 31- 35.

60. Lwamba, E. 2007, *Optimization of the grain size distribution of the raw material mixture in the production of iron ore sinter*, MSc Thesis, University of Pretoria. P.76-77.

61. ChambIR® Series - Model E4 Infrared heating system data sheet, Also available at : http://www.Researchinc.com, (accessed 14 April 2009)

62. Young, R.A. 1993. The Rietveld method, International Union Crystallography, *Oxford University Press*, Oxford, 298p.

63. Turriff, D.M.R. 2007. *Process kinetics of transient liquid phase sintering in a binary-isomorphous alloy system*, PhD Thesis, University of Waterloo, Ontario, Canada, p.65-135.

64. Verhoeven, J.D.1986. Scanning electron microscopy, Metal Handbook 9th Edition, vol. 10: Materials Characterization, *ASM Handbook Committee, ASM-International*, Metals Park, Ohio, p. 490-503.

65. Engineering statistics Handbook, p.1909-2081. Also available at: http://www.itl.nist.gov/div898/handbook/eda/eda.htm (accessed 22 September 2009)

66. Subra, P. & Jestin, P. 2000, Screening design of experiment (DOE) applied to supercritical antisolvent process, *Ind. Eng. Chem. Res, American Chemical Society*, vol. 39, No. 11, p. 4178-4184.

67. Blake, S., Launsby, R.G. & Weese, D.L. 1994. Experimental design meets the realities of the 1990s, *Quality Progress*, p.99-101.

68. Rekab, K. & Shaikh, M. 2005. Statistical design of experiments with engineering applications, *Chapman & Hall/CRC*, p.149-154.

69. Tonzětic´, I. & Dippenaar, A. 2011. An alternative to traditional iron-ore sinter phase classification. *Minerals Engineering*, *Elsevier*, vol.24, p.1-6.

70. Personal communication with Anglo American Kumba Iron Ore Personnel.

71. Harnett, D.L. & Murphy, J.L. 1975. Introductory statistical analysis, *Addison - Wesley Publishing, Inc.*, Menlo Park, California, A-23.

# Appendixes

Appendix 1

## Table of the Normal Distribution [71]


| z | 0.00 | 0.01 | 0.02 | 0.03 | 0.04 | 0.05 | 0.06 | 0.07 | 0.08 | 0.09 |
|---|---|---|---|---|---|---|---|---|---|---|
| 0.0 | 0.5000 | 0.5040 | 0.5080 | 0.5120 | 0.5160 | 0.5199 | 0.5239 | 0.5279 | 0.5319 | 0.5359 |
| 0.1 | 0.5398 | 0.5438 | 0.5478 | 0.5517 | 0.5557 | 0.5596 | 0.5636 | 0.5675 | 0.5714 | 0.5753 |
| 0.2 | 0.5793 | 0.5832 | 0.5871 | 0.5910 | 0.5948 | 0.5987 | 0.6026 | 0.6064 | 0.6103 | 0.6141 |
| 0.3 | 0.6179 | 0.6217 | 0.6255 | 0.6293 | 0.6331 | 0.6368 | 0.6406 | 0.6443 | 0.6480 | 0.6517 |
| 0.4 | 0.6554 | 0.6591 | 0.6628 | 0.6664 | 0.6700 | 0.6736 | 0.6772 | 0.6808 | 0.6844 | 0.6879 |
| 0.5 | 0.6915 | 0.6950 | 0.6985 | 0.7019 | 0.7054 | 0.7088 | 0.7123 | 0.7157 | 0.7190 | 0.7224 |
| 0.6 | 0.7257 | 0.7291 | 0.7324 | 0.7357 | 0.7389 | 0.7422 | 0.7454 | 0.7486 | 0.7517 | 0.7549 |
| 0.7 | 0.7580 | 0.7611 | 0.7642 | 0.7673 | 0.7704 | 0.7734 | 0.7764 | 0.7794 | 0.7823 | 0.7852 |
| 0.8 | 0.7881 | 0.7910 | 0.7939 | 0.7967 | 0.7995 | 0.8023 | 0.8051 | 0.8078 | 0.8106 | 0.8133 |
| 0.9 | 0.8159 | 0.8186 | 0.8212 | 0.8238 | 0.8264 | 0.8289 | 0.8315 | 0.8340 | 0.8365 | 0.8389 |
| 1.0 | 0.8413 | 0.8438 | 0.8461 | 0.8485 | 0.8508 | 0.8531 | 0.8554 | 0.8577 | 0.8599 | 0.8621 |
| 1.1 | 0.8643 | 0.8665 | 0.8686 | 0.8708 | 0.8729 | 0.8749 | 0.8770 | 0.8790 | 0.8810 | 0.8830 |
| 1.2 | 0.8849 | 0.8869 | 0.8888 | 0.8907 | 0.8925 | 0.8944 | 0.8962 | 0.8980 | 0.8997 | 0.9015 |
| 1.3 | 0.9032 | 0.9049 | 0.9066 | 0.9082 | 0.9099 | 0.9115 | 0.9131 | 0.9147 | 0.9162 | 0.9177 |
| 1.4 | 0.9192 | 0.9207 | 0.9222 | 0.9236 | 0.9251 | 0.9265 | 0.9279 | 0.9292 | 0.9306 | 0.9319 |
| 1.5 | 0.9332 | 0.9345 | 0.9357 | 0.9370 | 0.9382 | 0.9394 | 0.9406 | 0.9418 | 0.9429 | 0.9441 |
| 1.6 | 0.9452 | 0.9463 | 0.9474 | 0.9484 | 0.9495 | 0.9505 | 0.9515 | 0.9525 | 0.9535 | 0.9545 |
| 1.7 | 0.9554 | 0.9564 | 0.9573 | 0.9582 | 0.9591 | 0.9599 | 0.9608 | 0.9616 | 0.9625 | 0.9633 |
| 1.8 | 0.9641 | 0.9649 | 0.9656 | 0.9664 | 0.9671 | 0.9678 | 0.9686 | 0.9693 | 0.9699 | 0.9706 |
| 1.9 | 0.9713 | 0.9719 | 0.9726 | 0.9732 | 0.9738 | 0.9744 | 0.9750 | 0.9756 | 0.9761 | 0.9767 |
| 2.0 | 0.9772 | 0.9778 | 0.9783 | 0.9788 | 0.9793 | 0.9798 | 0.9803 | 0.9808 | 0.9812 | 0.9817 |
| 2.1 | 0.9821 | 0.9826 | 0.9830 | 0.9834 | 0.9838 | 0.9842 | 0.9846 | 0.9850 | 0.9854 | 0.9857 |
| 2.2 | 0.9861 | 0.9864 | 0.9868 | 0.9871 | 0.9875 | 0.9878 | 0.9881 | 0.9884 | 0.9887 | 0.9890 |
| 2.3 | 0.9893 | 0.9896 | 0.9898 | 0.9901 | 0.9904 | 0.9906 | 0.9909 | 0.9911 | 0.9913 | 0.9916 |
| 2.4 | 0.9918 | 0.9920 | 0.9922 | 0.9925 | 0.9927 | 0.9929 | 0.9931 | 0.9932 | 0.9934 | 0.9936 |
| 2.5 | 0.9938 | 0.9940 | 0.9941 | 0.9943 | 0.9945 | 0.9946 | 0.9948 | 0.9949 | 0.9951 | 0.9952 |
| 2.6 | 0.9953 | 0.9955 | 0.9956 | 0.9957 | 0.9959 | 0.9960 | 0.9961 | 0.9962 | 0.9963 | 0.9964 |
| 2.7 | 0.9965 | 0.9966 | 0.9967 | 0.9968 | 0.9969 | 0.9970 | 0.9971 | 0.9972 | 0.9973 | 0.9974 |
| 2.8 | 0.9974 | 0.9975 | 0.9976 | 0.9977 | 0.9977 | 0.9978 | 0.9979 | 0.9979 | 0.9980 | 0.9981 |
| 2.9 | 0.9981 | 0.9982 | 0.9982 | 0.9983 | 0.9984 | 0.9984 | 0.9985 | 0.9985 | 0.9986 | 0.9986 |
| 3.0 | 0.9987 | 0.9987 | 0.9987 | 0.9988 | 0.9988 | 0.9989 | 0.9989 | 0.9989 | 0.9990 | 0.9990 |

Appendix 2

**Interaction between 2 factors**

| | $X_1X_2$ | $X_1X_3$ | $X_1X_4$ | $X_2X3$ | $X_2X_4$ | $X_3X_4$ | Hem | SFCA | SFCA-I | Magn | C2S |
|---|---|---|---|---|---|---|---|---|---|---|---|
| **1** | + | + | + | + | + | + | 61.10 | 16.44 | 15.65 | 1.58 | 5.22 |
| **2** | - | - | - | + | + | + | 79.07 | 9.81 | 7.70 | 2.45 | 0.97 |
| **3** | - | + | + | - | - | + | 45.70 | 31.62 | 9.20 | 5.10 | 8.39 |
| **4** | + | - | - | - | - | + | 66.87 | 15.27 | 7.75 | 3.48 | 6.62 |
| **5** | + | - | + | - | + | - | 50.57 | 31.17 | 9.01 | 1.61 | 7.63 |
| **6** | - | + | - | - | + | - | 72.01 | 12.05 | 5.59 | 3.69 | 6.66 |
| **7** | - | - | + | + | - | - | 40.89 | 31.86 | 10.10 | 6.86 | 10.28 |
| **8** | + | + | - | + | - | - | 67.17 | 11.47 | 5.94 | 7.73 | 7.68 |
| **9** | + | + | - | + | - | - | 54.10 | 27.85 | 12.31 | 0.00 | 5.74 |
| **10** | - | - | + | + | - | - | 80.92 | 10.98 | 4.53 | 0.00 | 3.57 |
| **11** | - | + | - | - | + | - | 48.19 | 32.86 | 14.72 | 0.00 | 4.23 |
| **12** | + | - | + | - | + | - | 79.50 | 7.05 | 8.56 | 0.00 | 4.89 |
| **13** | + | - | - | - | - | + | 45.86 | 35.63 | 8.74 | 0.00 | 9.77 |
| **14** | - | + | + | - | - | + | 76.61 | 15.28 | 4.86 | 0.00 | 3.25 |
| **15** | - | - | - | + | + | + | 44.59 | 36.80 | 6.55 | 0.00 | 12.06 |
| **16** | + | + | + | + | + | + | 77.67 | 14.05 | 3.65 | 0.00 | 4.63 |

Hem: Hematite

Magn: Magnetite

C2S: Calcium silicate

XiXj: Interaction between $i^{th}$ factor and $j^{th}$ factor

**Mean effects and interaction effects between 2 factors**

| Phase | Factor | Average at high level | Average at low level | Main effect |
|---|---|---|---|---|
| Hematite | $X_1$ | 74.98 | 48.88 | 26.10 |
| | $X_2$ | 58.82 | 65.03 | -6.21 |
| | $X_3$ | 59.42 | 64.43 | -5.01 |
| | $X_4$ | 63.43 | 60.42 | 3.01 |
| | $X_1X_2$ | 62.86 | 61.00 | 1.86 |
| | $X_1X_3$ | 62.82 | 61.04 | 1.78 |
| | $X_1X_4$ | 64.12 | 59.73 | 4.39 |
| | $X_2X_3$ | 63.19 | 60.66 | 2.53 |
| | $X_2X_4$ | 64.09 | 59.77 | 4.33 |
| | $X_3X_4$ | 62.19 | 61.67 | 0.51 |
| SFCA | $X_1$ | 12.00 | 30.53 | -18.53 |
| | $X_2$ | 22.62 | 19.90 | 2.72 |
| | $X_3$ | 23.54 | 18.99 | 4.56 |
| | $X_4$ | 22.56 | 19.96 | 2.60 |
| | $X_1X_2$ | 19.87 | 22.66 | -2.79 |
| | $X_1X_3$ | 20.20 | 22.32 | -2.12 |
| | $X_1X_4$ | 19.81 | 22.72 | -2.91 |
| | $X_2X_3$ | 19.91 | 22.62 | -2.71 |
| | $X_2X_4$ | 20.03 | 22.50 | -2.47 |
| | $X_3X_4$ | 21.86 | 20.66 | 1.20 |
| SFCA-I | $X_1$ | 6.07 | 10.78 | -4.71 |
| | $X_2$ | 8.31 | 8.55 | -0.24 |
| | $X_3$ | 6.80 | 10.05 | -3.25 |
| | $X_4$ | 7.99 | 8.87 | -0.88 |
| | $X_1X_2$ | 8.95 | 7.90 | 1.05 |
| | $X_1X_3$ | 8.99 | 7.87 | 1.12 |
| | $X_1X_4$ | 8.19 | 8.66 | -0.47 |

| Phase | Factor | Average at high level | Average at low level | Main effect |
|---|---|---|---|---|
| SFCA-I | $X_2X_3$ | 8.30 | 8.55 | -0.25 |
| | $X_2X_4$ | 8.93 | 7.93 | 1.00 |
| | $X_3X_4$ | 8.01 | 8.84 | -0.83 |
| Magnetite | $X_1$ | 2.17 | 1.89 | 0.28 |
| | $X_2$ | 2.90 | 1.17 | 1.73 |
| | $X_3$ | 2.49 | 1.58 | 0.91 |
| | $X_4$ | 0.00 | 4.06 | -4.06 |
| | $X_1X_2$ | 1.80 | 2.26 | -0.46 |
| | $X_1X_3$ | 2.26 | 1.80 | 0.46 |
| | $X_1X_4$ | 1.89 | 2.17 | -0.28 |
| | $X_2X_3$ | 2.33 | 1.74 | 0.59 |
| | $X_2X_4$ | 1.17 | 2.90 | -1.73 |
| | $X_3X_4$ | 1.58 | 2.49 | -0.91 |
| Ca-silicates | $X_1$ | 4.78 | 7.92 | -3.13 |
| | $X_2$ | 7.35 | 5.35 | 2.00 |
| | $X_3$ | 7.75 | 4.95 | 2.79 |
| | $X_4$ | 6.02 | 6.68 | -1.07 |
| | $X_1X_2$ | 6.52 | 6.18 | 0.35 |
| | $X_1X_3$ | 5.73 | 6.97 | -1.25 |
| | $X_1X_4$ | 5.98 | 6.72 | -0.73 |
| | $X_2X_3$ | 6.27 | 6.43 | -0.16 |
| | $X_2X_4$ | 5.78 | 6.91 | -1.13 |
| | $X_3X_4$ | 6.36 | 6.34 | 0.03 |

Appendix 3

**Ordered mean, interaction effects and percentiles**

| Code | Main effect | i | (i – 0.5)/p | Zi |
|---|---|---|---|---|
| E | -18.53 | 1 | 0.01 | -2.33 |
| F | -6.21 | 2 | 0.03 | -1.88 |
| C | -4.71 | 3 | 0.05 | -1.65 |
| S | -4.06 | 4 | 0.07 | -1.48 |
| M | -3.25 | 5 | 0.09 | -1.34 |
| B | -3.13 | 6 | 0.11 | -1.23 |
| CA | -2.91 | 7 | 0.13 | -1.13 |
| AA | -2.79 | 8 | 0.15 | -1.04 |
| DA | -2.71 | 9 | 0.17 | -0.96 |
| EA | -2.47 | 10 | 0.19 | -0.88 |
| BA | -2.12 | 11 | 0.21 | -0.81 |
| QA | -1.73 | 12 | 0.23 | -0.74 |
| TA | -1.25 | 13 | 0.25 | -0.68 |
| wA | -1.13 | 14 | 0.27 | -0.61 |
| T | -1.07 | 15 | 0.29 | -0.56 |
| RA | -0.91 | 16 | 0.31 | -0.5 |
| R | -0.88 | 17 | 0.33 | -0.44 |
| LA | -0.83 | 18 | 0.35 | -0.39 |
| uA | -0.73 | 19 | 0.37 | -0.33 |
| IA | -0.47 | 20 | 0.39 | -0.28 |
| MA | -0.46 | 21 | 0.41 | -0.23 |
| OA | -0.28 | 22 | 0.43 | -0.18 |
| JA | -0.25 | 23 | 0.45 | -0.13 |
| H | -0.24 | 24 | 0.47 | -0.08 |
| vA | -0.16 | 25 | 0.49 | -0.03 |
| xA | 0.03 | 26 | 0.51 | 0.03 |

| Code | Main effect | i | (i – 0.5)/p | Zi |
|---|---|---|---|---|
| D | 0.28 | 27 | 0.53 | 0.08 |
| SA | 0.35 | 28 | 0.55 | 0.13 |
| NA | 0.46 | 29 | 0.57 | 0.18 |
| z | 0.51 | 30 | 0.59 | 0.23 |
| PA | 0.59 | 31 | 0.61 | 0.28 |
| N | 0.91 | 32 | 0.63 | 0.33 |
| KA | 1.00 | 33 | 0.65 | 0.39 |
| GA | 1.05 | 34 | 0.67 | 0.44 |
| HA | 1.12 | 35 | 0.69 | 0.5 |
| FA | 1.20 | 36 | 0.71 | 0.56 |
| I | 1.73 | 37 | 0.73 | 0.61 |
| v | 1.78 | 38 | 0.75 | 0.68 |
| u | 1.86 | 39 | 0.77 | 0.74 |
| J | 2.00 | 40 | 0.79 | 0.81 |
| x | 2.53 | 41 | 0.81 | 0.88 |
| Q | 2.60 | 42 | 0.83 | 0.96 |
| G | 2.72 | 43 | 0.85 | 1.04 |
| O | 2.79 | 44 | 0.87 | 1.13 |
| P | 3.01 | 45 | 0.89 | 1.23 |
| y | 4.33 | 46 | 0.91 | 1.34 |
| w | 4.39 | 47 | 0.93 | 1.48 |
| L | 4.56 | 48 | 0.95 | 1.65 |
| K | 5.01 | 49 | 0.97 | 1.88 |
| A | 26.10 | 50 | 0.99 | 2.33 |

**Normal distributions including interaction effects between 2 factors**

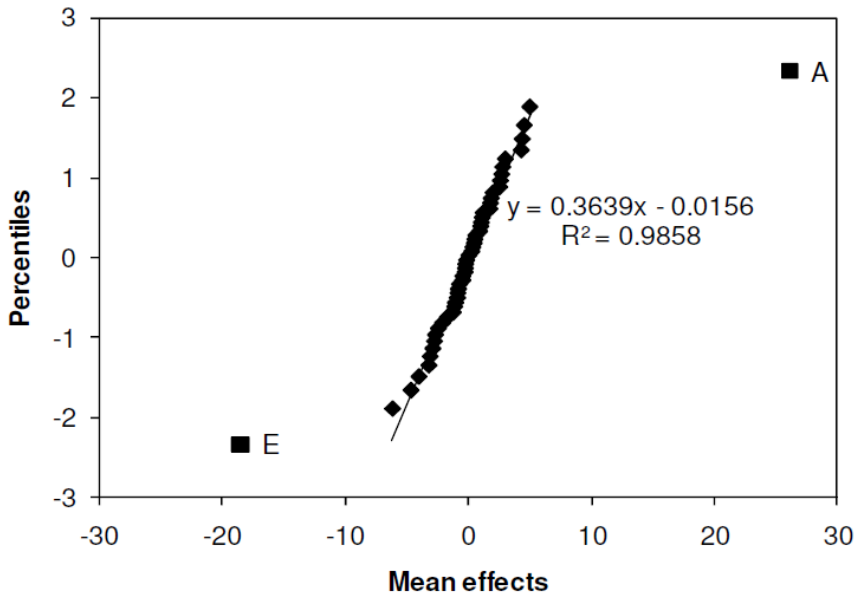


E (-18.53): Mean effect of coarse ore fraction on formation of SFCA

A (26.10): Mean effect of coarse ore fraction on assimilation of hematite

Appendix 4

## XRD analyses of sinters produced on laboratory scale

**Mix 1**

| | Phase compositions [mass%] | | | | | Average | STDEV |
|---|---|---|---|---|---|---|---|
| | Test 1 | Test 2 | Test 3 | Test 4 | Test 5 | | |
| **C2S** | 8.58 | 10.20 | 9.01 | 7.85 | 11.20 | 9.37 | 1.19 |
| **Hematite** | 54.23 | 56.58 | 57.02 | 55.98 | 55.11 | 55.78 | 1.01 |
| **SFCA-I** | 6.51 | 6.12 | 5.09 | 5.59 | 6.62 | 5.99 | 0.58 |
| **SFCA** | 30.68 | 27.1 | 28.88 | 30.58 | 27.07 | 28.86 | 1.59 |

**Mix 2**

| | Phase compositions [mass%] | | | | | Average | STDEV |
|---|---|---|---|---|---|---|---|
| | Test 1 | Test 2 | Test 3 | Test 4 | Test 5 | | |
| **C2S** | 9.51 | 7.52 | 5.68 | 6.56 | 8.68 | 7.59 | 1.38 |
| **Hematite** | 50.57 | 55.35 | 53.56 | 52.63 | 52.68 | 52.96 | 1.55 |
| **SFCA-I** | 7.95 | 6.07 | 5.23 | 6.52 | 4.89 | 6.13 | 1.08 |
| **SFCA** | 31.97 | 31.06 | 35.53 | 34.29 | 33.75 | 32.32 | 1.66 |

**Mix 3**

| | Phase compositions [mass%] | | | | | Average | STDEV |
|---|---|---|---|---|---|---|---|
| | Test 1 | Test 2 | Test 3 | Test 4 | Test 5 | | |
| **C2S** | 7.52 | 5.79 | 7.22 | 3.30 | 6.58 | 6.08 | 1.51 |
| **Hematite** | 65.26 | 64.11 | 66.13 | 67.94 | 65.98 | 65.88 | 1.25 |
| **SFCA-I** | 7.91 | 4.07 | 3.80 | 3.05 | 2.94 | 4.35 | 1.83 |
| **SFCA** | 19.31 | 26.03 | 22.85 | 25.71 | 24.5 | 23.68 | 2.45 |

**Mix 4**

| | Phase compositions [mass%] | | | | | Average | STDEV |
|---|---|---|---|---|---|---|---|
| | Test 1 | Test 2 | Test 3 | Test 4 | Test 5 | | |
| **C2S** | 4.62 | 2.01 | 3.26 | 1.98 | 3.17 | 3.01 | 0.97 |
| **Hematite** | 69.96 | 75.66 | 73.12 | 70.57 | 71.01 | 72.06 | 2.09 |
| **SFCA-I** | 7.91 | 6.85 | 7.23 | 10.42 | 9.65 | 8.41 | 1.39 |
| **SFCA** | 17.51 | 15.48 | 16.39 | 17.03 | 16.17 | 16.52 | 0.70 |

**Mix 5**

| | Phase compositions [mass%] | | | | | Average | STDEV |
|---|---|---|---|---|---|---|---|
| | Test 1 | Test 2 | Test 3 | Test 4 | Test 5 | | |
| **C2S** | 3.67 | 5.69 | 3.42 | 4.98 | 5.15 | 4.58 | 0.88 |
| **Hematite** | 75.29 | 74.96 | 77.78 | 78.59 | 74.58 | 76.24 | 1.62 |
| **SFCA-I** | 12.59 | 9.56 | 8.69 | 9.88 | 12.66 | 10.68 | 1.64 |
| **SFCA** | 8.45 | 9.79 | 10.11 | 6.55 | 7.61 | 8.50 | 1.33 |

Appendix 5

## Mix 1

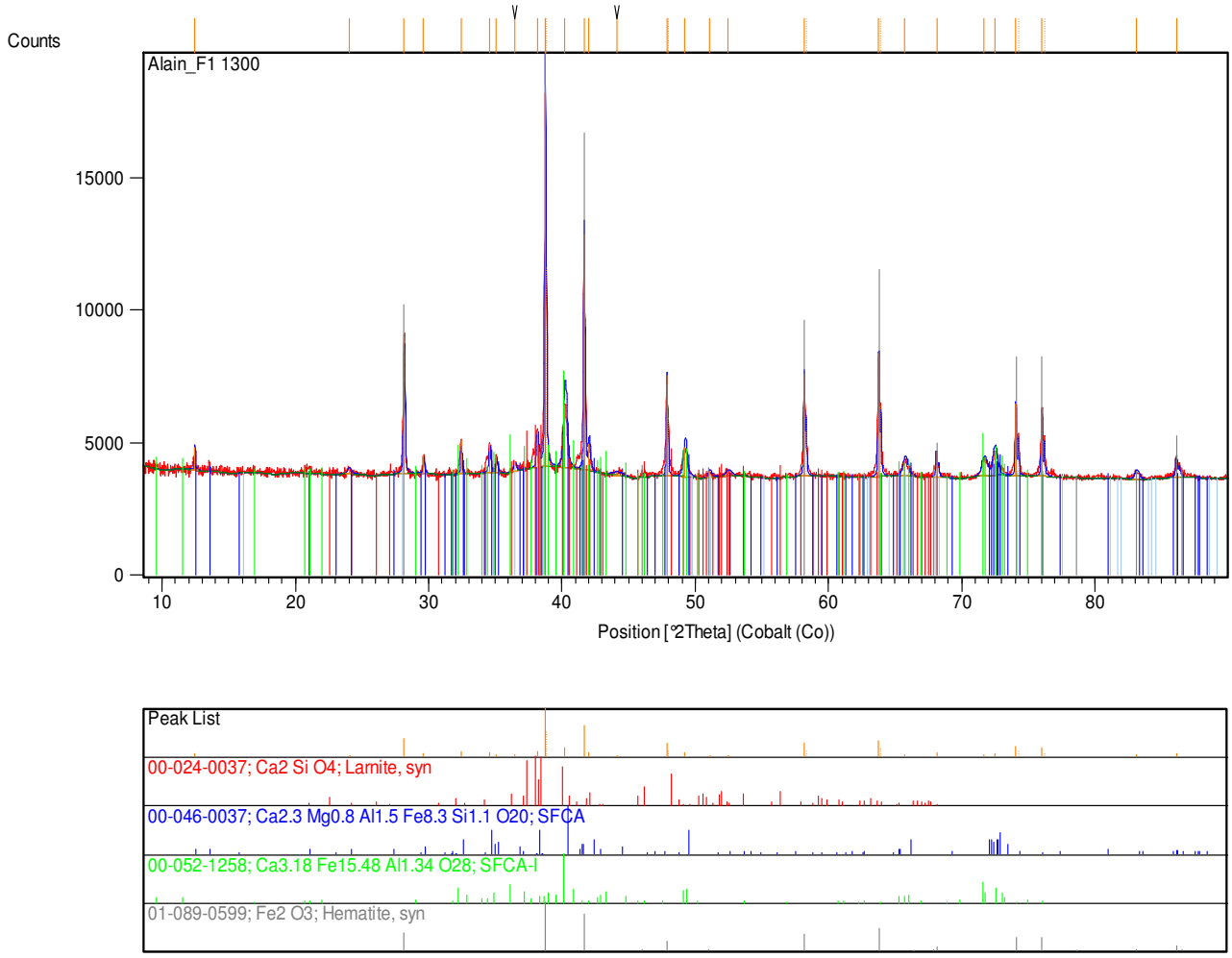

## Mix2

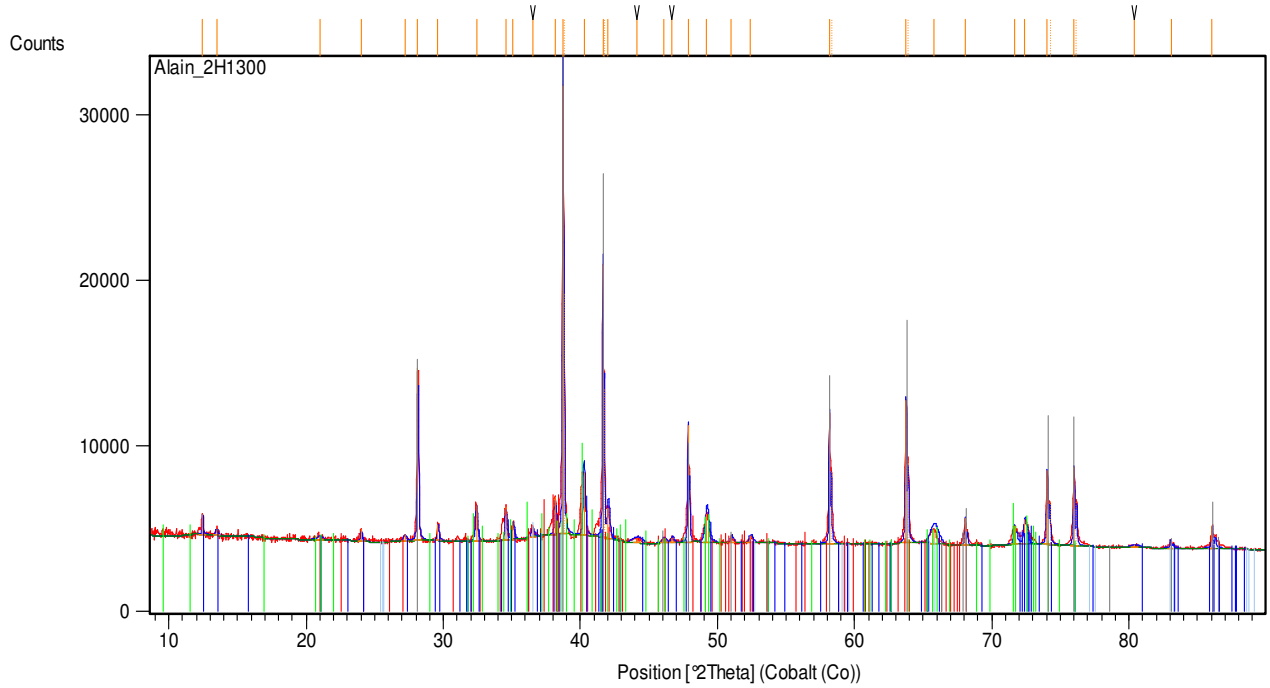
Counts
Alain_2H1300
30000
20000
10000
0
10
20
30
40
50
60
70
80
Position [°2Theta] (Cobalt (Co))

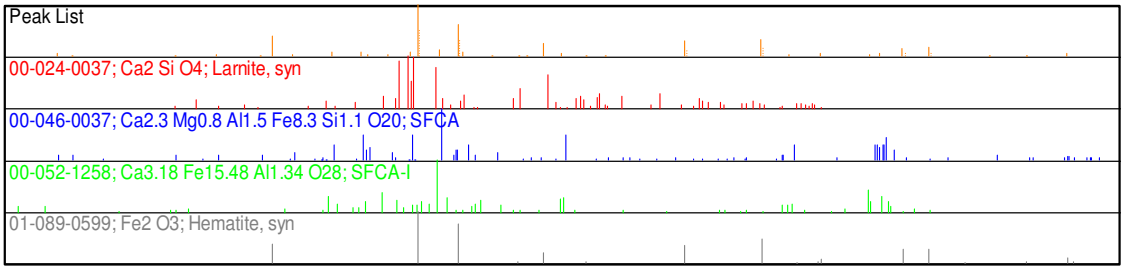
Peak List
00-024-0037; Ca2 Si O4; Larnite, syn
00-046-0037; Ca2.3 Mg0.8 Al1.5 Fe8.3 Si1.1 O20; SFCA
00-052-1258; Ca3.18 Fe15.48 Al1.34 O28; SFCA-I
01-089-0599; Fe2 O3; Hematite, syn

## Mix3

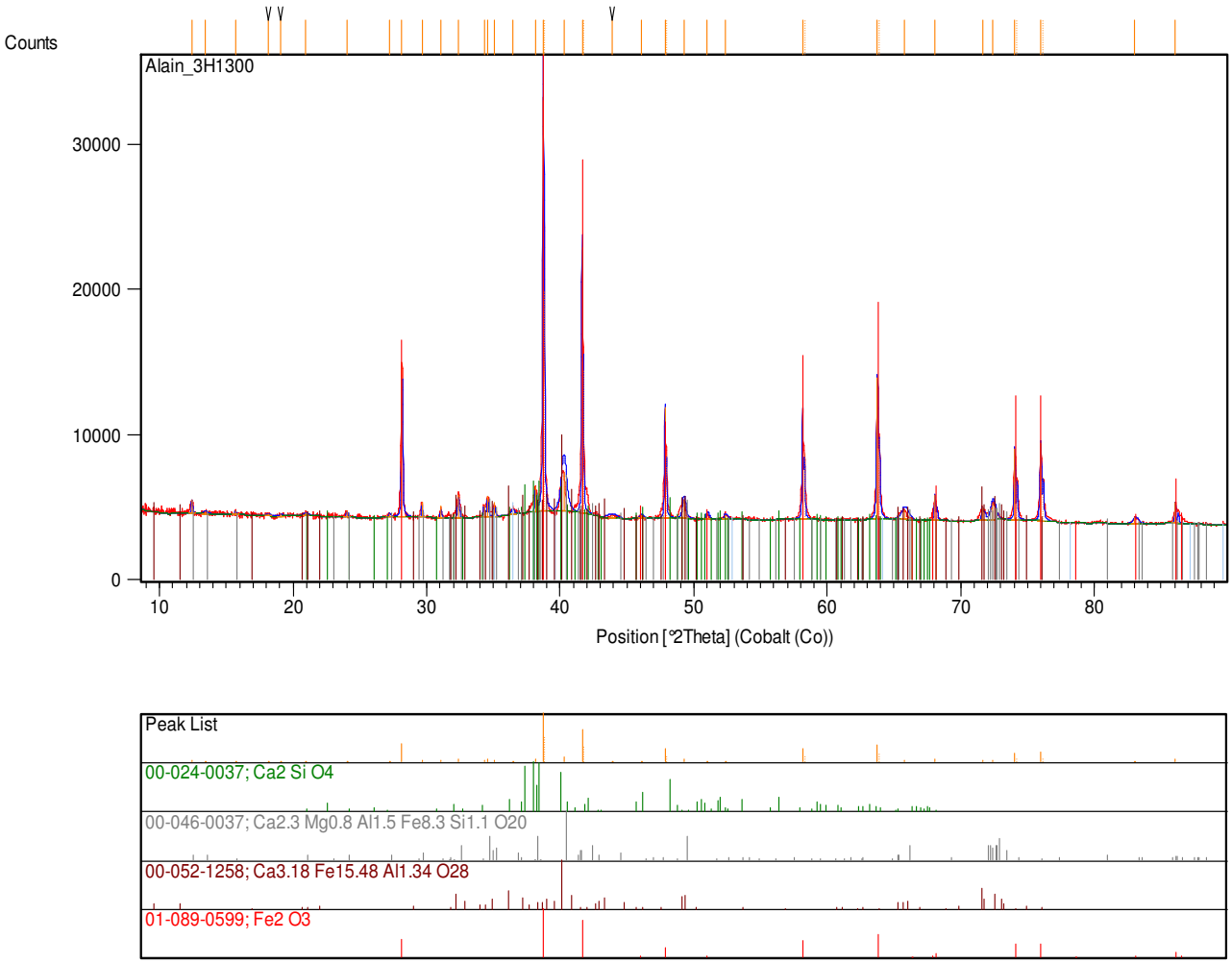
Counts
Alain_3H1300
30000
20000
10000
0
10
20
30
40
50
60
70
80
Position [°2Theta] (Cobalt (Co))
Peak List
00-024-0037; Ca2 Si O4
00-046-0037; Ca2.3 Mg0.8 Al1.5 Fe8.3 Si1.1 O20
00-052-1258; Ca3.18 Fe15.48 Al1.34 O28
01-089-0599; Fe2 O3

## Mix 4

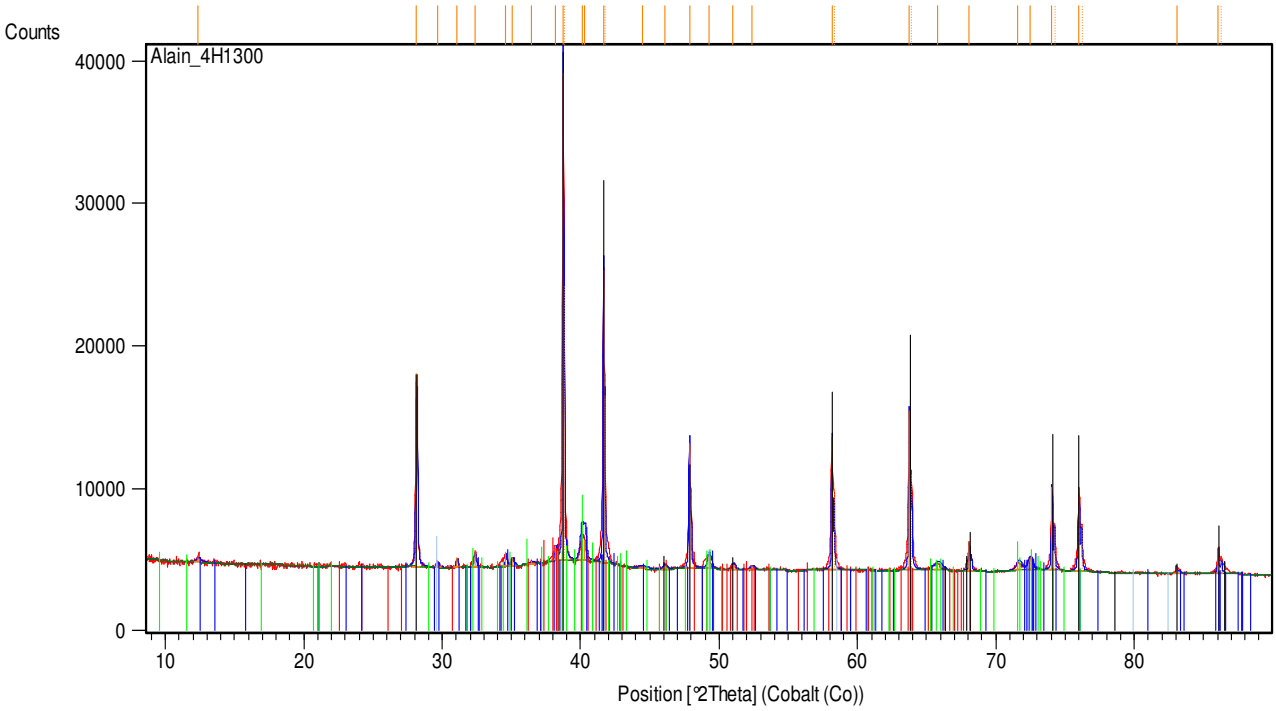
Counts
Alain_4H1300
40000
30000
20000
10000
0
10
20
30
40
50
60
70
80
Position [°2Theta] (Cobalt (Co))

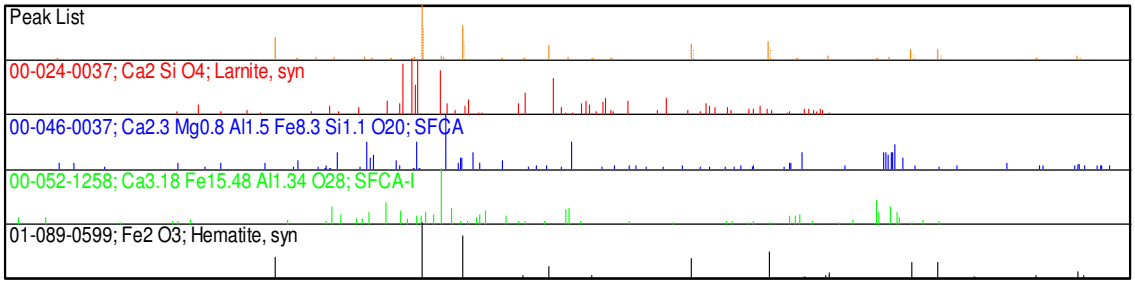
Peak List
00-024-0037; Ca2 Si O4; Larnite, syn
00-046-0037; Ca2.3 Mg0.8 Al1.5 Fe8.3 Si1.1 O20; SFCA
00-052-1258; Ca3.18 Fe15.48 Al1.34 O28; SFCA-I
01-089-0599; Fe2 O3; Hematite, syn

## Mix 5

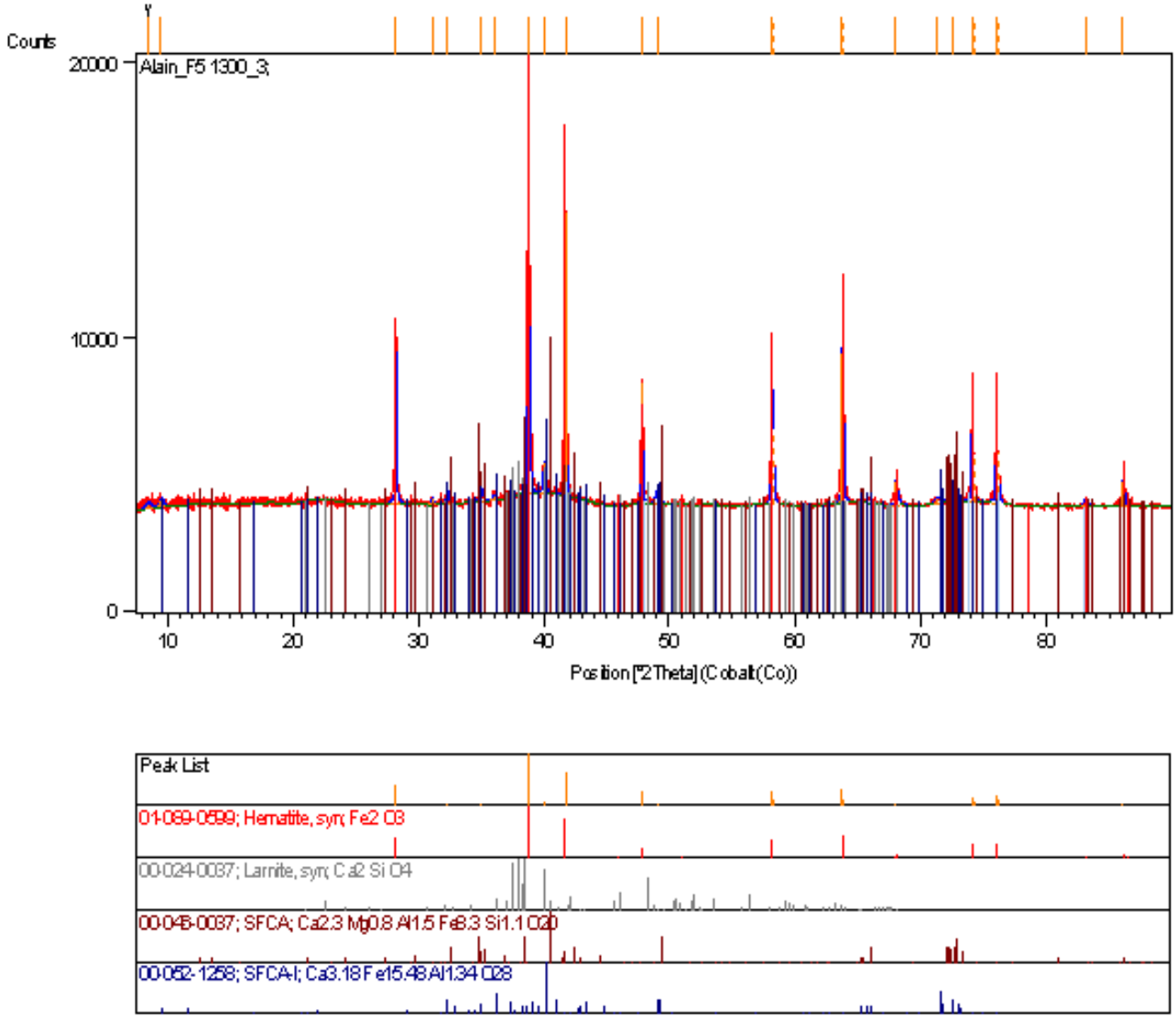
Counts
20000
10000
0
Alain_F5 1300_3;
10
20
30
40
50
60
70
80
Position [°2Theta] (Cobalt (Co))
Peak List
01-089-0599; Hematite, syn; Fe2 O3
00-024-0037; Larnite, syn; Ca2 Si O4
00-045-0037; SFCA; Ca2.3 Mg0.8 Al1.5 Fe8.3 Si1.1 O20
00-052-1258; SFCA-I; Ca3.18 Fe15.48 Al1.34 O28